JPRS L/9489

15 January 1981

USSR Report

ELECTRONICS AND ELECTRICAL ENGINEERING

(FOUO 1/81)

FBIS FOREIGN BROADCAST INFORMATION SERVICE

NOTE

JPRS publications contain information primarily from foreign newspapers, periodicals and books, but also from news agency transmissions and broadcasts. Materials from foreign-language sources are translated; those from English-language sources are transcribed or reprinted, with the original phrasing and other characteristics retained.

Headlines, editorial reports, and material enclosed in brackets [] are supplied by JPRS. Processing indicators such as [Text] or [Excerpt] in the first line of each item, or following the last line of a brief, indicate how the original information was processed. Where no processing indicator is given, the information was summarized or extracted.

Unfamiliar names rendered phonetically or transliterated are enclosed in parentheses. Words or names preceded by a question mark and enclosed in parentheses were not clear in the original but have been supplied as appropriate in context. Other unattributed parenthetical notes within the body of an item originate with the source. Times within items are as given by source.

The contents of this publication in no way represent the policies, views or attitudes of the U.S. Government.

APPROVED FOR RELEASE: 2007/02/08: CIA-RDP82-00850R000300070024-5

JPRS L/9489

15 January 1981

USSR REPORT

ELECTRONICS AND ELECTRICAL ENGINEERING

(FOUO 1/81)

CONTENTS

COMMUNICATIONS, COMMUNICATION EQUIPMENT, RECEIVERS AND TRANSMITTERS, NETWORKS, RADIO PHYSICS, DATA TRANSMISSION AND PROCESSING, INFORMATION THEORY

UDC 521.391.266

QUASI-OPTIMAL FILTERING OF TRAPEZOIDAL SIGNALS WITH VARYING RISE AND FALL TIMES

Kiev IVUZ RADIOELEKTRONIKA in Russian Vol 23,No 8,Aug 80 pp 85-86
manuscript received 15 Feb 79,after revision 31 Jan 80

[Paper by P.V. Gavrish]

[Text] The optimization of the electronic channel of a LIDAR polar coordinate meter reduces to the choice of the procedure for discriminating the detected signal in the receiver noise against the signal and interference background, referenced to the input of the time filter.

The received realization $u(t) = s(t-\tau, \beta) + n(t)$ consists of additive noise $n(t)$ and the signal $s(t-\tau, \beta)$, which is a determinate function of time, and some parameter β, which characterizes the law governing the image analysis; τ is the signal delay time.

The reception conditions are such that we consider the statistics of the photoelectric current to be normal while $n(t)$ is a steady-state normal uncorrelated process. In such situations, the reception of intensity modulated signals (with the exclusion of the constant component) is accomplished just as in the case of radar.

The sounding range is equal to $[R_1, R_2]$ for any distance R $[R_1, R_2]$ and uniformly distributed in $[R_1, R_2]$, the detected signal represents a symmetrical trapezoidal video pulse [1] with a width at the 0.5 level relative to the maximum value A of τ_c = const. and a width of the leading and trailing edges of $\tau_\phi \sim 1/R$. In this case, τ_ϕ is uniformly distributed in the segment $[\tau_{\phi 2}, \tau_{\phi 1}]$ $(0, \tau_s)$, where $\tau_{\phi 1} \sim 1/R_1$ and $\tau_{\phi 2} \sim 1/R_2$.

We shall take τ_ϕ as β. We then derive the likelihood function $p(u/\tau)$ which for a given nature of the signal and noise defines the structure

of the optimal receiving system, by means of statistically averaging the likelihood function $p(u/\tau, \tau_\phi)$ with respect to the minor parameter τ_ϕ. The practical realization of such an optimal receiver is complicated.

If the signal is considered to be a determinate function, the problem posed here can be solved by the method of optimal filtering (OF). However, since $\tau_\phi \sim 1/R$, the synthesis of a filter which is optimal for the set of signals encompassing $[R_1, R_2]$, is not feasible in practice. In such situations, quasi-optimal filters (KVOF) are used [2] which are matched to the signal in a portion of its spectrum selected in a specified manner.

It is proposed that an ideal low pass filter with a passband Δf be used as the KVOF, where the filter is designed to maximize the signal-to-noise ratio for the worst case situations which occur in the specified sounding band.

We shall designate the maximum value of the voltage signal-to-noise ratio at the output of the KVOF to the signal to noise ratio at the output of an optimal filter as ρ [2]:

$$\rho = \frac{\left| \int_{-\infty}^{\infty} S(j\omega) K(j\omega) e^{j\omega t} d\omega \right|}{\left| \int_{-\infty}^{\infty} |S(j\omega)|^2 d\omega \cdot \int_{-\infty}^{\infty} |K(j\omega)|^2 d\omega \right|^{1/2}}, \tag{1}$$

where

$$S(j\omega) = 4A \sin 0{,}5\,\omega\tau_c \sin 0{,}5\,\omega\tau_\phi/\omega^2\tau_\phi \tag{2}$$

is the spectrum of the received signal, while

$$K(j\omega) = ke^{-j\omega t_0}, \quad |\omega| < \Delta\omega \tag{3}$$

is the transfer function of the proposed KVOF. We define t_0 as the point in time when the signal is observed at the output of the KVOF; k is a constant factor.

After substituting (2) and (3) in (1), we obtain:

$$\rho = \frac{\left(1 - \frac{\tau_c}{\tau_\phi}\right) \mathrm{si}\,[\pi\Delta f(\tau_c - \tau_\phi)] + \left(1 + \frac{\tau_c}{\tau_\phi}\right) \mathrm{si}\,[\pi\Delta f(\tau_c + \tau_\phi)] - \frac{2}{\pi\Delta f\tau_\phi} \sin \pi\Delta f\tau_c \sin \pi\Delta f\tau_\phi}{\pi\sqrt{2/3\Delta f(3\tau_c - \tau_\phi)}}, \tag{4}$$

where si(z) is the integral sine.

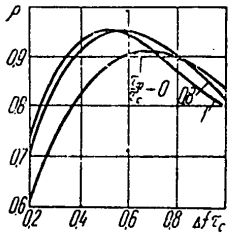

Figure 1.

The reduction in the signal-to-noise ratio at the output of a KVOF for various values of the normalized rise time of the pulses, computed on a computer using formula (4), is shown in Figure 1.

The quantity ρ, for a specified $[R_1, R_2]$ can be considered a function of two variables: τ_Φ and Δf, where

$$\tau_{\Phi 2} < \tau_\Phi < \tau_{\Phi 1},\ [\tau_{\Phi 2}, \tau_{\Phi 1}] \subset (0, \tau_c].$$

We shall specify the range of change for Δf by the condition of the most reliable isolation of the signal from the noise, i.e.,

$$\sup_{\Delta f} \{\rho(\tau_\Phi = \text{const}, \Delta f)\}, \text{ where } \tau_\Phi \in (0, \tau_c]. \qquad (5)$$

By studying the behavior of $\rho(\tau_\Phi = \text{const.}, \Delta f)$ by means of derivatives, we come to the conclusion that (5) is achieved when $0.52/\tau_c < \Delta f < 0.67/\tau_c$.

Making use of the minimax rule, we formulate the problem of selecting Δf in the following manner: maximize the lower bound of the numerical set formed by the values of the function $\rho(\tau_\Phi, \Delta f)$ with respect to Δf:

$$\sup_{\Delta f} \inf_{\tau_\Phi} \{\rho(\tau_\Phi, \Delta f)\}, \text{ where } \Delta f \in [0{,}52/\tau_c, 0{,}67/\tau_c),\ \tau_\Phi \in [\tau_{\Phi 2}, \tau_{\Phi 1}] \subset (0, \tau_c]. \qquad (6)$$

By analyzing the behavior of $\rho(\tau_\Phi, \Delta f = \text{const.})$ by means of derivatives, we conclude that the given function either increases in the segment $[\tau_{\Phi 2}, \tau_{\Phi 1}]$, or is convex upward with a maximum point determined by the equation $\rho'_{\tau_\Phi} = 0$.

The character of the behavior of $\rho(\tau_\Phi, \Delta f = \text{const.})$ depends on the position of the segment $[\tau_{\Phi 2}, \tau_{\Phi 1}]$ on the half-segment $(0, \tau_c]$ [sic] and the quantity Δf.

Consequently, $\inf_{\tau_\Phi} \{\rho(\tau_\Phi, \Delta f = \text{const})\}$ should be sought at the boundary points of the segment $[\tau_{\Phi 2}, \tau_{\Phi 1}]$.

The rule for selecting Δf follows from what has been presented here [3]. If in a specified $[\tau_{\Phi 2}, \tau_{\Phi 1}]$ there exists $\rho(\tau_{\Phi 2}, \Delta f) = \rho(\tau_{\Phi 1}, \Delta f)$, then (6) is determined by the solution of the given equation.

Otherwise, the desired Δf is equal to:

$$\sup_{\Delta f} \{\rho(\tau_{\phi 2}, \Delta f)\}, \text{ где } \Delta f \in [0{,}52/\tau_c, 0{,}67/\tau_c).$$

where

BIBLIOGRAPHY

1. Gavrish T.V., Tyrsa V.Ye., "O formirovanii signala v izmeritele polyarnykh koordinat ob"yekta metodom opticheskoy lokatsii" ["On the Signal Generation in a Meter for the Polar Coordinates of an Object by Means of Optical Detection and Ranging"], in the collection, "Optiko--kogerentnyye informatsionno-izmeritel'nyye sistemy" ["Coherent Optical Information and Measurement Systems"], Khar'kov, KhAI, 1977, No 1, pp 50-54.

2. Tikhonov V.I., "Statisticheskaya radiotekhnika" ["Statistical Radio Engineering"], Moscow, Sovetskoye Radio Publishers, 1966, p 677.

3. Fikhtengol'ts S.I., "Kurs differentsial'nogo i integral'nogo ischisleniya" ["Course in Differential and Integral Calculus"], Moscow, Nauka Publishers, 1970, 1, p 607.

8225
CSO: 1860

UDC 621.396.96:621.391.26

OPTIMAL WORD SELECTION FOR DIGITAL COHERENTLY WEIGHTED SIGNAL PROCESSING SYSTEMS

Kiev IVUZ RADIOELEKTRONIKA in Russian Vol 23, No 8, Aug 80 pp 86-89
manuscript received 2 Jul 79

[Paper by D.I. Popov and V.I. Koshelev]

[Text] In the analysis and optimization of digital quasi-optimal systems (KS) in [1], the losses due to the finite word length of the digital devices were not taken into account. Providing for a specified loss level involves the selection of the bit capacity of the appropriate devices, and in the final analysis determines the cost of the equipment. A procedure is proposed below for the selection of the optimum word length based on the criterion of minimal equipment cost.

The efficiency of a digital quasi-optimal system is reduced as a result of losses during analog-digital conversion of the input process, rounding-off the products in the multipliers and quantizing the coefficients in the digital filters. The first two types of losses are accounted for by the insertion of analog-digital converter (ATsP) noise having a dispersion of σ^2_{ADC} and the noise from rounding-off the products in a rejection filter (RF) having a dispersion of σ^2_{ro1} and in a bandpass filter (PF) having a dispersion σ^2_{ro2}. The analog-digital conversion noise is determined by the word length and the dynamic range of the A/D converter and consists of two terms: the quantization noise and the saturation noise, the dispersions of which are as follows respectively [2]:

$$\sigma^2_{кв} = (\delta_1^2/12)\{1 - 2\Phi(\zeta)\},$$

$$\sigma^2_{н} = 2\sigma^2_{(n+m)}\{((\zeta^2+1)\Phi(\zeta) - (\zeta/\sqrt{2\pi})\exp(-\zeta^2/2)\},$$

where $\delta_1 = \zeta\sigma_{(i+n)}/(2^{\nu-1} - 1)$ is the quantization step of the A/D converter; ζ is the dynamic range of the A/D converter; $\Phi(\zeta)$ is the

integral of the probabilities; $\sigma^2_{(п+ш)}$ [$\sigma^2_{(i+n)}$] is the dispersion of the mixture of interference and noise at the input; ν is the number of A/D converter bits.

For processes which take place in practice, the readouts of the rounding-off noise are not correlated with the input process or with each other, i.e., they take the form of discrete white noise. When rounding-off the products to the nearest quantization level, its mean mathematical value is equal to zero, while the dispersion, corresponding to one multiplication operation, is equal to $\delta_i^2/12$, where $\delta_i = \zeta\sigma'_{(i+n)}/(2^{\kappa} - 1)$ is the quantization step of the products in the corresponding digital devices; $\sigma'_{(i+n)}$ is the mean square value of the interference and the noise at the input to the filter under consideration; κ is the number of quantization bits in the corresponding digital device.

We shall take the losses due to the quantization of the coefficients of the digital filters into account directly in the calculations of the quasi-optimal system efficiency.

The losses in the threshold signal/(interference+noise) ratio [1], taking into account the errors considered here, can be estimated by the formula:

$$\Delta q = 1/\Delta\mu = 1 + (\sigma^2_{\upsilon\ \text{ацп}} + \sigma^2_{\upsilon\ \text{ок1}} + \sigma^2_{\upsilon\ \text{ок2}})/\sigma^2_{\upsilon\ (п+ш)}, \qquad (1)$$

where $\sigma^2_{\upsilon\ \text{ацп}}$ [$\sigma^2_{v\ \text{ADC}}$], $\sigma^2_{v\ \text{ОК1}}$ [$\sigma^2_{v\ \text{ro1}}$], $\sigma^2_{v\ \text{ОК2}}$ [$\sigma^2_{v\ \text{ro2}}$] and $\sigma^2_{v(п+ш)}$ [$\sigma^2_{v(i+n)}$] are the dispersions of the A/D converter noise, the rounding-off noise of the rejection and bandpass filter respectively as well as the mixture of interference and noise at the output of the linear part of the system. In this case, $\sigma^2_{v\ \text{ADC}} = \sigma^2_{\text{ADC}}H^{T*}G^{T}GH$, $\sigma^2_{v\ \text{ro1}} = (\delta_2^2/12)\mathcal{l}_1H^{T*}H$ and $\sigma^2_{v\ \text{ro2}} = (\delta_3^2/12)\mathcal{l}_2$,

$$\delta_2 = \zeta\sigma_{(n+ш)}/(2^{\beta-1} - 1),\ \delta_3 = \zeta\sqrt{D^T(R_п + \lambda I)D}\,\sigma_{(n+ш)}/(2^{\gamma-1} - 1),$$

where H is an n-dimensional complex column vector of coefficients of the pulse response of the bandpass filter; D is an m-dimensional column vector of the coefficients of the pulse response of the rejection filter; G is an n-dimensional rejection matrix with elements $G_{jk} = D_{j-k}$ where $k \leq j \leq \min(n, m+k)$ and $G_{jk} = 0$ otherwise, $R_п$ is an m-dimensional normalized correlation matrix of the interference; I is a unit matrix; λ is the ratio of the noise to interference at the input; $\mathcal{l}_1$ and $\mathcal{l}_2$ are the number of rounding-off operations respectively during the multiplication of fractional numbers in the rejection and bandpass filters; β and γ are respectively the number of rejection filter and bandpass filter bits. We will note that the square law shape of $D^T(R_п + \lambda 1)D$ determines the amount of reduction in the dynamic range of the interference at the output of the rejection filter.

It is obvious that requirement (1) can be met for various values of the vector $W = \{\zeta, \nu, \beta, \gamma\}$ by means of redistributing the losses among the components of the quasi-optimal system. In this case, the different variants prove to differ in terms of the complexity of the digital devices of the quasi-optimal system. Thus, a reduction in the A/D conversion losses by a specified amount, as a rule, requires greater outlays than an equivalent reduction in the losses in the digital filters. Because of this, it is expedient to choose the vector W which minimizes the overall equipment cost. For this, we shall introduce the conditional cost functions $f_1(\nu)$, $f_2(\beta)$ and $f_3(\gamma)$ which characterize the outlays for the realization of the A/D converter, rejection filter and bandpass filter respectively as a function of the number of bits for these devices. Then the problem of minimizing the overall conditional equipment cost is formulated as $P(W) = f_1(\nu) + f_2(\beta) + f_3(\gamma) \to \min$ with the limitation that $\Delta q \leq \Delta q_{max}$, where Δq_{max} are the maximum permissible losses in threshold signal. Because of the nonlinearity of the target function and the limitation imposed, this problem can be solved by the methods of nonlinear programing [3]. We shall transform the limitation to the form $g(W) = \Delta q - \Delta q_{max} \leq 0$, and relate it to the target function as a penalty function. Then:

$$P'(W, r) = f_1(\nu) + f_2(\beta) + f_3(\gamma) + r/g(W), \qquad (2)$$

where r is a parameter, the values of which fall off with each optimization cycle.

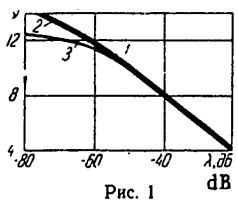

Рис. 1

Figure 1.

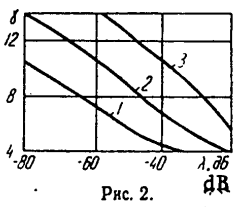

Рис. 2.

Figure 2.

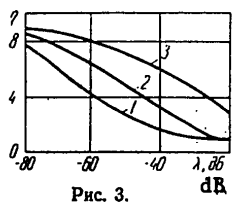

Рис. 3.

Figure 3.

Relationship (2) transforms the nonlinear programming problem for the case where limitations are present to a problem without limitations, which is solved by well known methods, for example, the method of variable metrics. The concluding step in the minimization is realized at a very small value of r, so that the resulting vector W_{opt} satisfies the limitation condition with a precision within the set tolerance, in this case, assuring a minimum of the function $P(W)$. The globality of the resulting solution is assured by resorting through the local extrema in the vicinity of the vector W_{opt}.

The solution of the nonlinear programming problem likewise makes it possible to obtain the optimal distribution of the overall losses $\Delta q = \Delta q_{ADC} \cdot \Delta q_{ro1} \cdot \Delta q_{ro2}$ among the components of the quasi-optimal system. Based on some variants of the solution of problem of (2), for the parameters treated below, it has been determined that the optimal relationship between the quantization and rounding-off losses has the form $\Delta q_{ro} \approx 0.1 \Delta q_{qu}$. If one considers the fact the losses in the individual components of the quasi-optimal system are equal to:

$$\Delta q_{ацп} \approx \Delta q_{кв} = 1 + \sigma^2_{v\,кв}/\sigma^2_{\sigma(п+ш)},\ \Delta q_{ок1} = 1 + \sigma^2_{v\,ок1}/(\sigma^2_{\sigma\,(п+ш)} + \sigma^2_{\sigma\,кв}),\ \Delta q_{ок2} = 1 + \sigma^2_{v\,ок2}/(\sigma^2_{\sigma\,(п+ш)} + \sigma^2_{v\,кв} + \sigma^2_{v\,ок1}),$$

then the desired parameters can be computed from the formulas:

$$\nu = \frac{1}{2}\log_2 \frac{\zeta^2 H^{T*} G^T G H}{3(\Delta q_{кв} - 1)(\sigma^2_v/\sigma^2)_{(п+ш)}},$$

$$\beta = \frac{1}{2}\log_2 \frac{\zeta^2 l_1 H^{T*} H}{3\Delta q_{кв}(\Delta q_{ок1} - 1)(\sigma^2_v/\sigma^2)_{(п+ш)}},$$

$$\gamma = \frac{1}{2}\log_2 \frac{\zeta^2 l_2 D^T (R_п + \lambda I) D}{3\Delta q_{кв}(\Delta q_{ок1} - 1)(\Delta q_{ок2} - 1)(\sigma^2_v/\sigma^2)_{(п+ш)}}.$$

The quantity ζ is chosen in this case as a function of the bit capacity of the A/D converter based on the recommendations of [2], something which makes it possible to neglect the saturation noise.

A gaussian apprximation was adopted in the numerical calculations for the energy spectrum of the interference with a normalized width of $p = 0.05$. The maximum losses Δq_{max} were limited to a value of 3 dB, while the conditional cost functions, because of practical consideration, were taken as $f_1(\nu) = 5\nu^2$, $f_2(\beta) = 0$ (since a rejection filter with integer coefficients is being considered where $m \leq 2$) and $f_3(\gamma) = n\gamma$. In all of the figures (1, 2, 3), curves 1 correspond to quasi-optimal systems with rejection filters in the form of second order interperiod compensation devices (ChPK2) and bandpass filters in the form of a coherently weighted store (VN), curves 2 correspond to ChPK1-VN [first order interperiod compensation circuit with a bandpass filter in the form of a coherently weighted store], and curves 3 correspond to the coherently weighted store.

A comparison of Figure 1 with the results shown in [1] shows that the high efficiency of quasi-optimal systems is achieved at the cost of multilevel quantization (up to 14 bits when $\lambda = -80$ dB). An increase in the internal noise level of the receiver leads to a reduction in

system efficiency, and as a consequence, to a lessening of the demands placed on the bit capacity of the A/D converter. In the cases of practical importance, the parameter λ falls in a range of -30 to -50 dB, and in this case, the requisite bit capacity of the A/D converter is equal to 6 to 10 bits and practically does not depend on the order of the rejection filter employed. The requisite dynamic range of the A/D converter is $\zeta = 3$ to 4.5 when $\nu = 6$ to 10 respectively.

The curves for the requisite bit capacity of the bandpass filter as a function of λ, which are shown in Figure 2, show that the presence of a bandpass filter permits a substantial reduction in the requisite bit capacity of the bandpass filter, in which case, the amount of the reduction is proportional to the rejection filer efficiency.

The influence of the internal noise level on the requirements placed on the number of bits for the representation of the weighting coefficients of the bandpass filter, η, is illustrated in Figure 3. The estimate of η is based on the average coefficient for the improvement in the signal/ /(interference + noise) ratio [1] from the condition for the reduction of this parameter by no more than 1 dB. The smoothed curves show that with an increase in λ, the requirements placed on the bit capacity fall off to a greater degree, the more efficient the rejection filter is. When $\lambda \geq -30$ dB, weighted processing in a ChPK2-VN quasi-optimal system has a poor efficiency and the weighted store degenerates into an equilibrium store. A similar situation is also observed in a ChPK1-VN quasi-optimal system when $\lambda \geq -20$ dB.

Thus, the analysis performed here and the proposed procedure for the optimization of the bit capacity of digital devices using the criterion of a minimum conditional equipment cost can be useful for the technical economic substantiation of the choice of the structure of digital quasi-optimal systems. The results obtained show that the requisite number of A/D converter bits is determined by the quasi-optimal system efficiency and for actual noise/interference ratio, depends little on its structure. The presence of a rejection filter in the quasi-optimal system reduces the requirements placed on the bit capacity of the weighting coefficients and the multipliers of bandpass filters to a greater extent, the higher the efficiency of the rejection filter.

BIBLIOGRAPHY

1. Popov D.I., Koshelev V.I., "Optimizatsiya tsifrovoy kogerentno-vesovoy radiolokatsionnykh signalov" ["The Optimization of the Digital Coherently Weighted Processing of Radar Signals"], IZV. VUZOV - RADIOELEKTRONIKA [PROCEEDINGS OF THE HIGHER EDUCATIONAL INSTITUTES - RADIOELECTRONICS], 1979, 22, No 8, p 90.

2. Gray G.A., Zeoli G.W., "Quantization and Saturation Noise due to Analog-Digital Conversion", IEEE TRANS., 1971, AES-7, No 1.

3. Khimmel'blau D., "Prikladnoye nelineynoye programmirovaniye" ["Applied Nonlinear Programming"], Moscow, Mir Publishers, 1975.

8225
CSO: 1860

UDC 621.391.2

STUDY OF BASE 4 FAST FOURIER TRANSFORMATION ALGORITHMS WITH CONSTANT STRUCTURE

Moscow RADIOTEKHNIKA I ELEKTRONIKA in Russian Vol 25, No 8, Aug 80 pp 1639-1647
manuscript received 5 Jan 79

[Article by A. A. Belyy, Ye. I. Bovbel', V. I. Mikulovich]

[Text] A study is made of base-4 fast Fourier transformation algorithms with constant structure under their properties. The presented results permit determination of the limiting possibilities of the systems containing no more than one arithmetic circuit operating in real time. The results of the studies are used to create algorithms with counterstructure which, in turn, permits the creation of deficient systems for simultaneous processing of two complex signals.

Introduction

Fast Fourier transformation algorithms (BPF algorithms) have had a great influence on the development of digital signal processing. They are widely used in determining the mutual spectral power density [1-3], the coherence function [4, 5], the mutual correlation function [1, 2, 6], and the indeterminacy function [2, 12]. The operation data play a defining role when solving various problems which arise, for example, in radar and also when processing the results of acoustic and vibration measurements. A characteristic feature when performing the given operations is simultaneous obtaining of the spectrum of two signals. The given signals are complex, for by assumption, the analytical model of a real signal is used [7, 8, 10].

The possibility of using BPF algorithms with substitution in the device realizing these operations has been investigated in detail in references [1, 9, 11]. The application of BPF algorithms with constant structure for the solution of a given problem has not in practice been investigated.

The purpose of this paper is the investigation of BPF algorithms with constant structure and the possibility of using the given algorithms in a specialized device designed for simultaneous obtaining of the spectra of two complex signals.

The limiting characteristics of the device operating in real time will depend on the speed of execution of the base operation of the BPF and the selected method of realizing the BPF. It is known that the execution of the BPF algorithm can be realized [1] by the methods of series, parallel and flow processing using bases 2, 4 and 8. Considering these methods, it is possible to draw the conclusion that from the point of view of equipment expenditures with timely development of an

element base it is possible to discuss the series method of executing the base 4 BPF algorithm when all of the base operations of the algorithm are performed in series by one arithmetic circuit.

1. Base 4 BPF Algorithm

The discrete Fourier transformation for samples of the time function s_i given at N discrete points is written in the form

$$A_k=\sum_{i=0}^{N-1} W^{ik}s_i, \quad k=0,1,\ldots,N-1, \tag{1}$$

where W = exp (-j2π/N), N is an integer.

If we introduce the N × 1 matrices

$$\underset{N\times 1}{\|s\|}=\mathrm{col}(s_0, s_1, \ldots, s_{N-1}); \quad \underset{N\times 1}{\|A\|}=\mathrm{col}(A_0, A_1, \ldots, A_{N-1})$$

and define the N × N matrix $\|W\|$, the coefficients of which are

$$w_{ik}=\exp\left[-j\frac{2\pi}{N}(ik)\bmod N\right],$$

expression (1) assumes the form

$$\underset{N\times 1}{\|A\|}=\underset{N\times N}{\|W\|}\ \underset{N\times 1}{\|s\|}. \tag{2}$$

In the case where the matrix $\|W\|$ is multiplied from the left by the permutation matrix $\|\Pi\|$, the newly obtained matrix can be represented in the form of the product of rarefied matrices. As the permutation matrix it is possible to use the digital inversion matrix $\|\Pi\| = \|Q\|$. In the case where a_{n-1}, a_{n-2}, ..., a_1, a_0) are n digits of the base 4 representation of the row number of the matrix $\|W\|$, then n digits (a_0, a_1, ..., a_{n-2}, a_{n-1}) define a new number of the given row in the matrix $\|T\|$. Let us also note that if an operation of the type (a_{n-1}, a_{n-2}, a_{n-3}, ..., a_2, a_1, a_0) ⇒ (a_0, a_{n-1}, a_{n-2}, ..., a_3, a_2, a_1) is performed, then the matrix $\|P\|$ is defined, and if the operation of the type (a_{n-1}, a_{n-2}, a_{n-3}, ..., a_2, a_1, a_0) ⇒ (a_{n-3}, a_{n-3}, a_{n-4}, ..., a_1, a_0, a_{n-1}) is valid, the matrix $\|M\|$ is defined.

Using the digital inversion matrix, expression (2) can be reduced to the form

$$\underset{N\times 1}{\|A\|}=\underset{N\times N}{\|Q\|}\ \underset{N\times N}{\|T\|}\ \underset{N\times 1}{\|s\|}, \tag{3}$$

where

$$\underset{N\times N}{\|\acute{T}\|}=\underset{N\times N}{\|Q\|}\ \underset{N\times N}{\|W\|}. \tag{4}$$

Entering the row number p of the matrix $\|T\|$ in the form

$$p=\sum_{k=0}^{n-1} d_k 4^k; \quad d_k=0, 1, 2, 3, \tag{5}$$

in equality (4), it is possible to note that the same row in the matrix $\|W\|$ will have the number

$$r_n(p)=\sum_{k=0}^{n-1} d_k 4^{n-1-k}. \tag{6}$$

In this case the elements of the matrix $\|T\|$ will be

$$t_{pq}=w_{r_n(p)q}=\exp\left(-j2\pi\frac{r_n(p)q}{N}\right). \tag{7}$$

Let us break down the matrix $\|T\|$ into blocks

$$\|T\|=\left\|\begin{array}{c|c|c|c} A^{00} & A^{01} & A^{02} & A^{03} \\ \hline A^{10} & A^{11} & A^{12} & A^{13} \\ \hline A^{20} & A^{21} & A^{22} & A^{23} \\ \hline A^{30} & A^{31} & A^{32} & A^{33} \end{array}\right\|, \tag{8}$$

where the matrices $\|A^{ik}\|$, $i=0, 1, 2, 3$; $k=0, 1, 2, 3$, has dimensions of $4^{n-1}\times 4^{n-1}$.

The elements of the matrix $\|A^{ik}\|$ are equal to:

$$\begin{gathered} a_{pq}^{ik}=t_{i\cdot 4^{n-1}+p,\ k\cdot 4^{n-1}+q}, \\ p=q=0, 1, \ldots, 4^{n-1}-1; \quad i=k=0, 1, 2, 3. \end{gathered} \tag{9}$$

If we consider the equality (7), expression (9) assumes the form

$$a_{pq}^{ik}=w_{r_n(p)q}=\exp\left\{-j2\pi\frac{r_n(i\cdot 4^{n-1}+p)(k\cdot 4^{n-1}+q)}{4^n}\right\}.$$

Since for i = 0, 1, 2, 3; p = 0, 1, ..., 4^{n-1} - 1 the equality

$$r_n(i\cdot 4^{n-1}+p)=4r_{n-1}(p)+i,$$

is valid, then

$$a_{pq}^{ik}=\exp\left\{-j2\pi\frac{ik}{4}\right\}\exp\left\{-j2\pi\frac{iq}{4^n}\right\}\exp\left\{-j2\pi\frac{r_{n-1}(p)q}{4^{n-1}}\right\}. \tag{10}$$

Considering expression (10), the equality (8) can be written as

$$\|T\|_{4^n\times 4^n}=\left\|\begin{array}{c|c|c|c} T_{n-1} & T_{n-1} & T_{n-1} & T_{n-1} \\ \hline T_{n-1}L_{n-1} & -jT_{n-1}L_{n-1} & -1T_{n-1}L_{n-1} & jT_{n-1}L_{n-1} \\ \hline T_{n-1}L_{n-1}^2 & -1T_{n-1}L_{n-1}^2 & T_{n-1}L_{n-1}^2 & -1T_{n-1}L_{n-1}^2 \\ \hline T_{n-1}L_{n-1}^3 & jT_{n-1}L_{n-1}^3 & -iT_{n-1}L_{n-1}^3 & -jT_{n-1}L_{n-1}^3 \end{array}\right\}=$$

$$=\left\|\begin{array}{c|c|c|c} T_{n-1} & 0 & 0 & 0 \\ \hline 0 & T_{n-1} & 0 & 0 \\ \hline 0 & 0 & T_{n-1} & 0 \\ \hline 0 & 0 & 0 & T_{n-1} \end{array}\right\|\left\|\begin{array}{c|c|c|c} I_{n-1} & 0 & 0 & 0 \\ \hline 0 & L_{n-1} & 0 & 0 \\ \hline 0 & 0 & L_{n-1}^2 & 0 \\ \hline 0 & 0 & 0 & L_{n-1}^3 \end{array}\right\|\times\left\|\begin{array}{c|c|c|c} I_{n-1} & I_{n-1} & I_{n-1} & I_{n-1} \\ \hline I_{n-1} & -jI_{n-1} & -1I_{n-1} & jI_{n-1} \\ \hline I_{n-1} & -1I_{n-1} & I_{n-1} & -1I_{n-1} \\ \hline I_{n-1} & jI_{n-1} & -1I_{n-1} & -jI_{n-1} \end{array}\right\},$$

where

$$\|L^m\| = \operatorname{diag}\left\{1, \exp\left(-j\frac{2\pi}{N}1\cdot m\right), \ldots, \exp\left[-j\frac{2\pi}{N}(4^{n-1}-1)m\right]\right\},$$

I_{n-1} is a unit matrix; let us also note that here the abbreviated notation for the $4^{n-1}\times 4^{n-1}$ matrix $\|A\|$ in the form $\|A\| = A_{n-1}$ is used for convenience.

If we introduce the notation

$$D_n = \text{quasi-diag}\,(I_{n-1}, L_{n-1}, L^2_{n-1}, L^3_{n-1})$$

and use the symbolic notation for the direct matrix product [11], then equality (11) assumes the form

$$T_n = (T_{n-1}\otimes I_1) D_n (I_{n-1}\otimes T_1), \tag{12}$$

where $\otimes$ is the direct product symbol.

If we express the matrix T_{n-1} in terms of the matrix T_{n-2} and this process is then repeated until the matrix T_n is fully expressed in terms of the matrix T_1, we obtain the base 4 BPF algorithm which considering equalities (2) and (3) is written in the form

$$\begin{aligned} W_n = {} & Q_n (T_1\otimes I_{n-1}) (D_2\otimes I_{n-2}) (I_1\otimes T_1\otimes I_{n-2}) \ldots \\ & \ldots (D_k\otimes I_{n-k}) (I_{k-1}\otimes T_1\otimes I_{n-k}) \ldots D_n (I_{n-1}\otimes T_1), \end{aligned} \tag{13}$$

where

$$D_{n-1} = \text{quasi-diag}\,(I_{n-i-1}, L^i_{n-i-1}, L^{2i}_{n-i-1}, L^{3i}_{n-i-1}),$$

$$L^m = \operatorname{diag}\,[0, m\cdot 4^i, m\cdot 2\cdot 4^i, \ldots, m(4^{n-i-1}-1)\cdot 4^i],$$

$$T_1 = \begin{Vmatrix} 1 & 1 & 1 & 1 \\ 1 & -j & -1 & j \\ 1 & -1 & 1 & -1 \\ 1 & j & -1 & -j \end{Vmatrix},$$

$k = 3, 4, \ldots, n-1$; $i = 0, 1, \ldots, n-2$; $m = 1, 2, 3$.

The symbolic notation m is used in place of W^m to designate the elements of the matrix L.

2. BPF Algorithm with Constant Structure

By analogy with what has been stated above, it is possible to obtain a class of BPF algorithms permitting the use of a set of structural diagrams for their equipment execution. From this class of algorithms we isolate the BPF algorithms with constant structure which are considered below.

APN Algorithms. If we isolate the matrix $S_n=I_{n-1}\otimes T_1$, in the equality (13), we obtain the BPF algorithm which is written in the form

$$W_n=Q_nP_nS_nP_n(I_{n-2}\otimes D_2)S_n\ldots P_n(I_{n-k}\otimes D_k)S_n\ldots P_nD_nS_n. \tag{14}$$

Example: for N = 64 expression (14) assumes the form

$$W_3=Q_3P_3S_3P_3(I_1\otimes D_2)S_3P_3D_3S_3,$$

where

$$D_3=\operatorname{diag}\begin{matrix}(0,&0,&0,&0,&0,&0,&0,&0,&0,&0,&0,&0,&0,&0,&0,&0,\\ 0,&1,&2,&3,&4,&5,&6,&7,&8,&9,&10&11,&12,&13,&14,&15,\\ 0,&2,&4,&6,&8,&10,&12,&14,&16,&18,&20,&22,&24,&26,&28,&30,\\ 0,&3,&6,&9,&12,&15,&18,&21,&24,&27,&30,&33,&36,&39,&42,&45),\end{matrix}$$

$$(I_1\otimes D_2)=\operatorname{diag}\begin{matrix}(0,&0,&0,&0,&0,&0,&0,&0,&0,&0,&0,&0,&0,&0,&0,&0,\\ 0,&0,&0,&0,&4,&4,&4,&4,&8,&8,&8,&8,&12,&12,&12,&12,\\ 0,&0,&0,&0,&8,&8,&8,&8,&16,&16,&16,&16,&24,&24,&24,&24,\\ 0,&0,&0,&0,&12,&12,&12,&12,&24,&24,&24,&24,&36,&36,&36,&36).\end{matrix}$$

The block diagram of the device executing the given algorithm is presented in Figure 1 and consists of one arithmetic circuit (AU), the input and output storage elements (ZU1 and ZU2 respectively) and permanent memory (PZU).

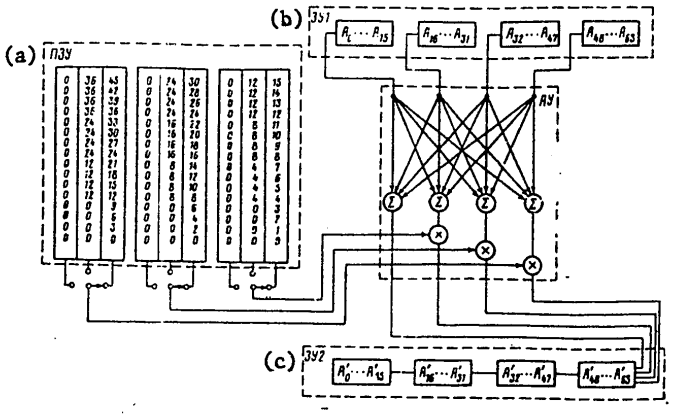

Figure 1. Block diagram of the device executing the APN algorithm.

Key: a. PZU b. ZU1 c. ZU2

The APS algorithm

$$W_n=Q_nP_nS_n\{P_n(I_{n-2}\otimes D_2)M_n\}\ldots \\ \ldots P_nS_n\{P_n(I_{n-k}\otimes D_k)M_n\}\ldots P_nS_n\{P_nD_nM_n\}P_nS_n. \tag{15}$$

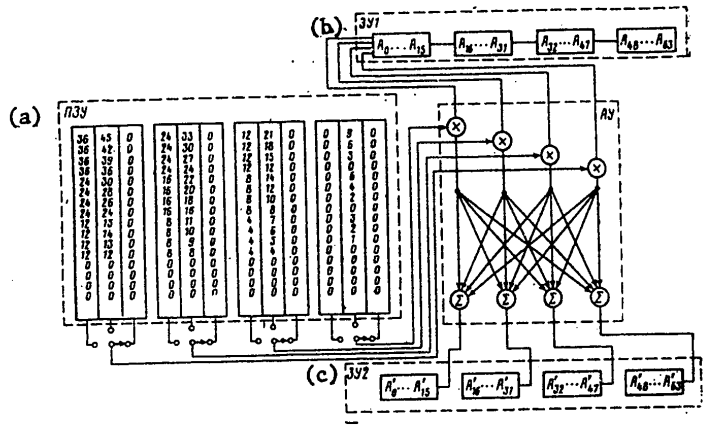

Figure 2. Block diagram of the device executing the BPS algorithm

Key: a. PZU b. ZU1 c. ZU2

The BPN algorithm

$$W_n = S_n M_n \{P_n [Q_n (D_2 \otimes I_{n-2}) Q_n] M_n\} S_n M_n \dots$$
$$\dots \{P_n^{k-1} [Q_n (D_k \otimes I_{n-k}) Q_n] M_n^{k-1}\} S_n M_n \dots \quad (16)$$
$$\dots \{P_n^{n-1} [Q_n D_n Q_n] M_n^{n-1}\} S_n M_n Q_n.$$

The BPS algorithm

$$W_n = S_n \{Q_n (D_2 \otimes I_{n-2}) Q_n\} M_n \dots$$
$$\dots S_n \{P_n^{k-2} [Q_n (D_k \otimes I_{n-k}) Q_n] M_n^{k-2}\} M_n \dots \quad (17)$$
$$\dots S_n \{P_n^{n-2} [Q_n D_n Q_n] M_n^{n-2}\} M_n S_n M_n Q_n.$$

Example: for N = 64 expression (17) assumes the form

$$W_3 = S_3 \{Q_3 (D_2 \otimes I_1) Q_3\} M_3 S_3 \{P_3 [Q_3 D_3 Q_3] M_3\} M_3 S_3 M_3 Q_3,$$

where

$$P_3 [Q_3 D_3 Q_3] M_3 = \text{diag}\ (0,\ 0,\ 0,\ 0,\ 0,\ 1,\ 2,\ 3,\ 0,\ 2,\ 4,\ 6,\ 0,\ 3,\ 6,\ 9,$$
$$0,\ 0,\ 0,\ 0,\ 4,\ 5,\ 6,\ 7,\ 8,\ 10,\ 12,\ 14,\ 12,\ 15,\ 18,\ 21,$$
$$0,\ 0,\ 0,\ 0,\ 8,\ 9,\ 10,\ 11,\ 16,\ 18,\ 20,\ 22,\ 24,\ 27,\ 30,\ 33,$$
$$0,\ 0,\ 0,\ 0,\ 12,\ 13,\ 14,\ 15,\ 24,\ 26,\ 28,\ 30,\ 36,\ 39,\ 42,\ 45),$$

$$Q_3 (D_2 \otimes I_1) Q_3 = \text{diag}\ (0,\ 0,\ 0,\ 0,\ 0,\ 0,\ 0,\ 0,\ 0,\ 0,\ 0,\ 0,\ 0,\ 0,\ 0,\ 0,$$
$$0,\ 0,\ 0,\ 0,\ 4,\ 4,\ 4,\ 4,\ 8,\ 8,\ 8,\ 8,\ 12,\ 12,\ 12,\ 12,$$
$$0,\ 0,\ 0,\ 0,\ 8,\ 8,\ 8,\ 8,\ 16,\ 16,\ 16,\ 16,\ 24,\ 24,\ 24,\ 24,$$
$$0,\ 0,\ 0,\ 0,\ 12,\ 12,\ 12,\ 12,\ 24,\ 24,\ 24,\ 24,\ 36,\ 36,\ 36,\ 36).$$

The block diagram of the hardware execution of the given algorithm is presented in Figure 2.

SPN algorithm

$$W_n=S_nD_nM_n\dots S_n(I_{n-k}\otimes D_k)M_n\dots S_n(I_{n-2}\otimes D_2)M_nS_nM_nQ_n. \tag{18}$$

SPS algorithm

$$\begin{aligned}W_n=&S_nM_n\{P_nD_nM_n\}S_nM_n\dots\\&\dots\{P_n(I_{n-k}\otimes D_k)M_n\}S_nM_n\dots\{P_n(I_{n-2}\otimes D_2)M_n\}S_nM_n.\end{aligned} \tag{19}$$

DPS algorithm

$$\begin{aligned}W_n=&Q_nP_nS_nP_n\{P_n^{n-2}[Q_nD_nQ_n]M_n^{n-2}\}S_n\dots\\&\dots P_n\{P_n^{k-2}[Q_n(D_k\otimes I_{n-k})Q_n]M_n^{k-2}\}S_n\dots\\&\dots P_n\{Q_n(D_2\otimes I_{n-2})Q_n\}S_n.\end{aligned} \tag{20}$$

DPN algorithm

$$\begin{aligned}W_n=&Q_nP_nS_n\{P_n^{n-1}[Q_nD_nQ_n]M_n^{n-1}\}\dots\\&\dots P_nS_n\{P_n^{k-1}[Q_n(D_k\otimes I_{n-k})Q_n]M_n^{k-1}\}\dots\\&\dots P_nS_n\{P_n[Q_n(D_2\otimes I_{n-2})Q_n]M_n\}P_nS_n.\end{aligned} \tag{21}$$

From the above-presented formulas it is obvious that each of the algorithms is executed in $n = \log_4 N$ steps. For each of the above-investigated algorithms the following basic property is satisfied: its structure is constant in all steps. The given structure permits the use of a memory with series access. The organization of the input or output memories can be parallel or series. The arithmetic circuit can be asymmetric (Figure 1) or symmetric (Figure 2). For convenience of use the basic distinguishing features of the given algorithms are presented in Table 1.

The processing in real time usually requires that the spectrum calculation time be equal to the signal duration T_p, that is, for the given algorithms the following equality must be satisfied

$$T_p=\tau\frac{N}{4}\log_4 N, \tag{22}$$

where τ is the time in seconds required for the performance of the basic base 4 operation including the memory access time and the operating time of the arithmetic circuit. Since the equality $F_B = N/2T_p$ is valid, where F_B is the Kotel'nikov frequency, the expression (22) assumed the form

$$T_p=2^{\left(\frac{4}{\tau F_B}-1\right)\log_4 2F_B}. \tag{23}$$

When using the equality (23), the graphs presented in Figure 3 were constructed which indicate the limiting possibilities of the systems, that is, they determine the minimum resolution or the admissible execution time for the given Kotel'nikov frequency. For comparison a curve is also presented for the base 4 BPF algorithm with substitution. The graphs were constructed under the condition that the memory access time is on the order of 1 microsecond, and the operating time of the arithmatic circuit is 2 microseconds. The values of F_B for the most widespread values of N are presented in Table 2.

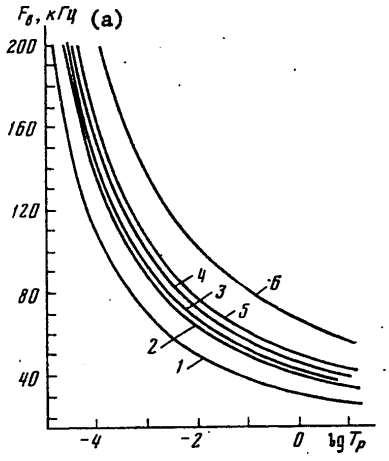

Figure 3. Ratio of the upper frequency and length of the realization during operation of a system for fast Fourier transformation in real time: 1 -- curve for the algorithm with substitution; 2 -- curves for the APN and the DPN algorithms; 3 -- curve for the BPN and SPN algorithms; 4 -- curve for the APS and DPS algorithms; 5 -- curve for the BPS and SPS algorithms; 6 -- curve for the algorithm with counterstructure.

Key: a. F_B, kilohertz

The above-investigated properties of the BPF algorithms with constant structure permit the development of algorithms that are more adaptable for simultaneous processing of two complex signals.

3. BPF Algorithms with Counterstructure

Let us propose that it is necessary to obtain the spectra of two complex signals in real times simultaneously. If we use the BPF algorithms with substitution for the given device, then from Table 2 and Figure 3 it is possible to determine the limiting characteristics of this system. The following belong to the basic equipment expenditures required for execution of the given system: two arithmetic circuits and a memory with a capacity of 2×2×N×k bits, where N is the signal length, and k is the number of binary bits required for representation of the input and intermediate values.

The application of BPF algorithms with constant structure, as is obvious from Table 2 and Figure 3 leads to expansion of the values of the limiting parameters and simplification of the hardware (the control circuit is simplified). It is necessary to note that these values are achieved as a result of increasing the memory size from 4×N×k bits to 2×4×N×k bits.

If among the algorithms with constant structure we isolate the algorithms which have a defined order of reading and writing data, then in it is possible to construct a

Table 1. BPF algorithms with constant structure

Algorithms		APN	APS	BPN	BPS	SPN	SPS	DPN	DPS
Read from memory	Series			+	+	+	+		
	Parallel	+	+					+	+
Enter in memory	Series	+	+					+	+
	Parallel			+	+	+	+		
Arithmetic circuit	Symmetric		+		+		+		+
	Asymmetric	+		+		+		+	
Order of execution of operation	Multiplication		+		+	+		+	
	Addition	+	+	+	+	+	+	+	+
	Multiplication	+		+			+		+

Table 2

N	Upper boundary frequency, kilohertz					
	Algorithm					
	with substitution	APN DPN	APS DPS	BPN SPN	BPS SPS	Optimal
64	81	108	114	126	135	185
256	61	81	86	94	102	138
1024	49	65	69	75	81	111
4096	41	54	57	63	68	92

a system having defined advantages. The block diagram of such a device using the APN and BPS is presented in Figure 4. The signal s_1 written in the memory ZU1 is the input signal for the algorithm APN, and the signal s_2 written in the ZU2 memory is the input signal for the BPS algorithm. For example, for N = 64, 0, 15, 31 and 47 samples of the signal s_1 arrived at the input of the arithmetic circuit of the APN algorithm, and 0, 1, 2 and 3 samples of the signal s_2 arrive simultaneously at the input of the arithmetic circuit of the BPS algorithm. After performance of the calculations at the output of the arithmetic circuit of the APN algorithm, data appear which are entered in the cells of the ZU2 memory where previously there were 0, 1, 2 and 3 samples of the signal s_2, and the data from the output of the arithmetic circuit of the BPS algorithm are entered in the corresponding cells of the ZU1 memory.

From the performed analysis it is obvious that the use of the BPF algorithms with constant structure and defined order of reading and writing (let us call the given algorithms BPF algorithms with counterstructure) permits the memory size to be cut in half.

The above-presented choice of BPF algorithms with counterstructure (APN and BPS) does not permit the organization of an optimal system, that is, a system in which the arithmetic circuit and memory operat without a pause. However, if we are limited to the algorithms, for example, SPN and DPN, for which a defined order of execution of the operations is fixed in each step, then in the block diagram presented in Figure

4, one arithmetic circuit will be excess. Accordingly, it is possible to create an optimal system (let us propose that for this purpose in the arithmetic circuit there are special buffer registers available), which will be capable of processing two complex signals with minimum equipment expenditures: one arithmetic circuit, a 4×N×k bit memory and control circuit. The limiting parameters of the given system can be determined from Table 2 and Figure 3.

THe algorithms APN and BPN; APS and BPS; SPN and DPN; SPS and DPS which differ from each other by the type of arithmetic circuit and the order of execution of the operation can be used as BPF algorithms with counterstructure. The given algorithms permits the developer to manifest defined flexibility when constructing systems designed for simultaneous processing of two complex signals.

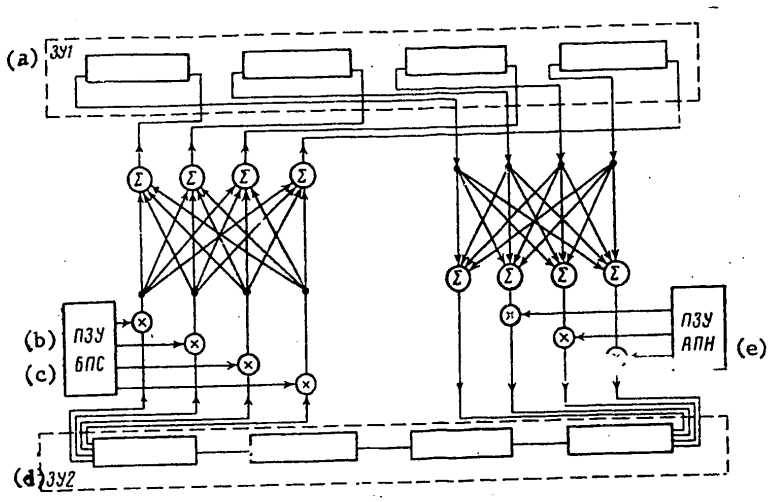

Figure 4. Block diagram of the device executing the BPF algorithm with counter structure.

Key: a. ZU1 memory b. PZU c. BPS d. ZU2 memory e. APN

Thus, the performed studies of the properties of the BPF algorithms with constant structure permitted determination of the algorithms with counterstructure which can be used for the creation of optimal devices that are efficient with respect to equipment expenditures designed for real time processing of two complex signals.

BIBLIOGRAPHY

1. L. Rabiner, B. Gould, TEORIYA I PRIMENENIYE TSIFROVOY ORPABOTKI SIGNALOV (Theory and Application of Digital Processing of Signals), Izd. Mir, 1978.

2. CINQUIEME COLLOQUE NATIONAL SUR LE TRAITEMENT DU SIGNAL ET SES APPLICATIONS, Nice, 1975.

3. ASPECTS SIGNAL PROCESS, Part II, Proc. NATO Adv. Study Inst., Portovenere, La Spezia, 1976.

4. W. G. Halvorsen, I. S. Bendat, SOUND AND VIBR., Vol 9, No 8, 1975, p 18.

5. V. A. Benignus, IEEE TRANS., AU-17, 1969, No 2, p 145.

6. B. I. Trampe, BRÜEL AND KJAER TECHN. REV., No 4, 1970, p 3.

7. D. Ye.Bakman, RADIOTEKHNIKA I ELEKTRONIKA (Radio Engineering and Electronics), Vol 21, No 6, 1976, p 1275.

8. D. Ye. Bakman, L. A. Vaynshteyn, USPEKHI FIZ. N. (Progress in the Physical Sciences), Vol 123, No 4, 1977, p 657.

9. V. M. Yefanov, N. I, Korshever, V. M. Lobastov, G. G. Mashutkin, AVTOMETRIYA (Autometry), No 3, 1973, p 3.

10. C. Berthomier, N. Cornilieau-Wehrlin, ANN. TELECOMMUNS, Vol 30, No 7-8, 1977, p 224.

11. H. Sloate, IEEE TRANS. CIRCUITS AND SYSTEM, Vol 21, No 1, 1974, p 109.

12. E. I. Bovbel', V. V. Izokh, I. Yu. Shmidov, RADIOTEKHNIKA I ELEKTRONIKA, Vol 18, No 11, 1973, p 2311.

10845
CSO: 1860

UDC 621.391.2

EFFECT OF THE FORM OF SEA WAVES ON THE SCATTERED RADIATION CHARACTERISTICS

Moscow RADIOTEKHNIKA I ELEKTRONIKA in Russian Vol 25, No 8, Aug 80 pp 1770-1774
manuscript received 28 Mar 79

[Article by I. F. Shishkin]

[Text] In recent decades, in the broad oceanographic literature a detailed study has been made of the relation of the characteristics of radiation scattered by the sea to the condition of the water surface. The dependence of the scattered signal parameters on the form of the sea waves constitutes an exception. This is explained by the inadequacy of the widely accepted two-scale model of the sea surface to the mechanisms present during scattering by waves of finite steepness.

Graphic results are obtained when investigating the diffraction of acoustic or electromagnetic waves on a trochoidal profile.

The expressions proposed in [1] for the angular factor determining the scattering indicatrix of a field incident on a segment of the surface with the simplest types of large-scale unevennesses are easily generalized to the case of symmetric periodic unevennesses of arbitrary form. For a reflection coefficient modulus equal to one, the dependence of the angular factor modulus of the form of the unevennesses, the angle of irradiation of the surface α_0 and the direction of the diffraction lobe peaks α_m has the form

$$f(\alpha_m)=\left|\frac{1-\cos(\alpha_m-\alpha_0)}{\sin\alpha_m-\sin\alpha_0}\sum_{t=-\infty}^{\infty}\cdots\sum_{p=-\infty}^{\infty}\sum_{l=-\infty}^{\infty}(-t)^{m-l-2p-\ldots-(n-t)}J_t(s_n)\ldots\right. \quad (1)$$

$$\left.\ldots J_p(s_3)J_l(s_2)J_{m-2l-3p-\ldots-nt}(s_1)\right|,$$

where the arguments s_n of the Bessel functions of different order are expressed in terms of the coefficients of expansion of the surface profile in a Fourier series a_n by the formula

$$s_n=ka_n(\sin\alpha_m-\sin\alpha_0) \quad (2)$$

(k is the emission wave number).

For profiles defined by the parametric equations

$$\begin{cases} x=\theta-\alpha\sin\theta, \\ y=\beta\cos\theta \end{cases}$$

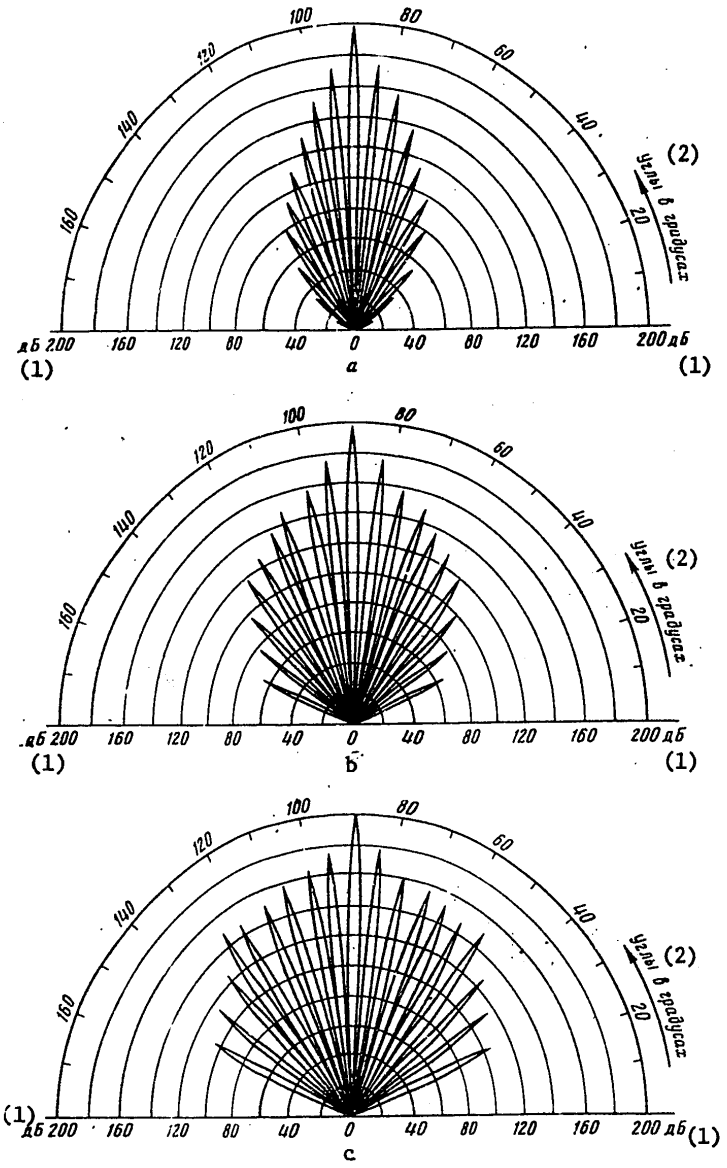

Figure 1: a -- $h/\Lambda = 0.05$, $\alpha = \beta = 0.157$; b -- $h/\Lambda = 0.1$, $\alpha = \beta = 0.314$; в -- $h/\Lambda = 0.1$, $\alpha = 0.65$, $\beta = 0.314$.

Key: 1. decibels 2. angles in degrees

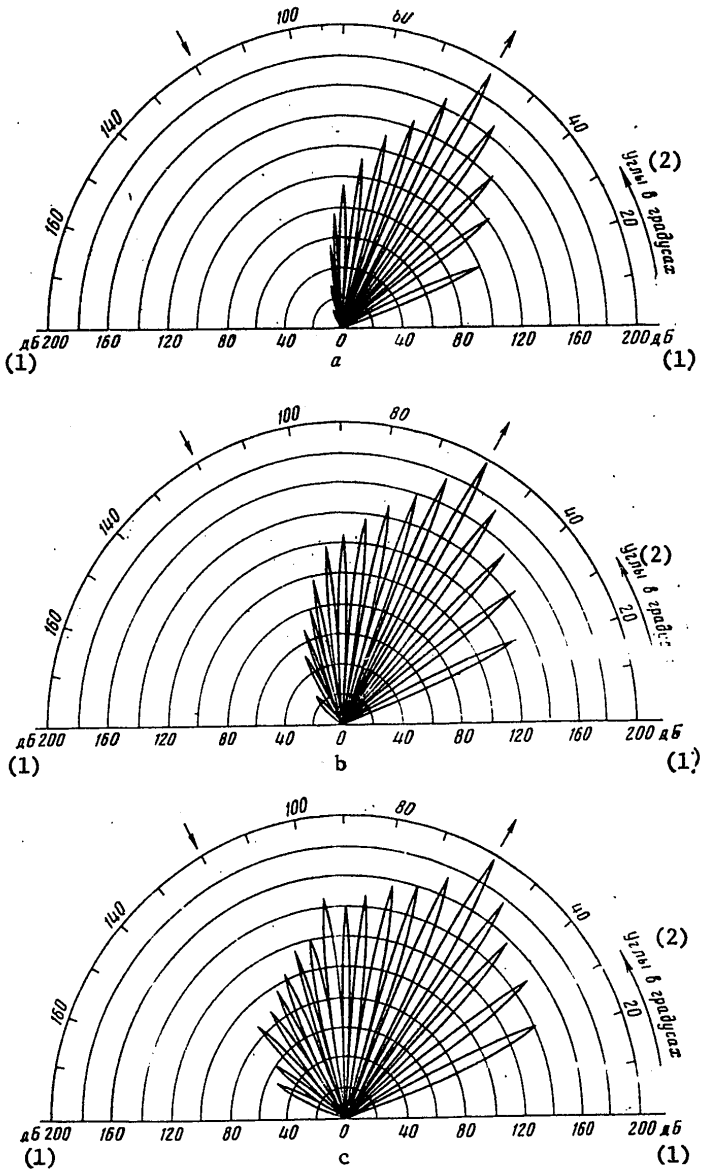

Figure 2. a -- $h/\Lambda = 0.05$, $\alpha = \beta = 0.157$; b -- $h/\Lambda = 0.1$, $\alpha = \beta = 0.314$; c -- $h/\Lambda = 0.1$, $\alpha = 0.65$, $\beta = 0.314$.

Key: 1. decibels 2. angles in degrees

for $n \geq 1$ [2],

$$a_n=\beta[J_{n-1}(n\alpha)+J_{n+1}(n\alpha)]-\alpha\beta J_n(n\alpha)-\frac{1}{2}\alpha\beta[J_{n-2}(n\alpha)+J_{n+2}(n\alpha)]. \quad (3)$$

The calculation by formula (1) is performed as follows. By the given values of α_0, the sea wave length Λ and the radiation wavelength λ from the condition

$$m=\frac{\Lambda}{\lambda}(\cos\alpha_m-\cos\alpha_0)$$

for $m = 0, \pm1, \pm2, \ldots$ the directions of the diffraction lobe peaks are defined. Then for each direction α_m by formula (2) all the arguments of the Bessel functions s_n are found in (1), after which $f(\alpha_m)$ is calculated. The number of harmonics n depends on the required accuracy of the calculations. In practice it is insured when using the following approximate expressions in place of (3)

$$\begin{aligned}
a_1&\simeq\beta(1-0{,}375\alpha^2+0{,}0026\alpha^4-0{,}000759\alpha^6),\\
a_2&\simeq\beta(0{,}5\alpha-0{,}333\alpha^3+0{,}0625\alpha^5),\\
a_3&\simeq\beta(0{,}375\alpha^2-0{,}359\alpha^4+0{,}1108\alpha^6),\\
a_4&\simeq\beta(0{,}333\alpha^3-0{,}4\alpha^5),\\
a_5&\simeq\beta(0{,}3255\alpha^4-0{,}475\alpha^6),\\
a_6&\simeq\beta0.3375\alpha^5,\\
a_7&\simeq\beta0{,}3647\alpha^6.
\end{aligned}$$

Since the Bessel functions are negligibly small for the values of the indexes greatly exceeding the magnitude of the argument, in (1) the summation is actually performed within bounded limits.

The form of the sea waves is given by the values of α and β. For $\alpha = \beta$ the wave profile is trochoidal, the case $\alpha > \beta$ corresponds to the so-called V. V. Shuleykin waves. The steepness of the waves defined as the ratio of their height h to length Λ increases as the values of α and β increase, and it reaches a maximum value of 0.143 for trochoidal waves with $\alpha = \beta = 0.45$, and for the V. V. Shuleykin waves, for $\alpha > \beta < 0.45$.

In Figure 1,a,b, the scattering indicatrices are calculated by formula (1) for the trochoidal waves of different steepness and Λ = 30 cm of radiation with λ = 3 cm for vertical ($\alpha_0 = 270°$) irradiation of a section of the water surface are presented. From the figures it is obvious that the variation in wave steepness leads to noticeable redistribution of the energy calculated in the surrounding space. Here a role is played by the variation of the wave height. For example, in the direction of the back scattering the amplitude of the echos as a result of an increase in h decreases by hundredths of a decibel. In pure form the dependence of the scattering indicatrix on the form of sea waves is traced on a model of the V. V. Shuleykin waves. The sharpening of the crests of these waves takes place as a result of an increase in the ellipticity of the orbits in which the surface particles of the wave move without variation of h and Λ. The transformation of the scattering indicatrix is illustrated in Figure 1,b,c. The amplitude of the back-scattered signals does not vary within the limits of accuracy of the calculations.

Analogous phenomena occur for slant irradiation of the water surface, which is illustrated by the scattering indicatrices constructed in Figure 2 for the same values of

Λ, λ and $\alpha_0 = 300°$. The difference is the absence of symmetry of the indicatrices with respect to the direction of mirror reflection. The amplitude of the signals started in mirror direction by trochoidal waves decreases by hundredths of a decibel as a result of an increase in their height. When scattering by V. V. Shuleykin waves, it remains constant.

Thus, whatever the angles of irradiation of the water surface (within the limits of applicability of the investigated method [1]), the amplitude of the signals scattered in the direction of the mirror reflection does not depend on the shape of the sea waves. Its value is determined by the angle α_0 and the amplitude of the first harmonic of the spatial spectrum of the surface waves a_1. The angular factor in the mirror direction is

$$f(\alpha_m) = \frac{1-\cos(\alpha_m-\alpha_0)}{\sin\alpha_m-\sin\alpha_0} J_0(s_1).$$

In practice the signals scattered in the mirror reflection direction are used for vertical sounding of the wave surface from aircraft in the combined reception-transmission mode. Here, consequently, it is impossible to obtain information about the shape of the sea waves. This fact must be considered when designing means of monitoring world ocean pollution by petroleum products based on recording the smoothing of the sea waves by surface-active films.

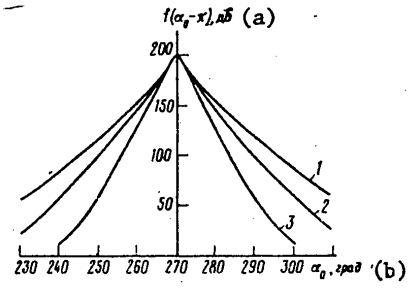

Figure 3: 1 -- $\alpha = \beta = 0.45$; 2 -- $\alpha = \beta = 0.314$; 3 -- $\alpha = \beta = 0.157$.

Key: a. decibels b. degrees

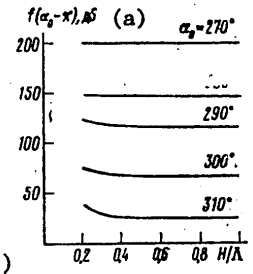

Figure 4: $\alpha = \beta$ cth $2\pi(H/\Lambda)$; $\beta = 0.314$.

Key: a. decibels

During inclined sounding the amplitude of the back-scattered signals depends on the shape of the waves. The greater the angle of incidence, the stronger this dependence. Figure 3 shows the case of active location of waves of trochoidal profile, and Figure 4 shows V. V. Shuleykin waves with $\beta = 0.314$ and $\alpha = \beta$ cth $2\pi(H/\Lambda)$, where H is the depth of a body of water. The presented relations confirm the conclusion that was drawn.

The consideration of the asymmetry of the sea waves can be considered a further development of the theory.

The author is grateful to I. K. Mileyeva for computer calculations by formula (1).

BIBLIOGRAPHY

1. L. M. Brekhovskikh, ZHETF (Journal of Experimental and Theoretical Physics), Vol 23, No 3(9), 1952, p 275.

2. L. A. Korneva, TRUDY KOORDINATSIONNYKH SOVESHCHANIY PO GIDROTEKHNIKE (Works of the Coordinating Conferences on Hydraulic Engineering), Izd. Energiya, 1972, p 36.

10845
CSO: 1860

UDC 621.396.669

A COMPARISON OF THE NOISE IMMUNITY OF TWO DETECTORS WHICH OPERATE USING THE METHOD OF BILATERAL SPATIAL CONTRASTS

Kiev IVUZ RADIOELEKTRONIKA in Russian Vol 23, No 8, Aug 80 pp 32-36
manuscript received 30 Mar 79, after revision 1 Nov 79

[Paper by V.T. Belinskiy, Yu.L. Mazor and R.M. Tereshchuk]

[Text] The noise immunity of two noise signal detectors which operate using the method of bilateral spatial contrasts is treated, where the detectors differ in the procedure for the comparison of the signal and reference voltages. The advantage of a detector where the signal voltage is compared to the average reference voltage over a detector in which the signal voltage is compared to each of two reference voltages is demonstrated.

In noise signal detectors which use the method of bilateral spatial contrasts, various methods are employed to compare the signal and reference voltages. Block diagrams of two detectors are shown in Figure 1, each of which contains a standard detection channel (TTO) and reference and signal voltage driver (FSON). The TTO consists of the antenna system (AS), the bandpass filter (PF), the detector (D) and a low pass filter (FNCh). The low pass filter storage interval T, is chosen equal to the time for sweeping the antenna system through an angle equal to the width of the main lobe of the directional pattern (DN). The reference and signal voltage driver consists of delay lines LZ1 and LZ2. The voltage $U_4 = U_4(t)$ is chosen as the signal voltage, which corresponds to the position of the antenna system directional pattern at the point in time t, while chosen as the reference voltages are $U_4 = U_4(t+T)$ and $U_4'' = U(t-T)$, which are shifted in time relative to the signal voltage by $\pm T$.

The basic distinction between the detectors consists in the method of comparing the signal and reference voltages. In the detector of Figure 1a, the signal voltage is compared in a threshold gate (PU) with the mean arithmetic value of the reference voltages, where this value is obtained by means of an adder (S) and a voltage divider (Del). The decision that a signal is present is made in the case where the threshold voltage U_{por} is exceeded by the signal voltage $U_s = U_4' > U_{por} = K_d(U_4 + U_4'')$, where K_d is the transmission factor of the voltage divider ($K_d > 0.5$).

In the detector shown in Figure 1b, the signal voltage is compared to each reference voltage. The decision that a signal is present is made in the case where the threshold voltage U_{por} in the threshold gates PU1 and PU2 is simultaneously exceeded by the output voltages of the subtraction gates VU1 and VU2 respectively:

$$\left.\begin{aligned} U_4' - U_4 > U_{пор} \\ U_4' - U_4'' > U_{пор} \end{aligned}\right\}. \qquad (1)$$

Decision (1) is made by a device which performs an AND logic operation. The specified false alarm probability (VLT) is achieved through the choice of the threshold voltage. In the following, the detectors considered are designated in accordance with the operational algorithm as ODKS - a detector with bilateral contrasts with respect to the mean value and ODKI - a detector with bilateral contrasts and an AND logic gate.

The noise immunity of an ODKS was treated in [1] with the following assumptions: the interference voltages corresponding to the adjacent directions of the antenna system directional pattern are independent; PF is an ideal bandpass filter with a bandwith of Δf; D is a linear detector with no inertia; SNCh [low pass filter] is an ideal integrator.

The case where $\Delta fT >> 1$ which is important in practice was analyzed.

We shall estimate the noise immunity of an ODKI, adopting the assumptions made above and $\Delta fT >> 1$. In this case, it can be assumed that the voltages at the outputs of the reference voltage and signal driver have a gaussian distribution both in the presence and the absence of a signal, mean values of:

$$a_4 = K_1\sigma_2;\ a_4' = K_1\sigma_2';\ a_4'' = K_1\sigma_2'' \qquad (2)$$

and mean square deviations of:

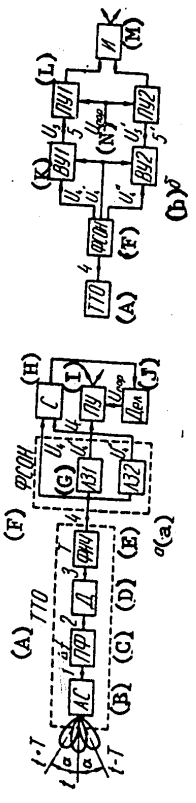

Figure 1.

Key: A. TTO [standard detection channel];
B. AS [antenna system];
C. PF [bandpass filter];
D. D [detector];
E. FNCh [low pass filter];
F. FSON [signal and reference voltage driver];
G. LZ1 [delay line 1];
H. S [adder];
I. PU [threshold gate];
J. Del [voltage divider];
K. VU1 [subtraction gate 1];
L. PU1 [threshold gate 1];
M. AND gate;
N. U_{por} [threshold voltage].

$$\sigma_4 = K_2\sigma_2;\ \sigma_4' = K_2\sigma_2';\ \sigma_4'' = K_2\sigma_2'', \tag{3}$$

where $K_1 = 1/\sqrt{2\pi}$, $K_2 = 0.2/\sqrt{\Delta f T}$, σ_2, σ_2' and σ_2'' are the mean square deviations of the interference voltage at the output of the bandpass filter corresponding to the three adjacent directions of antenna system directional pattern.

The probability that the voltages at the outputs of the subtraction gates U_5 and U_5' will simultaneously exceed the threshold voltage is:

$$P_{пр} = P(U_5 > U_{пор},\ U_5' > U_{пор}) = \int_{U_{пор}}^{\infty}\int w_2(y_1, y_2)\, dy_1 dy_2, \tag{4}$$

where $w_2(y_1,y_2)$ is the combined probability density of the two independent random quantities U_5, U_5', formed from the three independent ones U_4, U_4' and U_4''. In accordance with [2]:

$$w_2'(y_1, y_2) = \int_{-\infty}^{\infty} J_{4,5} w_1(x_1)\, w_1(x_2)\, w_1(x_3)\, dy_3,$$

where $w_1(x_1)$, $w_1(x_2)$, $w_1(x_3)$ are the one-dimensional probability densities of the random quantities U_4, U_4', U_4''; $J_{4,5}$ is the Jacobian of the transform from the random quantities U_4, U_4' and U_4'' to the random quantities $U_5 = U_4' - U_4$, $U_5' = U_4' - U_4''$ and $U_5'' = U_4'$.

In this case, $J_{4,5} = 1$, and therefore:

$$w_2(y_1, y_2) = \frac{1}{(2\pi)^{3/2}\sigma_4\sigma_4'\sigma_4''}\int_{-\infty}^{\infty} \exp\left[-\frac{(y_3 - y_1 - a_4)^2}{2\sigma_4^2}\right]\times$$
$$\times \exp\left[-\frac{(y_3 - a_4')^2}{2(\sigma_4')^2}\right]\exp\left[-\frac{(y_3 - y_2 - a_4'')^2}{2(\sigma_4'')^2}\right]dy_3. \tag{5}$$

Following the substitution of (5) in (4) and integrating with respect to y_3, taking (2) and (3) into account, we derive the expression for the probability that the threshold voltage will be exceeded simultaneously in PU1 and PU2 of the ODKI:

$$P_{пр} = \frac{C_1 C_2}{2\pi\sqrt{C_1^2 + C_1^2C_2^2 + C_2^2}}\exp\left\{K^2\left[\frac{C_1C_2(1 + C_1 + C_2)}{C_1^2 + C_1^2C_2^2 + C_2^2} - 1\right]\right\}\times$$
$$\times\int_{z_0}^{\infty}\int \exp\left[-\frac{C_1^2(1 + C_2^2)z_1^2 + 2KC_1(C_1 - C_2 - C_2^2 + C_1C_2^2)z_1}{2(C_1^2 + C_1^2C_2^2 + C_2^2)}\right]\times$$
$$\times\exp\left[\frac{2C_1C_2z_1z_2 - 2KC_2(C_2 - C_1 - C_1^2 + C_1^2C_2)z_2 - C_2^2(1 + C_1^2)z_2^2}{2(C_1^2 + C_1^2C_2^2 + C_2^2)}\right]dz_1dz_2, \tag{6}$$

$z_0 = U_{por}/\sigma_4'$ is the normalized threshold value and $K = K_1/K_2$.

The false alarm probability $P_{лт}$ and the detection probability $P_{по}$ are defined by the expression:

$$P_{пр} = \begin{cases} P_{лт} & \text{при } C_1 = \sigma_2/\sigma_2'; \; C_2 = \sigma_2''/\sigma_2; \quad (7) \\ P_{по} & \text{при } C_1 = \sigma_2/\sigma_2'\sqrt{1+\gamma}; \; C_2 = \sigma_2''/\sigma_2'\sqrt{1+\gamma}, \quad (8) \end{cases}$$

(when)

where $\gamma = \sigma_{2c}^2/\sigma_2^2$ is the ratio of the signal power to the interference power at the bandpass filter output.

By using expressions (6) and (7), one can select the value of Z_0 for which the specified false alarm probability is assurred. Shown in Figure 2 are the detection characteristics computed from formulas (6) and (8) for various kinds of interference field anisotropy and $\Delta fT = 10^4$, where the value of d_0 was established for the worst case nature of the anisotropy ($C_1 = C_2 = 0.95$), so that the maximum false alarm probability did not exceed 10^{-4}.

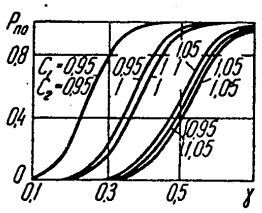

Figure 2.

In the comparison of an ODKI and ODKS, the change in the coefficients which define the nature of the interference field anisotropy for [illegible] adjacent directions of the antenna system directional pattern was taken in a range of 0.95 to 1.05. In the worst case as regards the false alarm flow for the nature of the anisotropy ($C_1 = C_2 = 0.95$, the values of the transmission factor of the voltage divider K_d (for the ODKS) and the normalized threshold z_0 (for the ODKI) were determined, for which a specified value of $P_{f.a.0}$ [false alarm probability] is assurred. Then, the threshold ratios $\gamma_{0.9}$, and the corresponding [detection] probabilities $P_{по} = 0.9$ (Table 1) and the values of the false alarm probability (Table 2) were determined for each detector using formulas [1] (for the ODKS) or (6)-(8) for the ODKI for various kinds of interference field anisotropy. For the ODKI, the values of z_0 and the threshold ratios $\gamma_{0.9}$ were determined on a computer using numerical integration and searching for the extremum of a one-dimensional quality function using the method of the golden mean [3]. The indicated calculations were performed for various values of ΔfT and $P_{лт0}$ (Tables 1 and 2).

Then, similar calculations were also performed for both detectors where the initial setting of the threshold z_0 (the coefficient K_d) was made

assuming that the interference field was isotropic ($C_1 = C_2 = 1$). The results of these calculations are shown in Tables 1 and 2.

TABLE 1 THRESHOLD RATIOS $\gamma_{0.9}$

Пороговые отношения $\gamma_{0,9}$

(1) $P_{лт\,0}$	ΔfT	(2) Структура обнаружителя	(3) Характер анизотропии поля помехи: $C_1=0,95$ $C_2=0,95$	$C_1=0,95$ $C_2=1$	$C_1=1$ $C_2=1$	$C_1=0,95$ $C_2=1,05$	$C_1=1$ $C_2=1,05$	$C_1=1,05$ $C_2=1,05$
(4) Установка порога при $C_1 = C_2 = 1$								
10^{-4}	10^3	ОДКС	0,095	0,15	0,21	0,21	0,27	0,34
		ОДКИ	1,08	1,23	1,31	1,42	1,46	1,54
	10^4	ОДКС	—	—	0,064	0,064	0,12	0,17
		ОДКИ	0,21	0,31	0,34	0,45	0,46	0,47
10^{-6}	10^3	ОДКС	0,13	0,19	0,26	0,26	0,32	0,38
		ОДКИ	1,41	1,57	1,67	1,80	1,84	1,95
	10^4	ОДКС	—	—	0,08	0,08	0,13	0,18
		ОДКИ	0,28	0,39	0,42	0,53	0,54	0,56
(5) Установка порога при $C_1 = C_2 = 0,95$								
10^{-4}	10^3	ОДКС	0,21	0,28	0,34	0,34	0,42	0,48
		ОДКИ	1,29	1,44	1,53	1,66	1,70	1,80
	10^4	ОДКС	0,06	0,12	0,18	0,18	0,24	0,30
		ОДКИ	0,33	0,45	0,47	0,60	0,62	0,63
10^{-6}	10^3	ОДКС	0,25	0,32	0,39	0,39	0,46	0,53
		ОДКИ	1,64	1,80	1,92	2,02	2,10	2,22
	10^4	ОДКС	0,08	0,13	0,19	0,19	0,25	0,31
		ОДКИ	0,41	0,52	0,56	0,66	0,69	0,71

ODKI

Key: 1. False alarm probability;
2. The detector structure;
3. The nature of the interference field anisotropy;
4. The setting of the threshold when $C_1 = C_2 = 1$;
5. The setting of the threshold when $C_1 = C_2 = 0.95$.

A comparison of the threshold ratios for both detectors (Table 1) shows the substantial advantage of the ODKS for both methods of setting the threshold (assuming $C_1 = C_2 = 1$ and $C_1 = C_2 = 0.95$) and any nature of the interference field anisotropy. In this case, the advantage of the ODKS in the threshold ratios is manifest more when the initial setting of the threshold is made assuming that the interference field is

isotropic and increases with a reduction in the product ΔfT and the probability $P_{лт0}$.

TABLE 2 THE FALSE ALARM PROBABILITIES

(1) $P_{лт0}$	ΔfT	Структура обнаружителя (2)	(3) Характер анизотропии поля помехи: $C_1=0{,}95$, $C_2=0{,}95$	$C_1=1$, $C_2=1$	$C_1=0{,}95$, $C_2=1{,}05$	$C_1=1{,}05$, $C_2=1{,}05$
	(4)	Установка порога при $C_1=C_2=1$				
10^{-4}	10^3	ОДКС	$1{,}5\cdot10^{-1}$	10^{-4}	10^{-4}	$1{,}4\cdot10^{-7}$
		ОДКИ	$1\cdot10^{-3}$	10^{-4}	$7{,}2\cdot10^{-5}$	$7{,}8\cdot10^{-6}$
	10^4	ОДКС	1	10^{-4}	10^{-4}	— / −11,8
		ОДКИ	$2{,}4\cdot10^{-2}$	10^{-4}	$4{,}7\cdot10^{-6}$	$3{,}5\cdot10^{-8}$
10^{-6}	10^3	ОДКС	$2{,}7\cdot10^{-2}$	10^{-6}	10^{-6}	$<10^{-11}$ / −7,2
		ОДКИ	$2{,}2\cdot10^{-5}$	10^{-6}	$6{,}5\cdot10^{-7}$	$3{,}3\cdot10^{-8}$
	10^4	ОДКС	1	10^{-6}	10^{-6}	— / −12,68
		ОДКИ	$1{,}4\cdot10^{-3}$	10^{-6}	$3{,}1\cdot10^{-5}$	$4{,}6\cdot10^{-11}$

(1) $P_{лт0}$	ΔfT	Структура обнаружителя (2)	(3) Характер анизотропии поля помехи: $C_1=0{,}95$, $C_2=0{,}95$	$C_1=1$, $C_2=1$	$C_1=0{,}95$, $C_2=1{,}05$	$C_1=1{,}05$, $C_2=1{,}05$
	(5)	Установка порога при $C_1=C_2=0{,}95$				
10^{-4}	10^3	ОДКС	10^{-4}	$6\cdot10^{-11}$	$6\cdot10^{-11}$	— / −9,04
		ОДКИ	10^{-4}	$6{,}1\cdot10^{-6}$	$4{,}1\cdot10^{-6}$	$2{,}8\cdot10^{-7}$
	10^4	ОДКС	10^{-4}	— / −12,2	— / −12,2	— / −20,4
		ОДКИ	10^{-4}	$1{,}7\cdot10^{-8}$	$4{,}4\cdot10^{-11}$	$1{,}8\cdot10^{-12}$
10^{-6}	10^3	ОДКС	10^{-6}	$<10^{-11}$ / −7,33	— / −7,33	— / −9,94
		ОДКИ	10^{-6}	$2{,}6\cdot10^{-8}$	$1{,}7\cdot10^{-8}$	$4{,}8\cdot10^{-10}$
	10^4	ОДКС	10^{-6}	— / −13,1	— / −13,1	— / −21,3
		ОДКИ	10^{-6}	$2\cdot10^{-11}$	$4\cdot10^{-12}$	$2{,}3\cdot10^{-17}$

Key: 1. False alarm probability;
2. The detector structure;
3. The nature of the interference field anisotropy;
4. The setting of the threshold when $C_1 = C_2 = 1$;
5. The setting of the threshold when $C_1 = C_2 = 0.95$.

[TABLE 2, continued: Note to Table 2: Indicated in the upper row are the false alarm probabilities and in the lower row, the value of the argument of the probability integral.]

A comparison of the threshold ratios for differing natures of the interference field anisotropy (Table 1) shows that the ODKI is less critical than the ODKS to a change in the nature of the anisotropy.

A comparison of the false alarm probabilities of both detectors (Table 2) shows the substantial advantage of the ODKS, which is more manifest when the threshold is set for $C_1 = C_2 = 0.95$. At the same time, the ODKI is distinguished by lesser criticality to a change in the nature of the interference field anisotropy as well as with respect to the threshold ratios.

The calculations which were performed demonstrate the preferability of setting the thresholds for the worst case with respect to the false alarm flow for the nature of the interference field anisotropy.

BIBLIOGRAPHY

1. Mazor Yu.L., Tereshchuk R.M., Chachkovskiy S.V., "Pomekhoustoychivost' obnaruzhitelya shumovogo signala, rabotayushchego po metodu dvukhstoronnego prostranstvennogo kontrasta" ["The Noise Immunity of a Noise Signal Detector Operating In Accordance with the Method of Bilateral Spatial Contrast"], IZV. VUZOV - RADIOELEKTRONIKA, 1978, 21, No 9, p 110.

2. Levin B.R., "Teoreticheskiye osnovy statisticheskoy radiotekhniki" ["The Theoretical Principles of Statistical Radio Engineering"], Moscow, Sovetskoye Radio Publishers, 1976, Book 1.

3. Wild, D.J., "Methods of Extremum Search", Translated from the English, Moscow, Nauka Publishers, 1969.

[11-8225]

8225
CSO: 1860

UDC 621.396.96

THE SEQUENTIAL DETECTION OF AN INCOHERENT SIGNAL

Kiev IVUZ RADIOELEKTRONIKA in Russian Vol 23, No 8, Aug 80 pp 61-64
manuscript received 14 May 79; after revision 1 Aug 79

[Paper by A.M. Shloma and G.B. Gol'fel'd]

[Text] Sequential algorithms are derived for the detection of an incoherent signal against a background of Markov interference.

We shall consider the problem of the sequential detection of an incoherent signal against a background of nonsteady-state gaussian interference. The relevant algorithms were derived in [1] for the case of independent interference, based on invariant and asymptotically invariant statistics. The results of [1] are generalized in this paper for the case of Markov interference.

The detection problem posed above is statically formulated in the following manner. There is a matrix set of n p-dimensional observations $\{x_{ij}: i = \overline{1,n};\ j = \overline{1,p}\}$. The sample is dependent with respect to the rows (i) and independent with respect to the columns (j). The elements of the sample are gaussian, $x_{ij} \sim N(\mu_{ij};\ \sigma_{ij}^2)$. The sample is steady-state with respect to the rows ($\mu_{ij} = \mu_i;\ \sigma_{ij}^2 = \sigma_i^2$) and is nonsteady-state with respect to the columns. Required is the organization of a sequential unbiased Wald procedure to check the hypothesis h_0: $h_0: \vec{\mu} = (\mu_1, \ldots, \mu_n) = 0$ (interference) as opposed to the alternative $H_1: \vec{\mu} \neq 0$ (signal and interference).

The major difficulty in solving this problem is the generation of the logarithm of the likelihood ratio, since the requirement of an unbiased procedure does not allow for direct use of the well known results for the detection of signals against a background of Markov interference [2]. The possibility of using functional models similar to an

autoregression model in the synthesis of unbiased procedures is studied in this paper.

1. *Interfering parameters are absent.* Let the relationship between the elements of the sample x_{ij} ($j = \overline{1,p}$) be a Markov simply connected function. Then, since the elements x_{ij} and $x_{i,j+1}$ are dependent, x_{ij} and $x_{i,j+2}$ are conditionally independent, one can obtain two samples from the original matrix sample $\{x_{ij}\}$, which consist of the conditionally independent elements: $\{x_{i,2l-1}: i=\overline{1,n}; l=\overline{1,p/2}\}$ and $\{x_{i,2l}: i=\overline{1,n}; l=\overline{1,p/2}\}$, and p is even for the sake of determinancy.

However, the matrices $\{x_{i,2l-1}\}$ and $\{x_{i,2l}\}$ are interdependent. Since the alternative is two-sided, then to construct an unbiased procedure to check the hypotheses, it is expedient to change over from the samples obtained to samples of the following form:

$$\{J_i^2 : i=\overline{1,n}\},\ \{Z_i^2 : i=\overline{1,n}\}, \tag{1}$$

where

$$J_i^2 = p|\bar{x}_i^{\mathrm{I}}|^2/(2\sigma_i^2),\quad Z_i^2 = p|\bar{x}_i^{\mathrm{II}}|^2/(2\sigma_i^2),$$
$$\bar{x}_i^{\mathrm{I}} = (2/p)\sum_{l=1}^{p/2} x_{i,2l-1},\quad \bar{x}_i^{\mathrm{II}} = (2/p)\sum_{l=1}^{p/2} x_{i,2l}.$$

We shall change over from samples (1) to the sample:

$$\{J_i^2, Z_i^2 : i=\overline{1,n}\}. \tag{2}$$

Since the pairs (J_i^2, Z_i^2) are independent with respect to i, then the logarithm of the likelihood ratio for (2) has the form:

$$\lambda_n = \sum_{i=1}^{n} \ln[W(J_i^2, Z_i^2 | H_1)/W(J_i^2, Z_i^2 | H_0)].$$

In accordance with the rule for the multiplication of probability densities, the likelihood function is factored as follows: $W(J_i^2, Z_i^2) = W(J_i^2)W(Z_i^2|J_i^2)$.

Consequently,

$$\lambda_n = \sum_{i=1}^{n}\left[\ln\frac{W(J_i^2|H_1)}{W(J_i^2|H_0)} + \ln\frac{W(Z_i^2|J_i^2, H_1)}{W(Z_i^2|J_i^2, H_0)}\right].$$

We shall adopt the following model of the function for (2):

$$Z_i^2 = \rho_i^2 J_i^2 + \varepsilon_i^2, \quad i = \overline{1, n}, \tag{3}$$

where $\varepsilon_i^2 = p|\varepsilon_i|^2/(2\sigma_i^2)$, ε_i is a sequence of independent random quantities; in the case of the hypothesis H_0: $\varepsilon_i \sim N(0; 2\sigma_i^2/p)$, and in the case of the hypothesis H_1: $\varepsilon_i \sim N(\mu_i; 2\sigma_i^2/p)$, and consequently, in the case of H_0: $\varepsilon_i^2 \sim \chi^2(2)$, and in the case of H_1: $\varepsilon_i^2 \sim \chi^2(2; \delta_i^2)$, where the noncentrality parameter is $\delta_i^2 = p\mu_i^2/(2\sigma_i^2)$; ρ_i is the correlation factor between the elements x_{ij} and $x_{i,j+1}$. It is interesting to note that the use of the model: $Z_i^2 - \delta_i^2 = \rho_i^2 (J_i^2 - \delta_i^2) + \varepsilon_i^2$, $\varepsilon_i^2 \sim \chi^2(2)$, $i = \overline{1,n}$, similar to a first order autoregression equation with an unknown mean [3], does not yield anything in the case, since when it is used, the logarithm of the likelihood ratio degenerates when $\delta_i^2 << 1$.

In contrast to the traditional approach, no centering of the observations is accomplished in model (3), but it is assumed instead of this that in the case of the hypothesis H_1, the "observations error" ε_i^2 contains a regular component. Since J_i^2 is generated on the basis of conditionally independent elements, then in line with [4], in the case of H_0: $J_i^2 \sim \chi^2(2)$, and in the case of H_1: $J_i^2 \sim \chi^2(2; \delta_i^2)$. By deriving the corresponding conditional distributions from (3) for Z_i^2, when $\delta_i^2 << 1$, one can write the following expression for the logarithm of the likelihood ratio:

$$\lambda_n \cong \frac{1}{4} \sum_{i=1}^{n} [\delta_i^2 [(1 - \rho_i^2) J_i^2 + Z_i^2] - \sum_{i=1}^{n} \delta_i^2. \tag{4}$$

2. *Interfering parameters are present.* In this case, one can make use of T^2 statistics, which differ in the invariant properties [4]. In arguing similar to section 1, one can change over from the initial sample $\{x_{ij}\}$ to the sample $\{(J_i^2)^T, (Z_i^2)^T : i = \overline{1, n}\}$, where $(J_i^2)^T = p|\bar{x}_i^{\mathrm{I}}|^2/[2(S_i^2)^{\mathrm{I}}]$, $(Z_i^2)^T = p|\bar{x}_i^{\mathrm{II}}|^2/[2(S_i^2)^{\mathrm{II}}]$. Here:

$$(S_i^2)^{\mathrm{I}} = \sum_{l=1}^{p/2} 2(x_{i,2l-1} - \bar{x}_i^{\mathrm{I}})^2/(p-2), \quad (S_i^2)^{\mathrm{II}} = \sum_{l=1}^{p/2} 2(x_{i,2l} - \bar{x}_i^{\mathrm{II}})^2/(p-2),$$

are the sample dispersions.

We shall take the following as the model of the function:

$$(Z_i^2)^T = r_i^2 (J_i^2)^T + (\varepsilon_i^2)^T. \tag{5}$$

Here, for the case of H_0: $H_0:(\varepsilon_i^2)^T \sim F(2; p/2-2)$, and in the case of H_1: $H_1:(\varepsilon_i^2)^T \sim F(2; p/2-2; \delta_i^2)$, $r_i = \left[\sum_{j=1}^{p}(x_{i,j+1}-\bar{x}_i)(x_{ij}-\bar{x}_i)\right]/S_i^2(p-1)$ is the sample correlation coefficient (we will note that in the steady-state case, one can use the paired sample correlation coefficient for the random quantities J_i^2 and Z_i^2 are the measure for the correlation of these random quantities, which, as follows from the formulation of the problem, is non-negative), $S_i^2 = \sum_{j=1}^{p}(x_{ij}-\bar{x}_i)^2/(p-1)$ is the sample dispersion;

$\overline{x_i} = \bar{x}_i = \sum_{j=1}^{p} x_{ij}/p$ is the sample mean.

It can be demonstrated that for large values of p: $S_i^2 \cong 0{,}5[(S_i^2)^I + (S_i^2)^{II}]$.

In subsequently reasoning completely on analogy with section 1, and considering the fact that the corresponding χ^2 distributions are replaced by the probability densities from the family of F distributions, when $\delta_i^2 << 1$, one can derive the following expression for the logarithm of the likelihood ratio:

$$\lambda_n \cong \frac{1}{4}\sum_{i=1}^{n}\delta_i^2[(1-r_i^2)(J_i^2)^T + (Z_i^2)^T] - \sum_{i=1}^{n}\delta_i^2. \qquad (6)$$

Since the sample estimates used are valid in the case of the hypothesis H_0 [3], then (4) and (6) are asymptotically equivalent for hypothesis H_0. In practice, one usually sets $\delta_i^2 = \delta_0^2$, $i = \overline{1,n}$, and therefore, the actual sequential analysis procedure itself can be written in the following form:

$$4(b/\delta_0^2 + n) \leqslant \lambda_n \cong \sum_{i=1}^{n}[(1-r_i^2)(J_i^2)^T + (Z_i^2)^T] \leqslant 4(a/\delta_0^2 + n),$$

where a and b are Wald thresholds [5].

3. A doubly connected Markov model of the function. The approach treated above can also be used in this case. Here, the element $x_{i,j+4}$ is conditionally independent of the elements x_{ij} and $x_{i,j+1}$ ($j = \overline{1,p}$), and for this reason, a transition can be made from the original sample $\{x_{ij}: i = \overline{1,n};\ j = \overline{1,p}\}$ to three samples which are independent of each other and consist of the conditionally independent elements: $\{x_{i,3l-2}: i = \overline{1,n};\ l = \overline{1,p/3}\}$, $\{x_{i,3l-1}: i = \overline{1,n};\ l = \overline{1,p/3}\}$, $\{x_{i,3l}: i = \overline{1,n};\ l = \overline{1,p/3}\}$, and for the sake of determinacy, p is a multiple of three. If the interfering parameters are not present, then one can change over from these samples

(7)

$$\{J_i^2, Z_i^2, R_i^2 : i = \overline{1,n}\}$$

where $$J_i^2 = p|\bar{x}_i^{\mathrm{I}}|^2/(3\sigma_i^2),\quad Z_i^2 = p|\bar{x}_i^{\mathrm{II}}|^2/(3\sigma_i^2),\quad R_i^2 = p|\bar{x}_i^{\mathrm{III}}|^2/(3\sigma_i^2),$$

$$\bar{x}_i^{\mathrm{I}} = \frac{3}{p}\sum_{l=1}^{p/3} x_{i,3l-2},\quad \bar{x}_i^{\mathrm{II}} = \frac{3}{p}\sum_{l=1}^{p/3} x_{i,3l-1},\quad \bar{x}_i^{\mathrm{III}} = \frac{3}{p}\sum_{l=1}^{p/3} x_{i,3l}.$$

Since the model of the dependence is doubly connected, the logarithm of the likelihood ratio for (7) can be written thus:

$$\lambda_n = \sum_{i=1}^{n}\left[\ln\frac{W(J_i^2|H_1)}{W(J_i^2|H_0)} + \ln\frac{W(Z_i^2|J_i^2,H_1)}{W(Z_i^2|J_i^2,H_0)} + \ln\frac{W(R_i^2|J_i^2,Z_i^2,H_1)}{W(R_i^2|Y_i^2,Z_i^2,H_0)}\right]. \tag{8}$$

For simplicity, we shall assume that the model of the function is expressed by the following relationships:

$$\left.\begin{aligned} Z_i^2 &= \rho_i^2 J_i^2 + \varepsilon_i^2 \\ R_i^2 &= \rho_i^4 J_i^2 + \rho_i^2 Z_i^2 + \varkappa_i^2 \end{aligned}\right\}. \tag{9}$$

Here, $\varepsilon_i^2 = p|\varepsilon_i|^2/(3\sigma_i^2),\ \varkappa_i^2 = p|\varkappa_i|^2/(3\sigma_i^2),$, where ε_i and κ_i $(i = \overline{1,n})$ are sequences of independent random quantities. For H_0: ε_i and κ_i have the distribution $N(0; 3\sigma_i^2/p)$, and for H_1: ε_i and κ_i have the distribution $N(\mu_i; 3\sigma_i^2/p)$. Consequently, the case of H_0: ε_i^2 and κ_i^2 have a $\chi^2(2)$ dustribution, and in the case of H_1: they have a $\chi^2(2; \delta_i^2)$ distribution, where the noncentrality parameter is $\delta_i^2 = p\mu_i^2/(3\sigma_i^2)$; ρ_i is the correlation coefficient between the adjacent elements of the original sample $\{x_{ij}\}$, located in one row (for simplicity, we assume that $\rho_{ij} = \rho_i$).

By using (9) and reasoning on analogy with section 1, it is easy to find that (8) assumes the following form when $\delta_i^2 << 1$:

$$\lambda_n \cong \frac{1}{4}\sum_{i=1}^{n}\delta_i^2[(1-\rho_i^2-\rho_i^4)J_i^2 + (1-\rho_i^2)Z_i^2 + R_i^2] - \frac{3}{2}\sum_{i=1}^{n}\delta_i^2.$$

If interfering parameters are present (σ_i^2 and ρ_i are unknown), then by employing T^2 statistics in a manner similar to section two, one

can obtain the corresponding sequential procedure for testing the hypotheses.

It should be noted in conclusion that in accordance with [5], the sequential procedures derived above for the selected models of the function are optimal, or in the presence of interfering parameters, asymptotically optimal for the hypothesis H_0 (i.e., assuming that only interference acts at the input to the receiver, and this is most important case of sequential detection in practice) in the sense of a minimum of the average analysis time. Moreover, the derived procedures are invariant, i.e., the probabilistic distributions of the corresponding statistics in the case of the hypothesis H_0 do not depend on the unknown interference power, and consequently, the detection is accomplished with a stable false alarm probability. The unbiased nature of the derived procedures makes it possible to accomplish incoherent detection of signals with a random phase.

BIBLIOGRAPHY

1. Shloma A.M., Gol'fel'd G.B., "Posledovatel'noye obnaruzheniye signalov na fone nestatsionarnykh normal'nykh pomekh" ["The Sequential Detection of Signals Against a Background of Normal Nonsteady-state Interference"], RADIOTEKHNIKA, 1979, 34, No 5, p 70.

2. Levin B.R., "Teoreticheskiye osnovy statisticheskoy radiotekhniki" ["The Theoretical Principles of Statistical Radio Engineering"], Moscow, Sovetskoye Radio Publishers, 1976, Book 3.

3. Anderson T., "The Statistical Analysis of Time Series", Translated from the English, Moscow, Mir Publishers, 1976.

4. Anderson T., "Introduction to Multidimensional Statistical Analysis", Translated from the English, Moscow, Fizmatgiz Publishers, 1963.

5. De Groot, M., "Optimum Statistical Solutions", Translated from the English, Moscow, Mir Publishers, 1974.

[11-8225]

8225
CSO: 1860

COMPONENTS AND CIRCUIT ELEMENTS, WAVEGUIDES, CAVITY RESONATORS AND FILTERS

UDC 621.372.54

QUADRATURE FILTERS USING INTEGRATED CIRCUITS FOR ANALOG SIGNAL MULTIPLEXERS

Kiev IVUZ RADIOELEKTRONIKA in Russian Vol 23, No 8, Aug 80 pp 25-31
manuscript received 4 Nov 78 after revision 5 Oct 79

[Paper by V.P. Tarasov and V.N. Timonteyev]

[Text] The design principles for symmetrical and asymmetrical quadrature filters (KF) are analyzed for the realization of panoramic comb filters. Based on the analysis, the properties are described and formulas are given for th transfer functions, the nonlinear distortion factor, the Q and the dynamic range of quadrature filters for various filter configurations in forward transmission channels. It is shown that the circuit of a symmetrical quadrature filter with high pass filters is the most suitable for integrated circuit design. The possibility of obtaining high Q tunable quadrature filters with a resonant frequency instability as a function of temperature of 10^{-6} 1/°C is indicated.

Panoramic comb filters are widely used in a number of radio electronic equipment components [1]. The demands of a high quality factor ($Q = 10^3 - 10^6$) and a low resonant frequency instability (down to 10^{-6} 1/°C), which can assume values in a range of from tens of hertz up to hundreds of megahertz, are placed on their selective elements.

Quasilinear quadrature filters (KF) best satisfy the indicated requirements [2]. They have a high Q, permit tuning of the resonant frequency in a wide range and in conjunction with crystal oscillators are frequency dividers, can assure a resonant frequency instability of 10^{-6} 1/°C and

less, including in the range of hundreds and tens of hertz, something which cannot be achieved by other means. Quadrature filters containing up to 100 active and passive components can be fabricated in an integrated circuit design. However, they have not found wide application up to the present time, since as a result of the poor quality of the analog signal multipliers, the major element of quadrature filters, the reference frequency signal voltage (tens of millivolts) has leaked through to the filter output. New designs of integrated circuit analog multipliers make it possible to reduce the reference frequency signal penetration to the output down to tenths of a millivolt [3]. For this reason, it is of considerable interest to select that quadrature filter circuit which most completely meets the requirements for panoramic comb filters and is the simplest to realize in an integrated circuit design.

This paper is devoted to the analysis of the structural configurations of quadrature filters, a theoretical study of them and an experimental investigation of a circuit proposed as an optimum one for integrated circuit realization.

At the present time, two variants of quadrature filter circuit configurations are known, which in accordance with the configuration, in the following we shall term either asymmetrical [2, 4, 5] (Figure 1, the switch in position a) or symmetrical [6] (Figure 1, the switch in position b) quadrature filters. Quadrature filter circuits contain two channels each, in each of which there are two analog signal multipliers, which are separated by filter elements (F). Low pass (FNCh) or high pass (FVCh) filters, as well as a combination of them can be used as the latter. The sinusoidal voltages, $U_{0\pi}$ and $U_{0\pi}'$, fed from the reference frequency generator $\Gamma_{0\pi}$, are phase shifted relative to each other by one-quarter of a period. The frequency f_0 of this generator is determined by the resonant frequency of the quadrature filter. The presence of two channels is needed to suppress spurious frequencies at the output which are generated by the multipliers. By presupposing that the analog multipliers are ideal, one can assume that in the case of a 90° phase shift of the quadrature components of the reference voltage and completely identical functionally similar components of both quadrature frequency channels, the output signal spectrum is not enriched with the frequencies of spurious harmonics.

The operational principle of a quadrature filter with a low pass filter in the channels consists in shifting the spectrum of the input signal to a low frequency range, then filtering and subsequently restoring the spectrum at the output. The working frequencies for this type of quadrature filter are the difference ($f - f_0$) components of the combination frequencies in each of the channels. The apperance of the signal at the output of the circuit is possible only when the frequencies f are close to the reference frequency, and other conditions, the difference components of the combination frequencies are suppressed by the channel low pass filters.

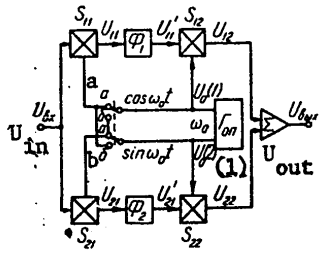

Figure 1.

Key: 1. Reference signal generator.

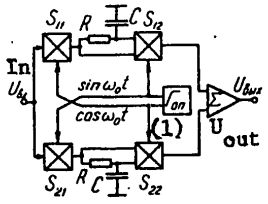

Figure 2.

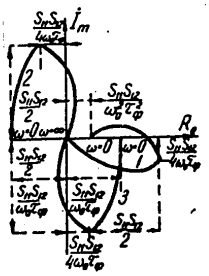

Figure 3.

The operational principle of a symmetrical quadrature filter and a high pass filter is based on the utilization of both the difference (f - f_0) and the sum (f + f_0) components of the combination frequencies. The appearance of a signal at the circuit output is assured just as in the preceding cases for asymmetrical and symmetrical quadrature filters with a low pass filter in the channels only at signal frequencies f which are close to the reference frequency f_0. The reason for this is the fact that the channel high pass filters suppress the difference components of the combination frequencies (f - f_0). At signal frequencies considerably different from the reference frequency, both components (the difference and the sum) get through to the output multipliers unimpeded and by virtue of the identical nature of the symmetrical quadrature filter channels, they are suppressed at the output.

The operation of a symmetrical quadrature filter circuit with a high pass filter is more clearly represented by analyzing the circuit equivalent to it which is shown in Figure 2. One can explain its operational principle by treating its components independently of the two circuits. One of them is the dual channel symmetrical circuit with direct coupling in the channel, having a zero transmission factor throughout the entire frequency range. The other is the symmetrical quadrature filter circuit with low pass filters in the channels which was treated earlier. Since the signals at the output are subtracted, the transmission function as

TABLE 1

Таблица 1

	(A) Симметричный квадратурный фильтр (АКФ)	(H) Симметричный квадратурный фильтр (СКФ)
(B) Выходные напряжения в операторной форме	$U_{вых1}(p)=\frac{S_{11}S_{12}}{4}\{U_{вх}(p)[h_1(p-j\omega_0)+h_1(p+j\omega_0)+\gamma[h_2(p-j\omega_0)+h_2(p+j\omega_0)]]+U_{вх}(p-j\omega_0)[h_1(p-j\omega_0)+\gamma e^{j2\varphi_0}h_2(p-j\omega_0)]+U_{вх}(p+j\omega_0)[h_1(p+j\omega_0)+\gamma e^{-j2\varphi_0}h_2(p+j\omega_0)]\}$ (3)	$U_{вых1}(p)=\frac{S_{11}S_{12}}{4}\{U_{вх}(p)e^{j\varphi_0}[h_1(p-j\omega_0)-\gamma h_2(p+j\omega_0)]-e^{-j\varphi_0}[\gamma h_2(p-j\omega_0)-h_1(p+j\omega_0)]+U_{вх}(p+j2\omega_0)e^{j\varphi_0}[h_1(p-j\omega_0)-\gamma h_2(p-j\omega_0)]+U_{вх}(p+j2\omega_0)e^{j\varphi_0}[h_1(p+j\omega_0)-\gamma h_2(p+j\omega_0)]\}$ (4)
(C) Передаточные функции КФ в операторной форме	$T(p)=\frac{U_{вых}(p)}{U_{вх}(p)}\frac{S_{11}S_{12}}{2}[h(p-j\omega_0)+h(p+j\omega_0)]$ (5)	$T(p)=\frac{U_{вых}(p)}{U_{вх}(p)}=j\frac{S_{11}S_{12}}{2}\sin\varphi_0[h(p-j\omega_0)-h(p+j\omega_0)]$ (6)
(D) Передаточная функция КФ при использовании в каналах ФНЧ первого порядка	$T(p)=S_{11}S_{12}(1+p\tau_\Phi)[(1+p\tau_\Phi)^2+\omega_0^2\tau_\Phi^2]^{-1}$ (7)	$T(p)=-S_{11}S_{12}\sin\varphi_0[(1+p\tau_\Phi)^2+\omega_0^2\tau_\Phi^2]^{-1}$ (8)
(E) Выходное напряжение КФ	$U_{вых2}(t)=U_c\{2B\cos[(\omega-\omega_0)t+\varphi+\varphi_1]\cos\omega_0 t+(A-B)\cos(\omega_0 t+\varphi+\varphi_1)\}$ (9)	
	$A=\frac{S_{11}S_{12}}{4}[h_{1(-)}^2+\gamma^2h_{2(+)}^2+2\gamma h_{1(-)}h_{2(+)}\cos\varphi_0]^{1/2}$, $B=\frac{S_{11}S_{12}}{4}[h_{1(-)}^2+\gamma^2h_{2(-)}^2+2\gamma h_{2(-)}\cos(2\varphi_0+\Delta\varphi_1)]^{1/2}$ (10)	$A=\frac{S_{11}S_{12}}{4}[h_{1(-)}^2+\gamma^2h_{2(-)}^2-2\gamma h_{1(-)}h_{2(+)}\cos(2\varphi_0+\Delta\varphi)]^{1/2}$, $B=\frac{S_{11}S_{12}}{4}(h_{1(-)}^2+\gamma^2h_{2(-)}^2-2\gamma h_{1(-)}h_{2(-)}\cos\Delta\varphi_1)^{1/2}$ (11)
(F) Коэф. нелинейных искажений КФ с ФНЧ	$K_{н.и}=\frac{1}{2}[1+\gamma^2\eta^2+2\gamma\eta\cos(2\varphi_0+\Delta\varphi_1)]^{1/2}$, $\eta=\frac{h_2}{h_1}$ (13)	$K_{н.и}=\frac{1}{2}(1+\gamma^2\eta^2-2\gamma\eta\cos\Delta\varphi_1)^{1/2}$, $\eta=\frac{h_2}{h_1}$ (14)
(G) Передат. функции КФ при последоват. соединении ФНЧ и ФВЧ в каналах	$T(j\omega)=\frac{1}{2}S_{11}S_{12}H_A(j\omega)$ (17)	$T(j\omega)=\frac{1}{2}S_{11}S_{12}]H_A(j\omega)\sin\varphi_0$ (18)
	где $H_A(j\omega)=\frac{\tau_{ФВЧ}(\omega-\omega_0)\exp[j\varphi(\omega)]}{\sqrt{[1-\tau_{ФВЧ}\tau_\Phi(\omega-\omega_0)^2]^2+\tau_{ФВЧ}^2(\omega-\omega_0)^2}}$	$\varphi(\omega)=\operatorname{arctg}\frac{1-\tau_{ФВЧ}\tau_\Phi(\omega-\omega_0)^2}{\tau_{ФВЧ}(\omega-\omega_0)}$

Принятые условные обозначения: h_1; h_2 - передаточные функции фильтров в 1-м и 2-м каналах КФ, причем $h_{1(-)}=h_1(p-j\omega_0)$; $h_{1(-)}=h_1(p+j\omega_0)$; $h_{2(+)}=h_2(p-j\omega_0)$; $h_{2(-)}=h_2(p+j\omega_0)$; $\tau_\Phi(\tau_{ФВЧ}, \tau_{ФНЧ})$ - постоянная времени фильтра; $H_A(j\omega)$, $\varphi(\omega)$ - передаточная и фазовая функции последовательно соединенных ФНЧ и ФВЧ

Key: A. Asymmetrical quadrature filter (AKF);
B. The output voltages in operator form;
C. The quadrature filter transfer functions in operator form;
D. The quadrature filter transfer functions when first order low pass filters are used in the channels;
E. The quadrature filter output voltage;
F. The nonlinear distortion factor of a quadrature filter with a low pass filter;
G. The quadrature filter transfer function when low pass and high pass filters are connected in series in the channels;
H. Symmetrical quadrature filter (SKF);

The following symbols were used: h_1 and h_2 are the transfer functions of the filters in the first and second quadrature filter channels, where:

$h_{1(-)} = h_1(p-j\omega_0)$; $h_{1(+)} = h_1(p+j\omega_0)$; $h_{2(-)} = h_2(p-j\omega_0)$;

$h_{2(+)} = h_2(p+j\omega_0$;

$\tau_\Phi(\tau_{ФВЧ}$ [$\tau_{h.p.f.}$], $\tau_{ФНЧ}$ [$\tau_{l.p.f.}$]) are the time constants of the filters;

$H_A(j\omega)$ $\phi(\omega)$ are the transfer and phase functions of the series connected low pass and high pass filters.

a whole will be determined by the symmetrical filter configuration with low pass filters and will differ from its transmission function only in the sign. The presence of a definite scatter in the parameters of the functionally similar components in the channels though leads to a reduction in the effectiveness of signal suppression outside the transmittance band.

In accordance with the symbols adopted in Figure 1, the following can be written for the asymmetrical quadrature filter circuit (AKF):

$$S_{1i}(t) = \frac{1}{2} S_{1i} \sum_{m=\pm 1} \exp(j\omega_0 mt);$$
$$S_{2i}(t) = \frac{1}{2} S_{2i} \sum_{m=\pm 1} \exp[jm(\omega_0 t + \varphi_0)], \quad (1)$$

where i = 1, 2, and for the symmetrical quadrature filter circuit (SKF):

$$S_{ii}(t) = \frac{1}{2} S_{ii} \sum_{m=\pm 1} \exp(j\omega_0 mt),$$
$$S_{in}(t) = \frac{1}{2} S_{in} \sum_{m=\pm 1} \exp[jm(\omega_0 t + \varphi_0)], \quad (2)$$

where i = 1, 2; n = 3 - i; $S_{11}(t)$ and $S_{21}(t)$ are the transmission factors of the input multipliers while $S_{12}(t)$ and $S_{22}(t)$ are the transmission factors of the output multipliers; ϕ_0 of the (quadrature) components of the reference voltage; ω_0 is the circular frequency of the reference voltage.

The analysis was made assuming the analog multipliers are identical, however, taking into account the scatter in the parameters of the functionally similar components of the different channels.

The basic results of the analysis of quadrature filter circuits obtained in this paper are summarized in Table 1.

Here, $\gamma = S_{21}S_{22}/S_{11}S_{12}$ is a coefficient which characterizes the nonidentical nature of the multipliers (when the multipliers are completely identical, $\gamma = 1$); $\eta = h_2/h_1$ is a coefficient which characterizes the nonidentical nature of the channel filters F1 and F2, which have an absolute value of the transition function in the passband of h_1 and h_2. As can be seen from expressions (3) and (4) for $U_{out}(p)$, which were

derived in operator form for the arbitrary transmission functions $h_1(p)$ and $h_2(p)$ of the channel filters F1 and F2, present at the output of both types of quadrature filters, besides the voltage which matches the frequency of the input signal, are the voltages of the combination signal frequencies ω and the frequency $2\omega_0$. We will note that the relative changes in the amplitude of the quadrature components $U_{0(1)}$ and $U_{0(2)}$ of the reference voltage do not have any influence on the amplitude of the voltages distorting the spectrum of the symmetrical quadrature filter, because of the constancy of γ, incorporated in expression (4).

The transfer functions of the asymmetrical quadrature filter (5) and the s-mmetrical quadrature filter (6) were found from (3) and (4) for the condition that $\gamma = 1$, $h_1(p) = h_2(p) = h(p)$ and $\phi_0 = \pi/2$. Just as in [5], assuming the use of extremely simple first order low pass filters (SNCh) with a time constant of $\tau\Phi$ in the quadrature filter channels, we obtain expresssions (7) and (8) based on (5) and (6). Hodographs of the transfer functions plotted on the basis of (7) and (8) are shown in Figure 3 (curves 1 and 2 respectively). The quality factor Q of both types of quadrature filters with low pass filters in the channel is defined by the ratio of the reference frequency f_0 to twice the passband of the channel low pass filters, i.e., $Q = f_0/2\Delta f_{1.p.f.}$. Quadrature filters, being quasilinear devices, introduce nonlinear distortions which occur because of the nonidentical nature of the functionally similar elements in the various channels and the deviations of the phase shift from the 90° value. These distortions of the output signal introduced by asymmetrical and symmetrical quadrature filters with low pass filters in the channel are characterized sufficiently clearly by expression (9). The coefficients A and B, incorporated in (9), take on different values depending on the type of quadrature filter of (10) and (11). Here:

$$h_{1(-)} = h_1[1 + (\omega - \omega_0)^2 \tau_{\phi 1}^2]^{-\frac{1}{2}},$$

$$h_{2(-)} = h_2[1 + (\omega - \omega_0)^2 \tau_{\phi 2}^2]^{-\frac{1}{2}},$$

$$\Delta\varphi_1(\omega) = \operatorname{arc\,tg}(\omega - \omega_0) \cdot \tau_{\phi 1} - \operatorname{arc\,tg}(\omega - \omega_0)\tau_{\phi 2}. \qquad (12)$$

As follows from (9), when $B \neq 0$, which corresponds to a definite scatter in the parameters of the quadrature filter components or the existence of an error in the phase shift ϕ_0 ($\phi_0 \neq 90°$) (for asymmetrical quadrature filters), distortions occur which are manifest in the form of amplitude modulation at the difference frequency $\omega - \omega_0$. The effectiveness of signal suppression at the output of a quadrature filter outside the transmittance band, as follows from (7), (8) and (9), is determined by the time constant τ_ϕ of the channel low pass filters and practically

does not depend either on the scatter in the parameters of the components of on ϕ_0. Expressions (13) and (14) for the nonlinear distortion factors, $K_{НИ}$, were derived from (9), (10) and (11) assuming that the first harmonic coefficient is equal to $(1/2)S_{12}S_{12}h_1$ [sic], the second harmonic coefficient is equal to B, while the third, fourth, etc. harmonic coefficients are equal to zero. It follows from (13) and (14) that $K_{НИ}$ [K_{n1d}] for both kinds of quadrature filters and low pass filters depends on the nonidentical nature of the functionally similar elements in the channels (including the presence of the phase shift $\Delta\phi_1$), while for symmetrical quadrature filters with low pass filters, K_{n1d} does not depend on ϕ_0 and $U_{0(1)}/U_{0(2)}$, i.e., for a symmetrical quadrature filter, the coefficient does not depend on $U_{0(1)}/U_{0(2)}$.

We shall now consider the factors limiting the dynamic range of quadrature filters.

In actual quadrature filter circuits using low pass filters, because of the thermal drift of the preceding stages, during the operation of the output multipliers it is possible for a noise voltage at a frequency of ω_0 with an amplitude of $U_{m\ noise}(\omega = \omega_0)$ to appear at the output. On the other hand, as follows from expression (9), derived assuming that the multipliers are ideal, when a noise signal at a frequency of $\omega \approx 3\omega_0$ is present at the quadrature filter input, a voltage at a frequency close to ω_0 having an amplitude of $U'_{m\ noise}$ $(\omega \approx \omega_0)$ will appear at the output.

Taking these specific features into account, we shall define the dynamic range of a quadrature filter by the following expression:

$$D = \frac{U_{m\ \text{вых макс}}\ \text{out max}_\phi}{U_{m\ \text{пом}} + U'_{m\ \text{пом}}} = \frac{D_{\text{др}} D_{3\omega_\phi}}{D_{\text{др}} + D_{3\omega_\phi}}. \qquad (15)$$

Here, $U_{m\ out\ max}$ is the maximum output signal amplitude of the quadrature filter; $D_{dr} = U_{m\ out\ max}/U_{m\ noise}$ is the dynamic range limited by the drift $D_{3\omega_0} = U_{m\ out\ max}/U'_{m\ noise}$ is the dynamic range limited by the presence of a noise signal at a frequency of $\omega \approx 3\omega_0$.

For both types of quadrature filters with low pass filters, we have:

$$D_{3\omega_0} = 4Q/K_{n.1.d.} = \qquad D_{3\omega_\phi} = 4Q/K_{НИ}, \qquad (16)$$

where $K_{n.1.d.}$ is determined by (13) or (14) depending on the type of quadrature filter.

With a scatter of 10% in the parameters, we find the following based on (13), (14) and (16): $K_{n.l.d.} = 20\%$ and $D_{3\omega_0} = 20Q$.

Galvanic coupling between the components in the channels is chracteristic of quadrature filter circuits with low pass filters, and this, as was shown in [4], leads to a substantial reduction in D_{dr}, and consequently, in D in the working range of temperatures. Quadrature filter circuits with series connected low pass and high pass filters in the channels are devoid of this drawback. Their transfer functions (17) and (18) (differing only in the 90° phase shift) were derived using (5) and (6) with the condition that $\omega_0\tau_\phi >> 1$, $\tau_{LPF} >> \tau_\phi$ and $\omega_0 > (1/3)\omega_0$. The amplitude-frequency (ACh) and phase-frequency response curves plotted using (17) are shown in Figure 4.

As can be seen from a comparison of Figures 3 (curves 1 and 2) and Figure 4, a characteristic feature of quadrature filters with series connected low pass and high pass filters in the channels is a region of maximum signal suppression at a quasiresonant frequency (ω_0), something which is not permissible for applications in panoramic filters.

This deficiency can be eliminated in the circuits of a symmetrical quadrature filter with high pass filters in the channels [6]. In fact, by substituting the expression $h(p) = p\tau_\phi(1+p\tau_\phi)^{-1}$ in (6), we prove the equivalency (within the precision of a 180° phase shift, see hodograph 3 in Figure 3) of the amplitude-frequency response of a symmetrical quadrature filter with high pass filters and a symmetrical quadrature with low pass filters. The conditions necessary to assure maximally high values of D_{dr} are also met at the same time, since the high pass filter capacitors perform the functions of galvanically decoupling the stages.

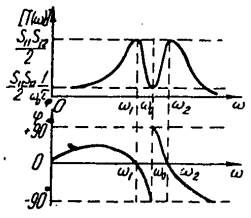

Figure 4.

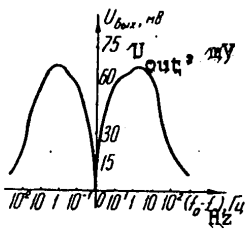

Figure 5.

As far as $D_{3\omega_0}$ and $K_{n.l.d.}$ are concerned, taking into account the scatter in the parameters of the circuit components for symmetrical quadrature

filters with high pass filters in the channel, we have:

$$D_{3\omega_0} = 2\sin\varphi_0(1-\gamma\eta)^{-1}, \tag{19}$$

$$K_{НИ} = 2\sin^{-1}\varphi_0\sqrt{3(1+\gamma^2\eta^2)-2\gamma\eta(2+\cos_{\Delta}\varphi_1)}. \tag{20}$$

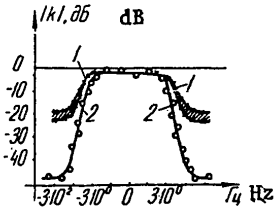

Figure 6.

As can be seen from a comparison of (19) and (16), the dynamic range of a symmetrical quadrature filter with high pass filters, in contrast to a quadrature filter with low pass filters, does not depend on the quality factor Q and can be made sufficiently high only in the case of a small disparity between the functionally similar elements in the various channels ($\nu\eta \to 1$).

It must be noted in particular that the signal suppression outside the transmittance band in a symmetrical quadrature filter circuit with high pass filters, when $\phi \neq 90°$, will be limited by the extent to which the elements in the channels are identical. Thus, the suppression factor given the condition that $|\omega - \omega_0|\tau_\phi >> 1$ is determined by the following expression:

$$K_{под} = T(\omega_0)/T(\omega) = 2\sin^{-1}\varphi_0[4(1-\gamma\eta)^2\cos^2\varphi_0 + (\omega-\omega_0)^{-2}\tau_\phi^{-2}h_i^{-2}\times \times(1+\gamma^2\eta^2-2\gamma\eta\cos\varphi_0)]^{-1}. \tag{21}$$

As follows from (21), when $\phi_0 = 90°$:

$$K_{под} = 2h_1^{-1}(1+\gamma^2\eta^2)^{-1/2}|\omega-\omega_0|\tau_\phi, \tag{22}$$

i.e., suppression of the first harmonic of the input signal at the output of a symmetrical quadrature filter with high pass filters, just as in the case of a quadrature filter with low pass filters, is proportional to the frequency offset.

Based on the analysis made here, the conclusion can be drawn that with completely identical parameters of the functionally similar elements in the channel, the asymmetrical quadrature filter configuration using low pass filters distorts (enriches) the signal spectrum at the output, i.e., as follows from (13), when $\gamma = \eta = 1$ and $\Delta\phi = 0$, the coefficients $K_{n.1.d.} = \cos\phi_0$, and as a consequence, $D_{3\omega_0} = 4Q/\cos\phi_0$.

A characteristic feature of symmetrical quadrature filter circuits where $\gamma = \eta = 1$ is the absence of nonlinear distortions and limitations of the dynamic range, regardless of the phase shift ϕ_0, i.e., $K_{n.l.d.} = 0$, while $D_{3\omega_0} = \infty$. These same properties are also extended to asymmetrical and symmetrical quadrature filters with series connected high and low pass filters in the channels respectively.

An extremely important fact is that when $\gamma \neq 1$ and $\eta \neq 1$, $K_{n.l.d.}$ does not depend on ϕ_0 for symmetrical quadrature filters with low pass filters and depends only slightly on ϕ_0 for symmetrical quadrature filters with high pass filters, something which can be used to widen the tuning range. Considering the minimum impact of temperature drift on the dynamic range, the symmetrical quadrature filter circuit using high pass filters, which provides for a passband type amplitude-frequency response without a region of maximum signal suppression at the quasiresonant frequency, is apparently the promising circuit for IC design as one or more microcircuits. The asymmetrical quadrature filter can find application as a high Q rejection filter when a parallel combination of high and low pass filters are used in its channels [7].

Because of the complexity of precision signal frequency measurement and control, an experimental study was made of a symmetrical quadrature filter using an SSB mixer, which made it possible to precisely lock together the indicated frequencies. The mixer made it possible to obtain the sum or difference of the frequencies generated by the reference voltage generator (G3-7A) and the infralow frequency generator (G3-39) respectively. All of the experimental circuits were designed around the K1NT291 integrated transistor pairs. Multipliers similar to those described in [3, 4], 140MA1 integrated circuits and miniature K50-6 capacitors with a capacitance from 15 to 450 microfarads were used in the symmetrical quadrature filter channels and the SSB mixer. The phase shift of 90° was accomplished by simple differentiating RC networks, tuned to the resonant frequency. The amplitude-frequency responses were recorded at freqeuncies of the reference voltage from 0.2 KHz up to 2 MHz.

The amplitude-frequency response obtained for a first order symmetrical quadrature filter with high and low pass filters for values of $\tau_\phi = 0.05$ sec and $\tau_{h.p.f.} = 1.5$ sec is shown in Figure 5. The signal suppression at the frequencies of spurious resonances amounted to no less than 33 dB, and in this case, the quality factor of the circuit at a frequency of $f_0 = 2$ MHz reached a value of $Q = 3 \cdot 10^5$. Curve 1 in Figure 6 shows the amplitude-frequency response of a first order symmetrical quadrature filter with a high pass filter. The shaded area, the lower boundary of which corresponds to room temperature, indicates the change in the amplitude-frequency response in a temperature range of -60 to +125 °C. Signal suppression outside the transmittance band amounted to -20 dB, which is in good agreement with the conclusions of the theoretical analysis.

Curve 2 in Figure 6 shows the amplitude-frequency response of a two stage symmetrical quadrature filter with high pass filters, which was recorded at room temperature ($K_{sup} \geq 40$ dB). The deviations of the phase shift p_0 and the reduction in the amplitude are one of the reference voltage components lead only to a decrease in $|T(\omega_0)|$ for the same level of nonlinear distortion registered with respect to the amplitude of the low frequency beat frequencies at the output. The dynamic range of the quadrature filter circuits studied here amounted to no less than 60 dB, and in a temperature range of -60 to +125 °C, $|T(\omega_0)| = 2U_{out} = 1.5$ volts.

We will note in conclusion that the most acceptable circuit for IC realization is the symmetrical quadrature filter configuration with high pass filters in the channels, in which at the price of a slight drop in the signal suppression coefficient outside the transmittance band, one can successfully provide for a maximum increase in the temperature stability and the dynamic range, while preserving the bandpass type of amplitude-frequency response.

BIBLIOGRAPHY

1. Finkel'shteyn M.I., "Osnovy radiolokatsii" ["Fundamentals of Radar"], Moscow, Sovetskoye Radio Publishers, 1973, pp 89-91, 111-114.

2. Rigby, "Integrated Selective Amplifiers Utilizing the Principle of Frequency Conversion", ZARUBEZHNAYA RADIOELEKTRONIKA [FOREIGN RADIO-ELECTRONICS], 1967, No 6.

3. Timonteyev V.N., et al., "Proyektirovaniye integral'nykh analogovykh peremnozhiteley signalov" ["The Design of Integrated Analog Signal Multipliers"], "Elektronnaya Tekhnika", "Seriya 3", "Mikroelektronika" ["Electronic Engineering" "Series 3" "Microelectronics"], 1977, No 6 (72).

4. Tarasov V.P., "Kvadraturnyy fil'tr" ["A Quadrature Filter"], IZV. VUZOV - RADIOELEKTRONIKA [PROCEEDINGS OF THE HIGHER EDUCATIONAL INSTITUTES. RADIOELECTRONICS], 1971, 14, No 12, p 1411.

5. Maslennikov V.V., Isaykin V.A., Tarasov V.P., "Izbiratel'nyye RC-Tsepi (obzor)" ["Selective RC Networks (Review)"], PTE [EXPERIMENTATATION INSTRUMENTS AND ENGINEERING], 1974, No 1.

6. Tarasov V.P., "Vozmozhnosti uvelicheniya postoyannoy vremeni RC-tsepey v kanalakh integriruyemykh kvadraturnykh fil'trov" ["The Possibilities of an Increase of the Time Constant of RC Networks in the Channels of Integrable Quadrature Filters"], in the collection, "Izbiratel'nyye sistemy s obratnoy svyaz'yu" ["Selective Systems with Feedback"], Taranrog, TRTI, 1974, No 2, p 106.

7. Tarasov V.P., "Sinkhronno-fazovyy rezhektronyy fil'tr" ["A Synchronous Phase Rejection Filter"], Patent No. 506112, BYULLETEN' IZOBRETENIY [BULLETIN OF INVENTIONS], 1976, No 9.

8225
CSO: 1860

PUBLICATIONS, INCLUDING COLLECTIONS OF ABSTRACTS

UDC 621.396.677.494

ANTENNA SYNTHESIS METHODS: PHASED ANTENNA ARRAYS AND CONTINUOUS-APERTURE ANTENNAS

Moscow METHODY SINTEZA ANTENNA: FAZIROVANNYYE ANTENNYYE RESHETKI I ANTENNY S NEPRERYVNYM RASKRYVOM in Russian 1980 signed to press 2 Oct 79 pp 2-5

[Annotation and table of contents from book by Ye. G. Zelkin, V. G. Sokolov, Sovetskoye radio, 4000 copies, 296 pages]

[Text] A study is made of the methods of determining the amplitudes and phases of antenna excitation currents, the coordinates of the location of its elements and other structural parameters of an antenna to insure the given radiation characteristics. Line, plane and curvilinear microwave antennas are investigated. Special attention is given to antenna arrays. Separate chapters are included on the phase synthesis and synthesis of nonequidistant antenna arrays. Solutions are presented for problems of optimizing antennas in the presence of various restrictions of a physical and technical nature. Along with the classical method of solving synthesis problems, some numerical methods which have been recently developed find reflection in the book. This book is illustrated by a large number of examples of solving various synthesis problems. Many examples in which important practical problems are considered have independent interest.

The book is designed for scientific and engineering-technical personnel engaged in antenna development and postgraduates.

There are 99 figures, 15 tables and 77 references.

Contents

10845
CSO: 1860

UDC 629.7.054

AUTOCOMPENSATION OF DRIFTS OF POWER GYROSTABILIZERS

Moscow AVTOKOMPENSATSIYA UKHODOV SILOVYKH GIROSTABILIZATOROV in Russian 1980 signed to press 24 Apr 80 pp 1, 2, 108, 109

[Annotation and table of contents from book by Georgiy Ambartsulovich Dzhagarov, Mashinostroyeniye, 780 copies, 109 pages]

[Annotation] The book presents theoretical principles of drifts of power gyrostabilizers. Versions of a method of autocompensation are examined, designs of hypothetical gyrostabilizers that realize the method of autocompensation are presented, and drifts as a consequence of deterministic perturbations are determined. An examination is also made of the drifts of various types of biaxial and uniaxial gyrostabilizers due to vibrations of the base relative to the unstabilized axes of the gyrostabilizer. Examples are given of calculation of drifts of various types of gyrostabilizers.

The book is written for engineers who work in the field of designing and studying gyroscopic devices and systems.

Contents

[50-6610]

6610
CSO: 1860

UDC 621.396.98:681.322.05

DIGITAL RADIO NAVIGATIONAL SYSTEMS

Moscow TSIFROVYYE RADIONAVIGATSIONNYYE USTROYSTVA in Russian 1980
signed to press 7 Sep 79 pp 2, 285-287

[Annotation and table of contents from book by V. V. Barashenkov, A. Ye. Lutchenko, Ye. M. Skorokhodov, V. B. Smolov, G. I. Stepashkin, Ye. Ye. Afanas'yev, edited by V.B. Smolov, Sovetskoye radio, 6000 copies, 288 pages]

[Text] In this book a description is presented of prospective digital radio navigation devices and their roles in navigational complexes. A study is made of the standard version of on-board equipment, automated methods of designing it, and the problems of servicing, operating and maintaining it. Flow charts are presented for the algorithms for processing the radio navigation information by computer engineering means. Much attention is given to integrated microcircuits which make it possible to build small, economical on-board radio navigational devices with high operating reliability which are convenient to service.

This book is designed for specialists in the development and servicing of radio navigational devices and will be useful to teachers and students of the navigational departments of the higher institutions of learning.

There are 12 tables, 175 figures and 110 references.

Contents

10845
CSO: 1860

UDC 621.396.6.002:621.9.047

ELECTROCHEMICAL PROCESSING IN THE TECHNOLOGY OF ELECTRONIC EQUIPMENT PRODUCTION

Moscow ELEKTROKHIMICHESKAYA OBRABOTKA V TEKHNOLOGII PROIZVODSTVA RADIOELEKTRONNOY APPARATURY in Russian 1980 signed to press 27 Jun 80 pp 1, 2, 136, 137

[Annotation and table of contents from book by Fedor Vladimirovich Sedykin, Lev Borisovich Dmitriyev, Viktor Vasil'yevich Lyubimov and Valentin Dmitriyevich Strukov, No 19 of the series "Biblioteka tekhnologa radioelektronnoy apparatury" (Library of the Electronic Equipment Technologist), Energiya, 4500 copies, 136 pp]

[Annotation] The book describes electrotechnological processing methods used in the production of electronic equipment. An examination is made of problems of the theory of the process, the feasibility of using electrochemical processing to make fittings and printed-circuit boards, for deburring and marking, data are given on the use of combined electrotechnological processes, and equipment for electrochemical machining is described.

For techologists and engineers in the radio and electronics industry.

Contents

[49-6610]

6610
CSO: 1860

UDC 656.254.16:621.317.2:629.114

MOBILE COMMUNICATIONS CENTER

Moscow AVTOMATIKA,TELEMEKHANIKA I SVYAZ' in Russian No 8, 1980 pp 18-21

[Article by B. P. Rol'shchikov, chief of the communications division of the Signal and Communications Service of Odessa Road]

[Text] The large-scales of introduction of new, more complex equipment have required a basic change in organization of its technical servicing.

Studying the system for servicing the communication systems at the Poletayevskaya and Kartalinskaya ranges of the Southern Urals Road and also considering the experience in the organization of the communications KIP [control and test points] on the Gor'kiy, Moscow and other roads, the collectives of communications specialists of some of the stations on the Odessa Road have gone over to an industrial base for servicing the communications media. At these stations independent communications repair shops (RTTs) have been created, advanced technology has been introduced, and the equipment servicing system has been changed.

The introduction of advanced servicing methods has made it possible sharply to improve the productivity of labor, improve the operating quality of communications equipment and achieve more reliable operation of the devices. The working conditions of the technical personnel have also been improved.

The introduction of new service technology at the Odessa, Odessa-Sortirovochnaya, Pomoshnyanskaya, Nikolayevsk and other stations has made it possible to exclude failures of the equipment at the communication terminals of the train dispatchers, the station and line-track communications. The number of cases of damage to station equipment, power supplies and cable communication lines has been reduced. Thus, at the Odessa-Sortirovochnaya [Odessa Shunting] station in 1979 the number of cases of damage was reduced by 4.3 times by comparison with 1976, and at the Pomoshnyanskaya station, by 11 times in the same period.

The creation of the communications RTTs has permitted technical servicing of the communications equipment to be converted to the centralized method.

Significant remoteness of the communications facilities from the large populated areas and absence of the required number of qualified specialists in the line sections have led to the necessity for organizing mobile groups in the communications RTTs. Such groups have been created at the Odessa, the Nikolayevsk, Pomoshnyanskaya and other stations. Mobile communications centers (PUS-LK) have been designed and built for them. The general view of a PUS-LK appears in Fig 1.

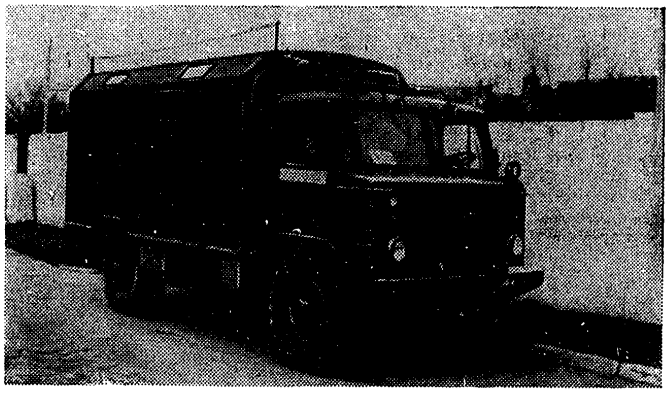

Figure 1. General view of a PUS-LK mobile communications center

The development of the structural design and the circuitry of the mobile communications center was the work of a creative group of road communications specialists. It was headed by chief engineer of the Signal and Communications Service V. M. Petrov. The group included the technical department head of the service E. A. Moshchuk, the communications department head of the service B. P. Rol'shchikov, senior engineer of the communications RTTs of the Odessa-Sortirovochnaya station S. I. Kremen', senior electrician of the communications RTTs of the Bel'tskaya station V. D. Kurbatov, senior electrician of the Odessa station K. D. Mal'tsev, and engineers of the road laboratory of automation, telemechanics and communications. The work was also participated in by the deputy chiefs of the stations with respect to communications and the engineers and senior electricians of a number of stations.

The PUS-LK mobile communications center permits insurance of the following: substitution of unmanned repeaters on the cable trunks multiplexed with K-60, KV-12 and V-3-3 equipment;

Replacement of the communications office equipment of the duty officer for the station with the organization of switch and operating communications of a limited number of subscribers;

Organization of five service connections on the cable trunk with respect to nonloaded pairs with replacement of them by spare pairs. Here, primarily provision is made for train dispatch communications (PDS), power dispatch communications (EDS), electrician's communications (SEM), station communications (PS) and line-track communications (LPS) and TU-TS [radio relay for remote control and remote signalling];

Substitution of the office systems of PSGO fleet public address communications;

Organization of communications between the operations leader from the point of performance of the operations with the department leader, road control and the Ministry of Railways;

Transportation of the replaced stock of dial communications equipment and long distance automatic telephone communications for complex replacement of instruments and also transportation of removable equipment taken out for preventive maintenance.

The substitution of the repeater stations operating on the trunk is being made by the SPUN-1-SK type repeaters available in the PUS-LK with the addition of the DK-88 filters. The presence of remote feed plates in the PUS-LK provides for feeding station power to adjacent unmanned repeaters on the cable trunk. For using the SPUN-1-SK on the trunk multiplexed by K-60 equipment and on the single-cable trunk multiplexed with KV-12 equipment, the DK-88 filter is used. The substitution of the repeater stations of the V-3-3 equipment is being done by equipment of the same time available in the NUP [unmanned repeater station] equipment room.

For replacement of the KASS equipment, the remote PRS-65 and KPS 2/3 panels and the redesigned USVR panels are used. They are connected to the PUS-LK circuitry. As a result of the presence of the multipair PTRK10x2 type cable they can be installed at a significant (up to 100 meters) distance from the place the PUS-LK is parked. The system for organizing the communications with the duty officer with respect to the station at the PUS_LK base is presented in Fig 2.

The communications lines (PDS, EDS, and so on) in one direction from the trunk cable box to a special protection circuit which is part of the equipment room, are connected to the on-board plug of the PUS-LK by PTRK10x2 cable and through the wiring of the PUS-LK equipment room, to the PTDU duplex repeater. The line in the opposite direction is connected through another PTRK10x2 cable to the other side of the same PTDU. The station duty officer line is connected in the wiring of the PUS-LK equipment room and is fed by the PTRK10x2 cable to the PRS-65 and KPS 2/3 panels installed in the station duty officer facility. The schematic of the organization of the PDS circuits is presented in Fig 3. The EDS, SEM and other links are organized analogously with some alterations. The presence in the equipment room of the required number of PTDU repeaters permits restoration of all of the technological communications on the trunk.

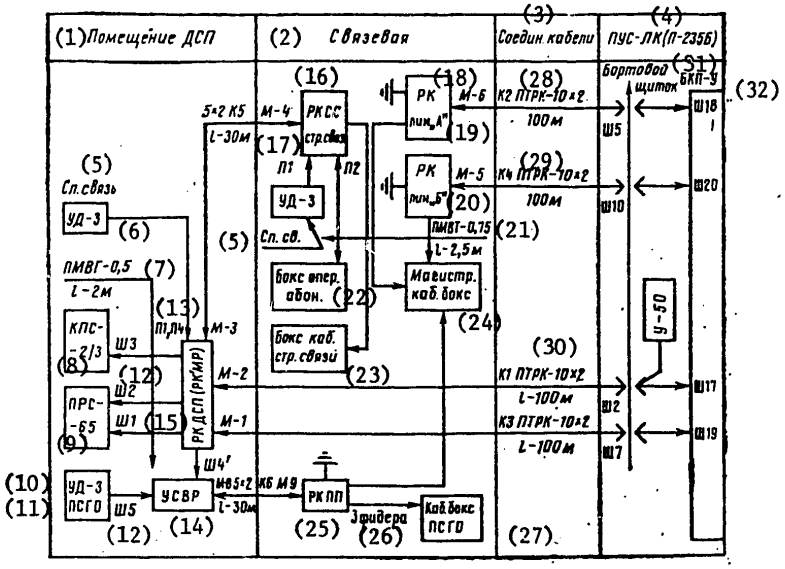

Figure 2. Schematic of the organization of the DSP [duty switchman's] communications

Key:

1. DSP facility
2. Communications office
3. Trunk cables
4. PUS-LK(P-235B)
5. Link between operators
6. UD-3
7. PMVG-0,5
8. KPS-2/3
9. PRS-65
10. UD-3
11. PSGO
12. Sh...
13. P1, P4
14. USVR
15. RK DSP(RK'MR)
16. RKSS
17. Switch communications
18. RK
19. Line A
20. Line B
21. PMVT-0,75
22. Operating subscriber box
23. Switch communications cable box
24. Trunk cable box
25. RKPP
26. 3 feeders
27. PSGO cable box
28. K2 PTRK-10x2
29. K4 PTRK-10x2
30. K1 PTRK-10x2
31. On-board panel
32. BKP-U

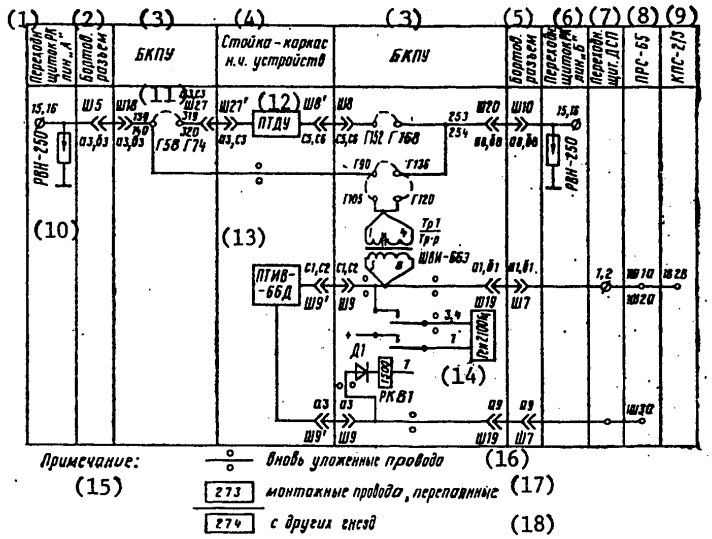

Figure 3. PDS [dispatch communications] system

Key:

1. RK line A junction panel
2. On-board plug
3. BKPU
4. Low-frequency circuit bay-flame
5. On-board plug
6. RK line B crossover panel
7. SP crossover panel
8. PRS-65
9. KPS-2/3
10. RVN-250
11. Sh ... = switch
12. PTDU
13. PTIV-66D
14. 2100 hertz oscillator
15. Note:
16. Newly laid lines
17. Resoldered wiring
18. Fron other jacks

Guaranteed servicing of the small automatic telephone offices with replacement of the DATS-60 sets and also replacement of the telephone sets of the operating communications and testing locally with respect to the PUS-LK instruments of the low-active sets without removal from the work places are carried out simultaneously (according to the annual schedule).

The replacement of the PSGO repeater for preventive maintenance is provided by the U-50 repeater installed in the PUS-LK. Here provision is made for connection of two switchable feeders with loudspeakers installed at the office to the repeater. The feeders are switched by the switches installed on the USVR panel (PSGO plate). For conversations, the station duty officer uses the UD-3 repeater, the control of which is by the switch on the USVR plate.

The intermediate sets are removed and sent for testing under the stationary conditions of the RTTs. Adjusted and tuned intermediate stations transferred from the RTTs to the PUS-LK are installed in their place.

The replacement of the communications equipment of the station duty officer by the equipment installed in the PUS-LK offers the possibility of performing any operations in the office communications circuits without disrupting the operation of the office. The replaced UKSS-6, PTDU and other equipment can be dismantled and replaced by other equipment or adjusted carefully in place. Prolonged interruptions of the communications between the station duty officer and the dispatcher or the office facilities are excluded.

All of the devices and instruments of the PUS-LK are mounted in the GAZ-66 truck bed. A K-66 type bed is used. It is sealed to keep dust from getting into the equipment room when moving the truck to the work place.

The arrangement of the equipment is shown: in front (Fig 4), on the left side (Fig 5), on the right side (Fig 6). An overall view of the equipment room appears in Fig 7.

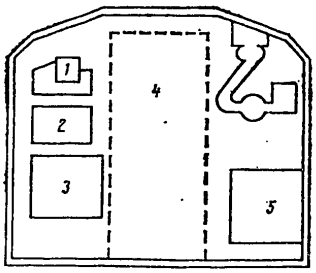

Figure 4. Arrangement of the equipment in the front of the truck body:
1 -- fan; 2 -- pharmacy; 3 -- spare parts box; 4-- SPUN-1-SK equipment; 5 -- ShchPOV panel

SPUN-1SK equipment is installed in the front part of the truck body. It is fastened to the front wall.

The PTDU type repeaters, the PTIV-66 harmonic selective signalling receivers and also the BV-24/2,5 and VSP 220/1,1 rectifiers are mounted on special bay-frames. The bay-frames are made of steel angles and installed on the left and right sides.

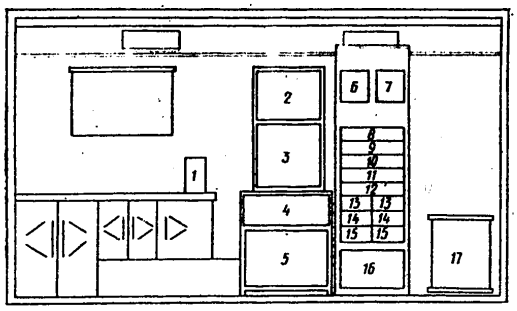

Figure 5. Arrangement of equipment on the left side of the truck body:
1 -- R-5-5 measuring instrument; 2 -- UU-110 level indicator; 3 -- LIG-60 oscillator; 4,5 -- P-303 equipment; 6, 7 -- PTIVy; 8-12 -- PTDU-67 repeater; 13-15 -- BOK, BRK remote feed plates; 16 -- VSP 220/1,1 rectifier; 17 -- cable

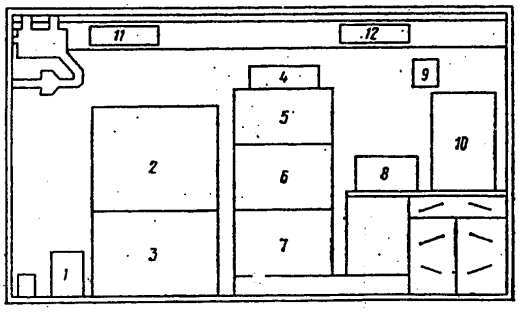

Figure 6. Arrangement of equipment on the right side of the truck body:
1 -- NO 24 V rectifier; 2 -- seat back; 3 -- container seat; 4 -- measuring instrument; 5, 6 -- switchboard; 7 -- PUS-LK power unit; 8 -- ZhR-3M power unit; 9 -- talk set; 10 -- ZhR-3M radio; 11, 12 -- window

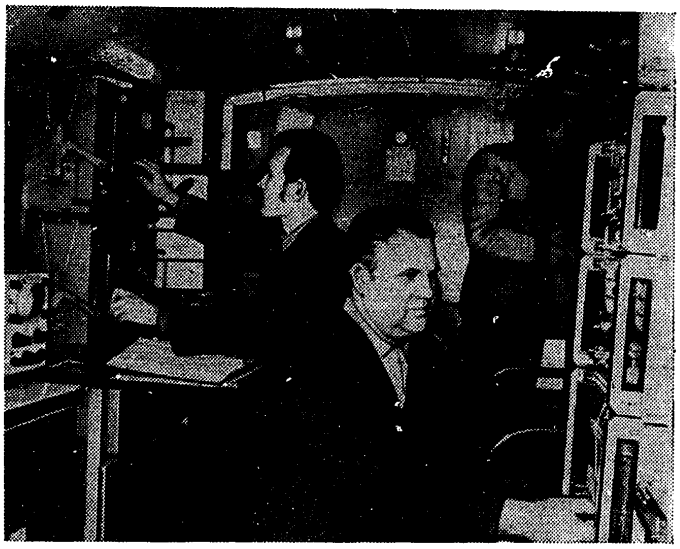

Figure 7. General view of the equipment room

The BKP-U type bay with variable wiring of the receptacles and plugs is used as the lead-in and switching equipment. The GS-300 oscillator and SPU-300 level indicator are used as measuring instruments.

The equipment is fastened to the floor and the sides of the body being sure to maintain the seal of the body.

The electric power supply for the PUS-LK communications equipment is provided by a bank of storage batteries consisting of 60 amp-hour alkaline batteries operating in the buffer mode. As the buffer rectifier in the PUS-LK equipment room the BV-24/2,5 rectifier is installed with the addition of an electronic voltage stabilization circuit to it. These power supplies feed the PTDU-M repeaters, the PTIV-66 harmonic signalling system receivers and also the remote devices installed at the office duty officer. The power supply for the AC equipment comes from the I-300-U inverter which operates from the truck engine shaft. In all of the rest of the cases the AC feed is from the external 220 volt electrical network. The connection of the equipment room to the AC network in this case is made by a power cable. It must be noted that the presence of storage batteries in the PUS-LK makes it possible also to provide electric power for the office communications equipment at the railroad station and, consequently, to disconnect the office storage battery and perform the required preventive operations.

The PUS-LK mobile communications center is subordinate to the communications RTTs section chief. The operating schedule is compiled by the RTTs section leader and is approved by the road department chief. This offers the possibility at the small railroad stations for the PUS-LK brigade to provide the station duty officer with communications from a remote panel and to perform the required operations. When compiling the schedule, consideration is given to the set of operations at the office (measurement of circuits and cables, preventive maintenance of the KASS equipment, replacement of the DATS devices, and so on).

The annual schedule is compiled on the basis of the requirements of the "Instructions for Technical Servicing of Wire Communications Systems" No TsSh/3417. Beginning with the annual schedule, monthly schedules for making calls are compiled. The makeup of the brigade for performing operations in the current month is also taken into account here.

The field brigade for the PUS-LK includes RTTs specialists in measuring communication cables, performing preventive maintenance on the selective communications systems, the KASS equipment and electric power supply devices. The brigade has a total of four people. The electrician for the electric power supply units is simultaneously the PUS-LK driver. Practice has demonstrated that this version of combining specialties is the most expedient. The local electrician also participates in the tuning, adjustment and testing of the communications equipment at the office. He makes all of the required entries in the station log.

An entry on the performed operations is also made in the PUS-LK log. The volume and the quality of these operations are confirmed by the signature of the local electrician or the senior section electrician.

The field brigade works on the line approximately 2 weeks out of the month. The rest of the time the brigade checks out and adjusts the removable modules of line equipment in the substitution stock under the stationary conditions of the RTTs. The same brigade checks out and performs preventive maintenance on the PUS-LK equipment.

The practice in operating the mobile communications center at the Odessa station has demonstrated that its use greatly improves the technical condition of the communications media at the small railroad stations. As a result of planned technical servicing of the communications equipment by the RTTs field brigade in 1978-1979, no damage to the station units was permitted.

However, not all of the stations on the road use this method of servicing communications at the railroad station. The basic cause for slow introduction of the PUS-LK is the absence of the required number of transport vehicles (trucks with sealed bodies), shortage of products and equipment to set them up (first of all the SPUN-1-SK repeaters, measurement equipment and switching modules).

On introduction of the PUS-LK it is necessary to warn against certain extremes. The directors of some of the stations at times try to load the mobile communications center down with an extremely large number of additional functions such as the repair and servicing of the train radio communications devices, provision of communications in the track repair section, servicing of the PONAB, checking out the measuring equipment, and so on.

This leads to great difficulties in resolving the structural makeup of the already mixed center. The center becomes overloaded with equipment, and it is extremely complicated to arrange it in the body. In addition, the performance of a large number of functions will lead to an increase in the number of people in the field brigade and the necessity for increasing the number of seats. This gives rise to complications in providing for the transportation of people. The application of one brigade for a large number of different operations causes difficulties in the technological level. It is necessary to define the work of each member of the brigade so that all will be loaded an identical amount of the time. Otherwise, there will be great losses of work time.

The industrial method of servicing communications equipment has found broad application on the railroad network. Its further improvement will be promoted by the introduction of the mobile communications centers. It will be expedient to create a standard mobile communications center, the development of which should be the responsibility of the KB TsSh design office or any other structural design organization. The technical drawings of the PUS-LK mobile communications center developed on the Odessa road can be taken as the basis for these developments.

[48-10845]

10845
CSO: 1860

PIEZOMAGNETIC CERAMICS

Leningrad P'YEZO-MAGNITNAYA in Russian 1980 signed to press 12 Dec 79 pp 204-206

[Annotation and table of contents from book by L. N. Syrkin, Energiya, 2d edition revised and supplemented, 3,700 copies, 208 pages]

[Text] A discussion is presented of the physical principles of the application of piezomagnetic ceramic materials (ferrites) in electroacoustics, ultrasonic and other fields of engineering. The problems of the theory of piezomagnetic oscillations in ferrites, the methods of measuring their parameters and the results of investigating the magnetic, mechanical and electromechanical (piezomagnetic) properties are considered. Reference material is presented. The first edition was published in 1972. The second edition includes a section on magnetoelastic properties of ferrites. Summary tables of parameters and so on are presented.

The book is intended for engineers and scientific workers specializing in electroacoustics, ultrasound, measurement engineering and the physics of magnetic materials. It can also be useful to postgraduates and students at the institutions of higher learning.

Contents

10845
CSO: 1860

UDC 681.84.081

RESOLUTION OF MAGNETIC RECORDING SYSTEMS

Moscow RAZRESHAYUSHCHAYA SPOSOBNOST' SISTEM MAGNITNOY ZAPISI in Russian 1980 signed to press 29 Jan 80 pp 1, 2, 113

[Annotation and table of contents from book by Yuriy Leonidovich Bogorodskiy, Energiya, 10,000 copies, 113 pages]

[Annotation] The book examines factors that influence the resolution of magnetic recording systems. Major emphasis is placed on analysis of various kinds of losses that arise in magnetic heads and recording media. The part played by active losses in an induction magnetic head is most completely demonstrated as the main factor that limits the theoretical resolution of the head.

The book is intended for engineering and technical workers engaged and the development and use of magnetic recording devices.

Contents

[54-6610]

6610
CSO: 1860

RADARS, RADIONAVIGATION AIDS, DIRECTION FINDING, GYROS

UDC 538.574.4:621.371.22

CHARACTERISTICS OF THE SEA WAVE IMAGE IN SIDE-LOOKING, SYNTHETIC-APERTURE RADAR

Kiev IVUZ RADIOFIZIKA in Russian Vol 23, No 8, 1980 pp 923-933 manuscript received 2 Apr 79
[Article by A. V. Ivanov, Institute of Radio Engineering and Electronics of the USSR Academy of Sciences]

[Text] On the basis of two-scale scattering model a study was made of the defocussing of the wave image connected with displacement of the waves, and some of the characteristics of the image brightness modulation caused by periodic variation of the velocities of elements of the suface layer.

Introduction

It has been demonstrated in a number of papers that it is possible to obtain very interesting information about the ocean surface by side-looking radar (RBO) [1-4]. Side-looking synthetic aperture radar (RSA) is prospective for use on oceanographic artificial earth satellites. This radar makes it possible to obtain a high-resolution image independently of the distance to the ocean surface with small dimensions of the real aperture. The resolution restrictions of RSA when observing stationary formations on the surface of the sea were investigated in reference [5].

One of the useful characteristics of RSA is the possibility of direct observation of quite long wind-driven waves and swells, measurement of their length and propagation direction. However, waves are not a stationary formation in the sense that the statistical parameters of the surface determining the scattering of the electromagnetic waves depend not only on the spatial coordinates, but also on time. Therefore the conclusions of reference [5], generally speaking, are inapplicable to the process of formation of the sea wave image in RSA.

In reference [7] a description is presented of an experiment demonstrating that the image of a wave system is defocused just as the image of a target moving with some velocity w parallel to the heading of the RSA carrier. The value of w in this case is close to the value of the projection of the phase velocity of the waves on the carrier course line. Focussing is restored by introducing the corresponding changes into the primary image processing system parameters. In explaining the experiment, the author proposes that all of the values describing the sea surface depend cylindrically on the coordinates and time: $f(K_{0x}+K_{0y}y-\omega t)$,

that is, they do not depend on the displacement in the direction perpendicular to the propagation direction K_0. Therefore the proposed explanation turns out to be unconvincing.

The presented interpretation is a special case of the model presupposing plane-parallel transport of a surface with wave phase velocity $v = \frac{\omega}{K_0}\frac{K_0}{K_0}$ (see, for example [8]). However, in this case the frequency of the back-scattered signal must be shifted on the average by $2v_r/\lambda$, where λ is the wavelength of the radio-emission, v_r is the projection of v in the direction of propagation of the radiation, which contradicts numerous experiments with respect to measuring the doppler shift indicating that the average shift is determined by the phase velocity of the resonance component of the swell and the drift velocity of the surface layer, which as a rule, are much less than the phase velocity of the predominant wave system [9-14].

Then the RSA, in contrast to incoherent RBO are sensitive not only to variation of the local angle of inclination of the surface and the variation in intensity of the resonance component of the swell on a large wave, but also the variation of the phase velocity of the resonance component caused by orbital movement in the surface layer. The possibility of additional brightness modulation of the image connected with the velocity gradients of the surface layer was indicated previously in references [4, 6], but the common characteristics of this modulation, the dependence of its parameters on the wave parameters were not presented.

In the proposed paper a theoretical study is made of the defocussing of the image connected with displacement of the wave and certain peculiarities of the "velocity" brightness modulation of the image. The analysis is based on a two-scale model of the scattering of ultrashort wave radiation by the wavy sea surface which today agrees most completely with the experimental data.

1. Wave Image Defocussing

In accordance with the two-scale model, the field backscattered by the sea surface can be written in the form

$$E(t) = \int_S e^{i\varphi(\rho,\ t)} F_0(\rho,\ t)\, e^{2ikr'(\rho)}\, z(\rho,\ t)\, d\rho,$$

where S is the illuminated section, $\rho = \{x, y\}$ are the coordinates of a point on the mean surface, $k = 2\pi/\lambda$, $\phi = -2kh(\rho, t) \sin\theta$ is the phase shift related to a large wave, h is the deviation of the surface level from the mean as a result of the large wave, θ is the mean glancing angle, F_0 is the coefficient describing the intensity of the back-scattered signal as a function of the local glancing angle, r' is the distance from the radiator to the point ρ of the mean plane, z is the variation of the level as a result of the small-scale component of the wave action (see the papers on the two-scale model in the bibliography [5, 13]).

The expression for the mean optical density with respect to a set of realizations of the image of a given surface obtained in RSA will have the form [5]

$$\langle P(x_0,\ y_0)\rangle \sim \int u(x_0 - x_1)\, u(x_0 - x_2)\, F\left(\rho_1,\ \frac{y_0 + \xi_1}{V}\right)\times$$

$$\times F^{*}\left(\rho_2,\ \frac{y_0+\xi_2}{V}\right)\exp\{2ik(x_1-x_2)\cos\theta\}\times$$

$$\exp\left\{\frac{ik}{r(x_0)}\left[(y_0+\xi_1-y_1)^2-(y_0+\xi_2-y_2)^2-a(\xi_1^2-\xi_2^2)\right]\right\}\times \qquad (1)$$

$$\times\left\langle z\left(\rho_1,\ \frac{y_0+\xi_1}{V}\right)z\left(\rho_2,\ \frac{y_0+\xi_2}{V}\right)\right\rangle d\rho_1\,d\rho_2\,d\xi_1\,d\xi_2,$$

where x_0, y_0 are the coordinates of a point in the image, the y-axis is directed along the course line of the carrier, $t = y_0/V$, V is the velocity of the carrier, u(x) is the range pulse characteristic of the RSA, $F = F_0 e^{i\Phi}$, r is the distance from the station to the point of the mean plane with the coordinates x_0, y_0.

The pulse characteristic of the primary image processing filter has the form $\exp\left[\frac{ik}{r(x_0)}ay^2\right]$ for $|y| < Vt_c/2$, where t_c is the coherent accumulation (synthesis) time, and a is a dimensionless coefficient. For a = 1 the filter is matched to the signal from a stationary target. The integration limits with respect to ξ_1 and ξ_2 are from $-Vt_c/2$ to $Vt_c/2$. The integration limits with respect to y_1 and y_2 are assumed to be infinite, for usually the observation time of any point of the surface is appreciably longer than the synthesis time. The limits are also infinite with respect to x_1 and x_2.

Hereafter, we shall consider one line of the image with respect to range, setting x_0 = const. Apparently, the slow variation of the intensity of a small-scale ripple on a large wave can be considered by writing

$$\langle z(\rho_1,\ t_1)\,z(\rho_2,\ t_2)\rangle = \sigma_0(\rho_1,\ t_1)\,\sigma_0(\rho_2,\ t_2)\,R(\rho_1-\rho_2,\ t_1-t_2),$$

where R is the normalized correlation function and σ_0 varies much more slowly than R. The mean statistical value of the intensity of the ripple σ_0 at some point of the surface with the coordinates ρ also depends on the position of this point on the large wave. The value of F(ρ, t) depends only on the large-scale wave action by definition. Then, assuming a strictly cylindrical shape of the large-scale wave action, it is possible to write $F\sigma_0 = \sigma(K_0\rho - \omega t)$.

Let us consider the value of the surface deviation from the mean level normalized for σ_0 as a result of the small-scale component. If in the absence of a large wave this value has the form $z_H(\rho, t)$, then on a large wave it is written as $z_H(\rho - st, t)$, where $s = s(K\rho - \omega t)$ is a vector in the plane x, y, the components s_x and s_y of which are equal to the projections of the orbital velocity on the plane tangent to the large-scale wave in the directions perpendicular and parallel to the heading, respectively. Of course, we shall consider that s(ρ, t) varies much more slowly than $z_H(\rho, t)$. Now the normalized correlation function assumes the form

$$R = R\left[\rho_1-\rho_2-s(\rho_1,\ t_1)t_1+s(\rho_2,\ t_2)t_2,\ t_1-t_2\right].$$

Let us substitute the indicated expression for σ and R in (1), substituting $(y_0 + \ _i)/V$ for t_i. Then, in the integral (1) we set $\exp\left\{\frac{ik}{r}[(y_0 - y_1)^2 - (y_0 - y_2)^2]\right\} \approx 1$ (see [5]), we replace the variables: $y_i' = y_i - \frac{v^{(y)}}{V}(y_0 + \xi_i)$, where $v^{(y)} = \omega/K_{0y}$, we compress (extend) the scale of the image with respect to y:

$$y_0\left(1 - \frac{v^{(y)}}{V}\right) \to y_0.$$

As a result, we obtain, considering $v^{(y)} \ll V$,

$$\langle P(x_0, y_0)\rangle \sim \int u(x_0 - x_1)u(x_0 - x_2)\exp[2ik(x_1 - x_2)\cos\theta] \times$$
$$\times \exp\left\{\frac{ik}{r}\left[2(y_0 - y_1')\xi_1 - 2(y_0 - y_2')\xi_2 + \left(1 - a - \frac{2v^{(y)}}{V}\right)(\xi_1^2 - \xi_2^2)\right]\right\} \times$$
$$\times \sigma(\rho_1')\sigma(\rho_2')R_3\Big[x_1 - x_2 - \frac{s_{x1}}{V}(y_0 + \xi_1) + \frac{s_{x2}}{V}(y_0 + \xi_2), \qquad (2)$$
$$y_1' - y_2' + \frac{v^{(y)}}{V}(\xi_1 - \xi_2) - \frac{s_{y1}}{V}(y_0 + \xi_1) + \frac{s_{y2}}{V}(y_0 + \xi_2),$$
$$\frac{\xi_1 - \xi_2}{V}\Big] d\rho_1' d\rho_2' d\xi_1 d\xi_2,$$

where $\rho' = \{x, y'\}$, $s_{x,yi} = s_{s,v}(\rho_i')$.

Let us substitute the variables

$$y_1' - y_2' = 2\eta, \qquad x_1 - x_2 = 2\chi,$$
$$y_1' + y_2' = 2y, \qquad x_1 + x_2 = 2x.$$

It is possible to postulate that $R(\chi, \eta, t)$ decreases to zero more rapidly than σ, u and s vary as functions of the same variables, and on integration with respect to χ and η it is possible to set $\chi = \chi_0$, $\eta = \eta_0$ in the arguments σ, u, s, where χ_0, η_0 are values for which the arguments R are equal to zero. In turn, for $t_c \ll T$, where T is the wave period, and for $s_x t_c$ much lower than the range resolution, it is possible to consider $|\sigma(\chi_0, \eta_0)| \approx |\sigma(0, 0)|$ and $u(\chi_0) \approx u(0)$ in the entire integration region with respect to ξ_1 and ξ_2. Let us also set $s(\chi_0, \eta_0) \approx s(0, 0)$. Then

$$2\chi_0 = \frac{s_x(\rho)}{V}(\xi_1 - \xi_2),$$
$$2\eta_0 = \frac{s_y(\rho) - v^{(y)}}{V}(\xi_1 - \xi_2).$$

Let us expand the phase ϕ in a series with respect to powers of χ_0, η_0 in the vicinity of the point x, y limiting ourselves to the linear terms:

$$\varphi(x+\chi_0,\ y+\eta_0)-\varphi(x-\chi_0,\ y-\eta_0)\approx\frac{2k}{V}(\xi_1-\xi_2)\sin\theta\left[\frac{\partial h}{\partial x}s_x+\frac{\partial h}{\partial y}(s_y-v^{(y)})\right].$$

In the coordinate system used for integration which is moving with a velocity $v^{(y)}$ parallel to the heading, the orbital velocity vector must lie in the plane tangent to the surface, at each point of the surface inasmuch as the form of the surface does not change in time; s_x and $s_y - v^{(y)}$ are components of this vector in the tangential plane, and, consequently, the value in brackets is equal simply to the vertical component of the orbital velocity s_z. Summing up, we obtain

$$\varphi(x+\chi_0,\ y+\eta_0)-\varphi(x-\chi_0,\ y-\eta_0)\approx\frac{2k}{V}(\xi_1-\xi_2)\,s_z\sin\theta.$$

The integral (2) now assumes the form

$$\langle P(x_0,\ y_0)\rangle\sim\int\Phi u^2(x_0-x)\,|\,\sigma(\rho)\,|^2\exp\left\{\frac{ik}{r}\left[2\left(y_0-y-\right.\right.\right.$$

$$\left.\left.\left.-\frac{r}{V}s_z\sin\theta\right)(\xi_1-\xi_2)+\left(1-a-\frac{2v^{(y)}}{V}\right)(\xi_1^2-\xi_2^2)\right]\right\}d\rho\,d\xi_1\,d\xi_2\,d\eta\,d\chi,$$

where

$$\Phi=\exp(4ik\chi\cos\theta)\exp\left[-\frac{2ik}{r}\eta(\xi_1+\xi_2)\right]\times$$

$$\times R\left[2\chi-\frac{s_x}{V}(\xi_1-\xi_2),\ 2\eta-\frac{s_y-v^{(y)}}{V}(\xi_1-\xi_2),\ \frac{\xi_1-\xi_2}{V}\right].$$

Let us form the integration with respect to χ and η:

$$\int\Phi\,d\chi\,d\eta=\tilde{R}_{12}\left[2k\cos\theta,\ \frac{k}{r}(\xi_1+\xi_2),\ \frac{\xi_1-\xi_2}{V}\right]\times$$

$$\times\exp\left[2ik\cos\theta\,\frac{s_x}{V}(\xi_1-\xi_2)\right]\exp\left[\frac{ik}{r}\,\frac{v^{(y)}-s_y}{V}(\xi_1^2-\xi_2^2)\right]\approx \tag{3}$$

$$\approx\tilde{R}(2k\cos\theta,\ 0)\exp\left(i\Omega_0\,\frac{\xi_1-\xi_2}{V}\right)\exp\left[2ik\cos\theta\,\frac{s_x}{V}(\xi_1-\xi_2)\right]\times$$

$$\times\exp\left[\frac{ik}{r}\,\frac{v^{(y)}-s_y}{V}(\xi_1^2-\xi_2^2)\right].$$

Here $\tilde{R}$ is the spatial spectral density of the small-scale part of the wave; the Fourier transform R with respect to the first two variables is designated by $\tilde{R}_{12}$.

The second argument $\tilde{R}$ is replaced by zero inasmuch as $(k/r)Vt_c$ (the maximum value of $|\xi_1 + \xi_2|$ in the integration region is Vt_c) is much less than the width of $\tilde{R}$ with respect to y [5], $\Omega_0 = \Omega_0(2k\cos\theta, 0)$ is the natural oscillation frequency of the resonance component of the ripple.

Substituting (3) in (2), we finally obtain

$$\langle P(x_0, y_0)\rangle \sim \iint_{-\infty}^{\infty} d\rho\, |\sigma(\rho)|^2 u^2(x_0 - x) \times$$
$$\times \int_{-Vt_c/2}^{Vt_c/2}\int \exp\left\{\frac{2ik}{r}\left[(y_0 - y - \Delta)(\xi_1 - \xi_2) + \right.\right. \tag{4}$$
$$\left.\left. + \frac{1}{2}\left(1 - a - \frac{v^{(y)} + s_y}{V}\right)(\xi_1^2 - \xi_2^2)\right]\right\} d\xi_1 d\xi_2,$$

where

$$\Delta = \frac{r}{V}\left[-\frac{\Omega_0}{2k} - s_x\cos\theta + s_z\sin\theta\right] = \frac{r}{V}\left[-v_\phi\cos\theta + s_r(\rho)\right],$$

v_ϕ is the natural phase velocity of the resonance component, s_r is the projection of the orbital velocity in the direction of the station (the x-axis is directed away from the path line, the z-axis is directed upwards).

The presence of the value of $\Delta(\rho)$ in the exponent indicates distortion of the grave image connected with orbital movement (see below), and the quadratic phase factor describes the defocussing of the image. Let us remember that the value of a = 1 corresponds to ordinary tuning of the filter to observation of the stationary surface; $v^{(y)} = s_y = 0$.

Generally speaking, inasmuch as the value of s_y depends on the coordinates, it is entirely impossible to restore the focussing by varying the value of a. However, since the values of the orbital velocity are usually significantly lower than $v^{(y)}$, it is possible to state that the best focussing can be achieved near the value

$$a = 1 - \frac{v^{(y)}}{V} \tag{5}$$

or in any case for some a in the limits

$$1 - \frac{v^{(y)} + |s_y|_{\max}}{V} < a < 1 - \frac{v^{(y)} - |s_y|_{\max}}{V}.$$

Here, the resolution of the system becomes somewhat worse, and it depends on the oscillation amplitude s_y. For

$$|s_y|_{\max} t_c < \Delta y_0, \tag{5a}$$

where $\Delta y_0 = \frac{r}{V}\frac{\lambda}{t_c}$ is the resolution of the RSA with respect to the stationary surface, it is possible to neglect the worsening of the resolution ([16], page 173).

In the case of plane-parallel the displacement of the observed surface in the direction y with the velocity w, the best focussing is reached for $a = 1 - 2w/V$. This result is easily obtained, for example, setting $z = z(x, y - wt)$ in the initial integrals. This means that the processing system characterized by the coefficient [5] is also focused on observation of a surface moving parallel to the heading with a velocity $w = v^{(y)}/2$. Let us remember that $v^{(y)} = \omega/(K_0 \cos \alpha)$ is the phase velocity of the wave formed by the section of the investigated three-dimensional wave by the plane x = const (K_0 is the wave vector, α is the angle between K_0 and the y-axis). In reference [7], the achievement of the best focussing is predicted for tuning of the processing system to the velocity $w = v_y = \omega \cos \alpha/K_0$. In order to make a choice in favor of one of the two indicated values of w, additional experiments are needed.

For completely isotropic small-scale waves, the expression of [3] must be supplemented by a second term of the same type, but with opposite sign Ω_0. This means that on the average the wave image will be the sum of two identical images shifted with respect to y in opposite directions with respect to the true position by $\Delta_c = \frac{r}{V} v_\phi \cos \theta$, and the wave image disappears for $2\Delta_c = \Lambda_y/2 = \pi/K_{0y}$, which corresponds to values of $\Lambda_y = 100$ to 150 meters for $\lambda = 3$–25 cm, $r/V = 100$ second and $\theta = \pi/4$. Within the framework of the given model this is the primary restriction on the resolution of the RSA when observing cylindrical waves.

Expression (4) relates the wave and image characteristics nonlinearly, that is, if the waves are formed by two cylindrical systems with essentially different values of $v^{(y)}$, the image of neither of them can be focused as in the absence of the other, or, in other words, the integral (4) cannot be represented in the form of the sum of two terms, in one of which time is excluded. This also pertains to the case of observation of a stationary formation on the sea surface (a system with $v^{(y)} = 0$) under wave conditions with which a somewhat different approach to this problem and additional restrictions on the resolution are related [5].

Finally, let us note that even for $|\sigma| = \text{const}$ and $\Delta = 0$ the integral (4) depends on x_0, y_0 as the result of the presence in it of the function $s_y(\rho)$, that is, a different position of the image focal point for different sections of the wave can theoretically lead to brightness modulation of the image [4, 17]. However, this modulation mechanism must not play a significant role inasmuch as the condition (5a), as a rule, is satisfied.

Let us estimate the error contained in the approximation $s(\chi_0, \eta_0) \approx s(0, 0)$. For this purpose, in the arguments R let us consider the terms of the first order of the expansion of s with respect to χ_0, η_0, defining the values of χ_0, η_0 as before with an accuracy to the zero-order terms of the same expansion. The most significant among the additional terms obtained as a result have the form $\frac{\partial s_x}{\partial y}\frac{v}{V^2}$ $y_0(\xi_1 - \xi_2)$ and $\frac{\partial s_x}{\partial y}\frac{v}{V_2}\xi_2^2$ (here $v^{(y)} \approx v$ is the wave phase velocity). The first of them leads to the appearance of the factor $\left(1 + \frac{r}{V}\frac{v}{V}\frac{\partial s_x}{\partial y}\right) y_0$ in the right-hand side

of (4). This factor does not play a role even for observations from an aircraft and disappears on observation from space. The second of the additional terms gives a disappearing term also in the exponent for observations from space. The second gives a term of the type $ik\frac{\partial s_x}{\partial y}\frac{v}{V^2}\xi_2^2$ in the exponent. Requiring that for all ξ it be less than one, setting $\left|\frac{\partial s_x}{\partial y}\right|_{max} \approx \frac{|s|_{max}}{\Lambda}$ and $|s|_{max} \approx cv$, we obtain the condition $t_c^2 < \lambda/cg$, where g is the gravitational acceleration, $c \approx 0.2$ for developed wave action (see below) and still less for ripple. An analogous condition figures in [5] as a result of the effect of the nonlinearity of the movement of the reflectors and can significantly limit the resolution.

The quadratic terms in the expansion of s and the third-order terms in the expansion of ϕ (it does not contain quadratic terms) impose weaker restrictions on the synthesis term.

2. Image Brightness Modulation by Orbital Movement

Let in the integral (4) $a = 1 - v^{(y)}/V$, and the condition (5a) be satisfied. Then, assuming very high resolution of the RSA with respect to both coordinates and omitting the parameter x_0, from (4) we obtain

$$\langle P(y_0)\rangle = \rho(y_0) = \int_{-\infty}^{\infty} \rho_0(y)\,\delta[y_0 - y - \Delta(y)]\,dy, \tag{6}$$

where $\rho_0(y) = |\sigma(y)|^2$. It is necessary to compare the optical density of the image obtained using the RSA, that is, $\rho(y)$ with the optical density obtained using the ordinary RBO, that is, with $\rho_0(y)$. It is possible to write

$$\rho(y_0) = \int_{-\infty}^{\infty} \rho(y')\,\delta(y_0 - y')\,dy' = \int_{-\infty}^{\infty} \rho(y+\Delta)\left(1 + \frac{d\Delta}{dy}\right)\delta(y_0 - y - \Delta)\,dy, \tag{7}$$

where $y' = y + \Delta(y)$.

Comparing (6) and (7), for $\rho(y)$ we obtain

$$\rho(y+\Delta) = \rho_0(y)\left(1 + \frac{d\Delta}{dy}\right)^{-1} \tag{8}$$

or, what amounts to the same thing,

$$\rho(y')dy' = \rho_0(y)dy, \quad y' = y + \Delta(y). \tag{9}$$

(see also [4, 6]).

This means that in the synthesized image each point is carried over from position y to the position $y + \Delta(y)$ by comparison with the image obtained on the incoherent RBO, and equation (9) describes the variation of the linear density of the points occurring in this case.

If the values of $\Delta'(y) < -1$ are encountered, then, first, $\rho(y)$ is ambiguous, and, secondly, it has negative branches. In Figure 1 (the dotted line) the form of the

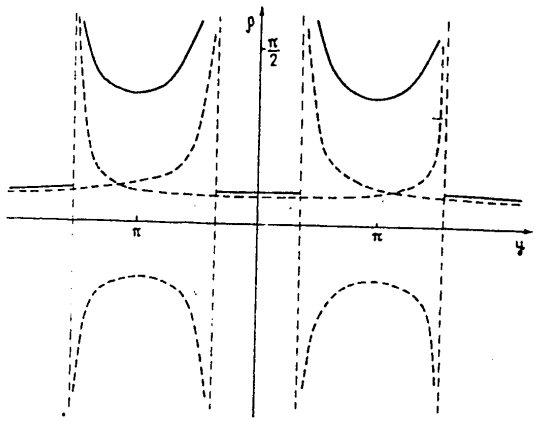

Figure 1.

function $\rho(y)$ defined from formula (8) for $\rho_0 = 1$ and $\Delta = \pi \sin y$ is depicted as an illustration. Returning to the problem of conversion of the linear plane of the points, it is easy to see that equation (8) must in this case be satisfied:

$$\rho(y) = \sum_n |\rho_n(y)|, \tag{10}$$

where ρ_n are different branches of the function (8). The solid curve in the figure corresponds to this predetermination of the function $\rho(y)$.

The spectrum of the function $\rho(y)$

$$\tilde{\rho}(\varkappa) = \int_{-L}^{L} \rho(y') \exp(-i\varkappa y')\, dy',$$

where 2L is the line length. If the transformation $y(y')$ is unique, then, proceeding from y' to y, we obtain

$$\rho(\varkappa) = \int_{L_1}^{L_2} \rho_0(y) \exp[-i\varkappa y - i\varkappa\Delta(y)]\, dy. \tag{11}$$

By subsitution of variables within the limits of the uniqueness sections it is easy to see that the expansion of (11) remains valid also for the ambiguous function $y(y')$ for the function $\rho(y)$ defined in accordance with the expressions (8) and (10).

Let us first postulate that $\rho_0 = \text{const}$ and $\Delta = \Delta_0 \sin K_{oy} y$ (the constant component plays a role). Obviously, in this case the function $\rho(y)$ is periodic with the period $2\pi/K_{0y}$ and the coefficients of its expansion in a series are

$$\tilde{\rho}_n = \frac{\rho_0 K_{0y}}{2\pi} \int_{-\pi/K_{0y}}^{\pi/K_{0y}} \exp(-in K_{0y} y - in K_{0y} \Delta_0 \sin K_{0y} y) \times dy = (-1)^n \rho_0 J_n(n\Delta_0 K_{0y}), \tag{12}$$

where J_n is the Bessel function, n are integers from $-\infty$ to $+\infty$. The finiteness of the resolution of the RSA with respect to y, including doubling of the image, will be expressed in the restriction of the number of harmonics in this expansion. It is possible to consider the amplitudes of the components with n such that $2/nK_{0y} \gtrsim 100$ m to be nonzero (see section 2). This means that in the majority of cases of practical interest it is possible to limit ourselves to the consideration of two or three first harmonics. If the first harmonic is zero, and the second harmonic and subsequent ones do not pass with respect to resolution, then the wave image will not be obtained, or it will have half the true spatial period if only the second harmonic passes.

The amplitude of the reflector velocity projection in the direction of the station for the gross assumption of large orbital movement is equal to $v_0 = v_{orb}(\sin^2\alpha\cos^2\theta + \sin^2\theta)^{1/2}$, where α is the angle between the direction of the wave propagation and the path line. Assuming for developed wind waves that $v_{orb} = cv$, where v is the wave phase velocity and substituting the values of $\Delta_0 = (r/V)\, v_0$ and $K_{oy} = K_0 \cos\alpha$, in (12) instead of $\tilde{\rho}_1 = 0$, we obtain

$$J_1\left[\frac{cr}{V}\cos\alpha\sqrt{K_0 g(\sin^2\alpha\cos^2\theta + \sin^2\theta)}\right] = 0. \qquad (13)$$

The value of c was determined in [5] under the assumption of the sinusoidal wave profile by equating the value of the mean square deviation of the surface (sinusoidal) from the mean level to the corresponding value obtained from the adopted expressions for the spectral wave density. If A is the amplitude of the sinusoidal wave obtained in this way and the orbits are circular, then $c = 2\pi A/\Lambda$, where Λ is the wavelength. However, the assumption of a sinusoidal nature, that is, smoothing of the profile by comparison with the actual one, led to a low estimate of c: $A/\Lambda \approx 10^{-2}$ was obtained. For a wave peaked to the maximum (the maximum steep windless wave) a value of $A/< \approx 7\cdot10^{-2}$ is given [15], but is indicated that the wind-driven waves have smaller amplitudes. Let us take a value of $3\cdot10^{-2}$. Then, assuming circular orbital movement as before, although this does not entirely correspond to the truth [15], we obtain $c \approx 0.2$ for developed wind wave action.

Then for different α for $0 < \theta < 45°$ and r/V = 100 sec the values of Λ_y corresponding to the first root of the equation (13) encompass the range from 0 to 700 meters, and the second root, from 0 to 200 meters. Hence, it follows that observation of premature disappearance of the wave image or doubling of its spatial frequency theoretically is possible.

Now let $\rho_0(y) = \rho_0[1 + m\sin(K_{0y}y + \phi)]$. Then instead of (13) we have the system

$$\operatorname{Re}\tilde{\rho}_1 = -J_1(z) + \frac{m}{2}\sin\varphi[J_0(z) - J_2(z)] = 0,$$

$$\operatorname{Im}\tilde{\rho}_1 = \frac{m}{2}\cos\varphi[J_0(z) + J_2(z)] = 0,$$

where $z = \Delta_0 K_{0y}$.

For $\phi = \pi/2$ this system becomes the equation

$$J_1(z) - \frac{m}{2}\,[J_0(z) - J_2(z)] = 0. \tag{14}$$

The value of the second route of equation (14) with respect to the values within the limits from 0 to 0.8 for m varying from 0 to 1, respectively. In this range of values of z for different θ and α it is possible to obtain in practice any value of Λ_y. The values of m and ϕ depend on the wave conditions and, in addition, on θ and α. These relations are still not exactly known, and therefore it is necessary to consider the possibility of the above-described distortions of the wave images.

We have investigated the characteristics of a sea wave image in RSA by comparison with the images obtained using the incoherent RBO, beginning in this case with a two-scale model of the scattering of ultrashort radio waves by the wavy surface of the sea.

The performed investigation demonstrated that for ordinary tuning of the processing system the image of the cylindrical wave system must be defocused just as the image of a target moving in the wide direction parallel to the heading of the RSA carrier with a velocity $v^{(y)}/2$, where $v^{(y)}$ is the phase velocity of the wave formed by the section of the investigated wave system by a plane parallel to the y-axis. For $v^{(y)} \ll V$ the focussing can in practice be completely restored by the corresponding tuning of the processing system.

The spatial variations of the velocities of the surface elements must lead to additional modulation of the optical density of the image. It is demonstrated that for sinusoidal variation of the velocities of the surface elements and the box scattering coefficient the first harmonic in the expansion of the density in a series can vanish. Here the image can in general be absent if the second and subsequent harmonics are not permitted, and doubling of the spatial frequency of the wave in the image can take place if the harmonics beginning with the third harmonic are not permitted.

It is also demonstrated in the investigated model the primary specific (by comparison with the case of observation of a stationary surface) restriction on the azimuthal resolution of the RSA when observing cylindrical waves is connected with the possible isotropicity of the small-scale oscillations of the surface and doubling of the image following from this.

The author thanks A. A. Kalinkevich for the many discussions of this paper.

BIBLIOGRAPHY

1. P. S. Belousov, et al., SOVETSKO-AMERIKANSKIY EKSPERIMENT"BERING"(Soviet American "Bering" Experiment), Leningrad, Gidrometeoizdat, 1975.

2. C. Elachi, J. GEOPHYS. RES., Vol 81, No 15, 1976, p 2655.

3. W. E. Brown C. Elachi, T. W. Thompson, J. GEOPHYS. RES., Vol 81, No 15, 1976, p 2657.

4. T. R. Larson, L. I. Moskowitz, J. W. Wright, IEEE TRANS, AP-24, 1976, No 3, p 393.

5. A. V. Ivanov, IZV. VUZOV -- RADIOFIZIKA (News of the Institutions of Higher Learning -- Radiophysics), Vol 21, No 12, 1978, p 1750.

6. C. Elachi, W. E. Brown, IEEE TRANS., AP-25, No 1, 1977, p 84.

7. A. Jain, APPL. PHYS. Vol 15, No 3, 1978, p 323.

8. B. S. Mush, ZARUBEZHNAYA RADIOELEKTRONIKA (Foreign Radioelectronics), No 6, 1978, p 63.

9. W. J. Plant, IEEE TRANS, AP-25, No 1, 1977, p 28.

10. A. D. Rozenberg, I. Ye. Ostrovskiy, A. I. Kalmykov, IZV. VUZOV -- RADIOFIZIKA, Vol 9, No 2, 1966, p 234.

11. A. D. Rozenberg, et al., IZV. AN SSR, SER. FIZIKA ATMOSFERY I OKEANA (News of USSR Academy of Sciences, Physics of the Atmosphere and Ocean Series), Vol 9, No 12, 1973, p 1323.

12. V. I. Zel'dis, et al., AKUST. ZH. (Acoustics Journal), Vol 20, No 2, 1974, p 235.

13. J. W. Wright, W. C. Keller, PHYS. FLUIDS, Vol 14, No 3, 1971, p 466.

14. J. W. Duncan, W. C. Keller, I. W. Wright, RADIO SCI., Vol 9, No 10, 1974, p 809.

15. V. V. Shuleykin, FIZIKA MORYA (Physics of the Sea), Moscow, Nauka, 1968.

16. Ch. Kuk, M. Berifel'd, RADIOLOKATSIONNYYE SIGNALY (Radar Signals), Moscow, Sov. radio, 1971.

17. G. R. Valenzuela, IN SURVEILLANCE OF ENVIRONMENTAL POLLUTION AND RESOURCES BY ELECTROMAGNETIC WAVES, Ed. by T. Lund. Dordrecht, Holland, 1978.

10845
CSO: 1860

UDC 621.396.965

FREQUENCY SCANNING IN RADIOVISION

Kiev IVUZ RADIOFIZIKA in Russian Vol 23,No 8,1980 pp 934-941 manuscript received 3 Jul 79

[Article by I. Ya. Brusin, T. G. Vlasova, E. I. Gel'fer, V. A. Zverev, A. D. Krasnyanskiy, S. Ye. Finkel'shteyn, Gor'kiy State University]

[Text] A study is made of the application of aperture synthesis in the frequency plane in radiovision. The possibilities of implementing the method in the passive operating mode, the achievable parameters and the possibility of target identification are discussed.

In variousradiovision systems (construction of the target image in the radio range [1, 2]), the requirement of high resolution is in contradiction with the size restriction of the real systems shaping the image. The application of aperture synthesis by displacement of the receiving element in space as is done in radioastronomy [3] and radar (RSA [synthetic aperture radar]) [4] can be a way out. A deficiency of the spatial aperture synthesis is low speed determined by the time for mechanical filling of the synthetic aperture.

It is proposed in this article that the method of aperture synthesis on the frequency plane be used in radio vision. The theoretical possibility of obtaining target images by using frequency scanning was demonstrated in [5-7]. A discussion is presented of the possibility of implementing the method in the millimeter radio wave band in the passive operating mode, achievable parameters and restrictions of the system, the possibility of reproducing the target image or, at least, its identification by partial information in the spectral plane.

In the active operating mode the frequency aperture synthesis can be realized by varying the frequency of the emitting oscillator. In the passive mode when the image is constructed by the natural emission of the target, it is necessary to perform a spectral analysis of the correlation function of the wide-band signals received at separated points [5, 6]. In view of the absence of band filters in the millimeter band, it is proposed that the superheterodyne signal reception system be used to isolate a narrow band with respect to the intermediate frequency from the obtained correlation function and then perform a successive spectral analysis by varying the heterodyne frequency.

Accordingly, a passive radiovision system with frequency scanning can be constructed.

Let the system consist of N separate receiving antennas and be a distance z from the observed target. Figure 1 shows the simplest case of a two-element receiving system

with the base 2ρ. The field component on a frequency ω at the reception points 1 and 2 can be written in the form

$$E_{1,2}(\omega) = \mathrm{Re}\iint p(x, y, \omega)\exp\left[i\omega\left(t - \frac{r_{1,2}}{c}\right)\right]dxdy, \qquad (1)$$

where p(x, y, ω) is the complex amplitude of the field at the targent on a frequency ω,

$$r_{2,1} = \sqrt{z^2 + (x \pm \rho\cos\alpha)^2 + (y \pm \rho\sin\alpha)^2},$$

α is the angle between the x-axis and the base of the system. In (1) and subsequent formulas, insignificant constant factors are omitted.

The spatial method of obtaining the correlation function of two signals is measurement of the mean value of the square of their sum [8, 9].

The signals received by the point antennas 1, 2, are summed, then the total signal is heterodyned, after which the intermediate frequency amplifier defines the frequency band from it

$$\omega_r - \Omega_2 < \omega < \omega_r - \Omega_1,$$
$$\omega_r + \Omega_1 < \omega < \omega_r + \Omega_2, \qquad (2)$$

where Ω_1 and Ω_2 are the lower and upper bounds of the pass band of the intermediate frequency amplifier.

The relative band width of the obtained high frequency filter usually is small: $2\Omega_2/\omega_r \ll 1$, and it is tuned by varying the heterodyne frequency ω_r within the limits from $\omega_1 = 2\pi c/\lambda_1$ to $\omega_2 = 2\pi c/\lambda_2$.

Squaring and averaging the total signal after the intermediate frequency amplifier are realized using a low-frequency quadratic detector. After averaging with respect to time $T \gg 2\pi/\Omega_1 \gg 2\pi/\omega$ in the expression for the signal at the output of the low-frequency detector section terms of the following type

$$\iiiint\!\!\iint \langle p(x, y, \omega)\, p^*(x', y', \omega')\rangle \exp\left[i(\omega-\omega')t - i\omega\frac{r_{1,2}}{c} + i\omega'\frac{r'_{1,2}}{c}\right]dxdx'dydy'd\omega\, d\omega'$$

and terms conjugate to them remain.

Since the natural emission of the target is not correlated with respect to space and frequency, the correlation function of the complex amplitudes of the field at the target will be

$$\langle p(x, y, \omega)\, p^*(x', y', \omega')\rangle = J(x, y, \omega)\,\delta(x-x')\,\delta(y-y')\,\delta(\omega-\omega'). \qquad (3)$$

Also proposing that the intensity of the target emission does not depend on the frequency in the heterodyne tuning range

$$J(x, y, \omega) = J(x, y),$$

considering (3), after integration with respect to x', y' and ω' we obtain the expression for the signal at the receiver output:

$$S = \iiint J(x, y)\left[1 + \cos\left(\omega \frac{r_1 - r_2}{c}\right)\right] dx\, dy\, d\omega. \tag{4}$$

Integrating (4) with respect to ω within the limits defined by the inequalities (2), we obtain

$$S = \iint J(x, y)\, dx\, dy + \iint J(x, y) \operatorname{sinc}\left[\frac{\Omega_2 - \Omega_1}{2c}(r_1 - r_2)\right] \times$$

$$\times \cos\left[\frac{\Omega_2 - \Omega_1}{2c}(r_1 - r_2)\right] \cos\left[\frac{\omega_r}{c}(r_1 - r_2)\right] dx\, dy. \tag{5}$$

Obviously, in the second integral the most rapidly varying is the last cofactor. If the following condition is satisfied for all points of the target

$$\frac{\Omega_2 - \Omega_1}{2c}(r_1 - r_2) < \frac{\pi}{4},$$

the first two cofactors can be considered constant within the integration limits, and the expression (5) assumes the simple form:

$$S = \iint J(x, y)\, dx\, dy + \iint J(x, y) \cos\left(\omega_r \frac{r_1 - r_2}{c}\right) dx\, dy. \tag{6}$$

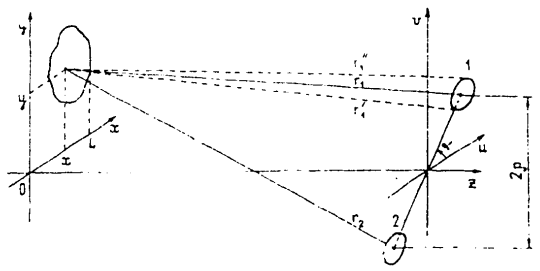

Figure 1. Radiovision system in the passive mode.

When deriving the expression (6), the receiving antennas were assumed to be points. For the real antenna of diameter D this is admissible if the phase difference for the edge points of the antenna (see Figure 1) is sufficiently small. In the Fresnel approximation

$$r_1'' - r_1' \approx \frac{D(L + \rho)}{z} < \frac{\lambda}{2}.$$

Thus, we obtain the following restriction on the size of the antenna:

$$D < \frac{\lambda z}{2(L+\rho)}. \tag{7}$$

If we turn both antennas so that the centers of their radiation patterns coincide, then the requirement (7) will be relaxed:

$$D < \frac{\lambda z}{2L}.^{1} \tag{8}$$

In the Fresnel approximation

$$r_1 - r_2 = \frac{2\rho}{z}(x\cos\alpha + y\sin\alpha),$$

and then (6) assumes the form

$$S(u, v) = \iint J(x, y)dx\,dy + \iint J(x, y)\cos(ux + vy)dx\,dy, \tag{9}$$

where

$$u = \frac{2\rho\omega_r}{cz}\cos\alpha, \qquad v = \frac{2\rho\omega_r}{cz}\sin\alpha \tag{10}$$

are the spatial frequencies along the x and y axes.

From formula (9) it is obvious that the signal at the output of the radiometer is defined by the values of the spatial spectrum

$$G(u, v) = \iint J(x, y)e^{-iux - ivy}dx\,dy \tag{11}$$

and can be written in the form

$$S(u, v) = G(0, 0) + \mathrm{Re}\,G(u, v). \tag{12}$$

The Fourier transformation of the signal obtained gives information about the target in the form

$$\int_{-\infty}^{\infty}\int S(u, v)e^{i(ux+vy)}du\,dv =$$

$$= \frac{1}{2}J(x, y) + \frac{1}{2}J(-x, -y) + G(0, 0)\delta(x)\delta(y). \tag{13}$$

It is possible to record the signal so that J(x, y) = 0 for $x \leq 0$ (or $y \leq 0$). Here

---

[1] The inequalities (7) and (8) can be obtained also from the condition of finding the entire target in the field of the main lobes of the radiation patterns of both antennas.

the superposition of the different terms in (13) is excluded, and later it is possible to limit ourselves to the investigation of only the spectrum G(u, v) instead of the full signal S(u, v).

It must be noted that although G(u, v) is a function of two variables during the measurement, as follows from (10), it is defined along a straight line forming the angle α with the u-axis. Thus, only the one-dimensional spectrum along the straight line connecting the reception point is measured. With an increase in the number of receivers in space (N > 2) we obtain the values of the spectrum along all segments of straight lines joining the reception points.

This characteristic of the signal recording can be taken into account as the effect of the filter, the transmission function of which H(u, v) differs from zero only along the indicated segments. The signal at the output of this filter is written as the product

$$H(u, v) \times G(u, v).$$

The Fourier transformation of this product can be represented as follows:

$$s(x, y) = \int_{-\infty}^{\infty}\int J(x', y')h(x-x', y-y')\,dx'\,dy', \tag{14}$$

where

$$h(x, y) = \frac{1}{4\pi^2}\int_{-\infty}^{\infty}\int H(u, v)e^{i(ux+vy)}\,du\,dv \tag{15}$$

is the response of the filter to the point effect.

For analysis of the obtained image first we assume that the signal is recorded only along a straight line coinciding with the u-axis, and the transfer function has the form

$$H(u, v) = \left[\Pi\left(\frac{u-u_0}{U}\right) + \Pi\left(\frac{u+u_0}{U}\right)\right]\delta(v), \tag{16}$$

where

$$\Pi(u) = \begin{cases} 1 \text{ for } & |u| \leqslant 1 \\ 0 \text{ for } & |u| > 1 \end{cases},$$

$$U = \frac{u_2-u_1}{2}, \qquad u_0 = \frac{u_2+u_1}{2}, \tag{17}$$

$$u_{1,2} = 2\frac{p\omega_{1,2}}{cz} = 4\pi\frac{p}{\lambda_{1,2}z}.$$

It is obvious that

$$\frac{u_0}{U} = \frac{\lambda_1+\lambda_2}{\lambda_1-\lambda_2} > 1. \tag{18}$$

For this type of filter the response to a point effect does not depend on y:

$$h(x,\ y) = h(x) = 2\,\frac{\sin Ux}{\pi x}\cos u_0 x. \tag{19}$$

Therefore, for example, the point target $J(x, y) = \delta(x - x_0)\ \delta(y)$ is a band parallel to the y-axis, with dependence on x described by the function $h(x - x_0)$.

According to (18) $U < u_0$; therefore $h(x)$ can be represented by an envelope of the type $\sin Ux/\pi x$ with high-frequency filling $\cos u_0 x$. The information about the target is included in the envelope; the high-frequency filling does not have great significance for target recognition.

It is obvious that the resolution is determined by the distance from the principal peak to the first zero in the course of the envelope; it is equal to

$$R = \frac{\pi}{U} = \frac{z\lambda_1\lambda_2}{2\rho(\lambda_2 - \lambda_1)}.$$

A point, a segment and either of their sets on a straight line x = const form a class of equivalent targets not distinguishable with respect to shape of the output signal if the signal recording in the spectral plane was made along the u-axis parallel to the x-axis.

Let us consider targets with sharp boundary in which

$$J(x,\ y) = \begin{cases} J_0 = \text{const}, & x,\ y \in \sigma \\ 0, & x,\ y \notin \sigma \end{cases},$$

where σ is the domain of the plane (x, y) bounded by the closed curve K. In this case the double integral (14) over the domain σ can be reduced to the integral with respect to the curve K:

$$s(x) = J_0 \oint_K P[x - x'(l)]\,dl \sin\varphi, \tag{20}$$

where ϕ is the angle between the element $d\ell$ and the x-axis, $x'(\ell)$ is the x-axis of the outline point considered as a function of the length ℓ of the corresponding section of the curve K, and

$$P(x) = \int_0^x h(\xi)\,d\xi.$$

This function is expressed in terms of an integral sine curve, but a more obvious representation is given by the approximate formula which is valid for $u_0 >> U$:

$$P(x) \approx \frac{2}{u_0}\,\frac{\sin Ux}{\pi x}\sin u_0 x. \tag{21}$$

Expression (20) shows that the contributions of the individual parts of the curve do not depend on each other. The segment of the curve parallel to the x-axis makes no contribution to the integral. The maximum contribution is obtained from the segments parallel to the y-axis. However, this contribution begins to drop sharply when the parallelness is disturbed. The harmful effect from the high-frequency factor in (19) and (21) is manifested in this characteristic. The spacing between the zeros of this factor is

$$d = \frac{\pi}{u_0} = \frac{2\pi}{u_2 + u_1} = \frac{z}{2\rho}\,\frac{\lambda_1\lambda_2}{\lambda_2 + \lambda_1}. \tag{22}$$

If the projection of the segment of the curve on the x-axis satisfies the condition

$$\Delta x < \frac{d}{2}, \tag{23}$$

then the function x'(ℓ) in the integral (20) can be taken as the constant x', and then the contribution of this segment turns out to be proportional to its length multiplied by the function P(x - x').

If

$$\Delta x \geqslant d, \tag{24}$$

then the individual parts of the investigated segment make contributions in counterphase, and the total results drops results.

For illustration of the conclusions obtained above regarding the possibility of reproducing the target image when recording the spectrum along a straight line, the following experiment was performed. An optical system was assembled, the schematic diagram of which appears in Figure 2. A diaphragm was located in the (x, y) plane. It was illuminated by a pencil of rays converging at the point f. The amplitude distribution of the light oscillations in the hole in the diaphragm simulated the object -- the function J(x, y). The light source (a helium-neon laser) and the lenses used to shape the converging beam are not shown in the figure. In the plane passing through the point f, the spectrum G(u, v) was formed. If a lens L was placed on the path of the rays, an image of the target was obtained in the X, Y plane.

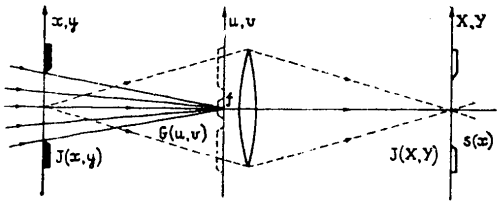

Figure 2. System for optical simulation of the recording and reproduction of an image by the frequency scanning method.

However, if a filter with pass band (16) was placed in the u, v plane, also, then light distribution proportional to $s^2(x)$ was obtained in the X, Y plane.

A slit located located along the u axis was used as the filter. Its width was about 4 microns. By using an additional diaphragm at the slit, the central part $|u| \leq u_1$ and continuations $|u| \geq u_2$ were covered, creating the expression

$$\frac{u_0}{U} = \frac{u_2 + u_1}{u_2 - u_1} \approx 8.$$

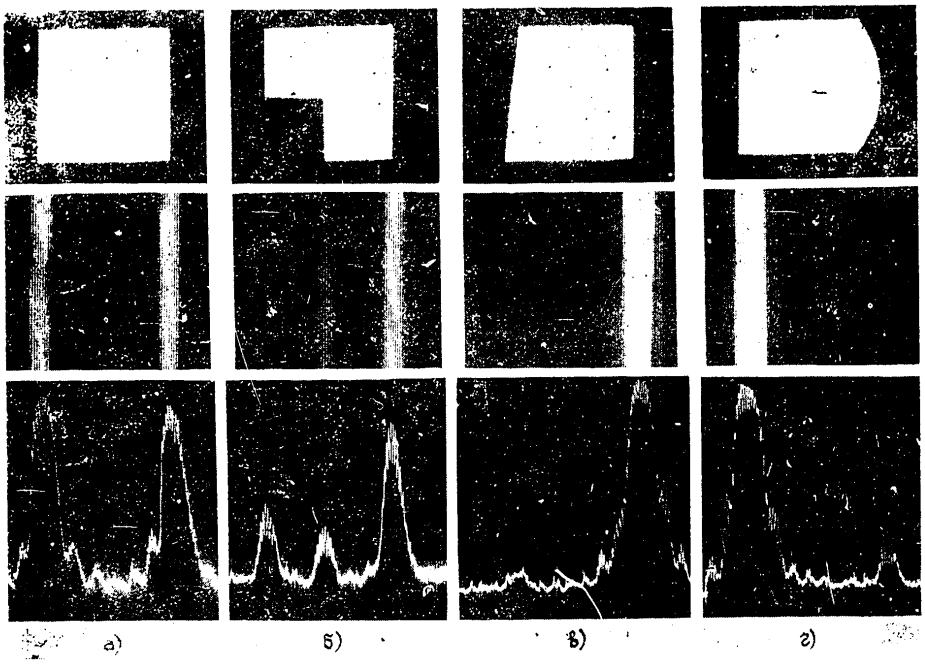

a) b) c) d)

Figure 3. The upper row is a photograph of the target; the middle row is the photographs of the same targets obtained on simulation of the frequency scanning method with two antennas; the lower row is the result of photometric measurement of the negative images of the middle row.

Figure 3 shows photographs of targets obtained without and with a filter. On the photographs with a filter (the middle row) the sides of the targets parallel to the x-axis were not represented. This coincides completely with the theoretical conclusions. The sides perpendicular tc the x-axis were transmitted the most intensely. The illumination distribution in their image is proportional to $P^2(x)$. The function (21) explains the appearance of fine structure with a period d and the course of the envelope in the image.

In the image of the figure with the step (photograph b) the intensity is appreciably less in the transmission of the short vertical segments than in the transmission of the long one. This is connected with the fact that when representing the vertical segments the illumination must be proportional to the square of their length.

The sloping side of the trapezoid was not represented in photograph c. The reason was the following. Considering the photograph, it is possible to see that the projection of the sloping side on the x-axis contains several periods of fine structure d, that is, the inequality (24) exists and, as a consequence, there is a strong drop in illumination which is intensified by the nonlinearity of the photographic process.

In photograph d the image of the art cf a circle is attenuated significantly. Only the segment close to the vertical tangnet for which inequality (23) is satisfied was actually depicted.

If smooth variations are characteristic for the function J(x, y), then by the output signal s(x) the corresponding target will be equivalent to the target with sharp variation of J(x, y), but with curvilinear outline.

In conclusion let us note that when observing targets of simple shape which is a priori known, the described setup permits determination of the overall dimensions of the target just as during spatial synthesis of the aperture along one straight line. The advantage of the radiovision system with frequency scanning is speed and absence of complex devices for mechanical movement of the antennas. More complete information about the target can be obtained as a result of complicating the system: either increasing the number of antennas or rotating one antenna around the other.

BIBLIOGRAPHY

1. E. I. Gel'fer, Yu. V. Lebskiy, S. Ye. Finkel'shteyn, N. A. Yakun', IZV. VUZOV -- RADIOFIZIKA (News of the Institutions of Higher Learning -- Radiophysics), Vol 19, No 10, 1976, p 1512.

2. E. I. Gel'fer, S. N. Mensov, RADIOTEKHNIKA I ELEKTRONIKA (Radio Engineering and Electronics), Vol 22, No 5, 1977, p 914.

3. A. A. Pistol'kors, RADIOTEKHNIKA I ELEKTRONIKA, Vol 11, No 10, 1966.

4. A. P. Reutov, B. A. Mikhaylov, G. S. Kondratenkov, B. V. Boyko, RADIOLOKATSIONNYYE STANTSII BOKOVOGO OBZORA (Side-Looking Radar), Moscow, Sov. radio, 1970.

5. V. A. Zverev, RADIOOPTIKA (Radiooptics), Moscow, Sov. radio, 1975.

6. E. I. Gel'fer, V. A. Zverev, S. Ye. Finkel'steyn, TEZISY II VSESOYUZNOGO SIMPOZIUMA PO MILLIMETROVYM I SUBMILLIMETROVYM VOLNAM (All-Union Symposium on Millimeter and Submillimeter Waves), Khar'kov, No 2, 1978, p 210.

7. G. Berbekar, S. Tökes, ULTRASONICS, Vol 16, No 6, 1978.

8. A. A. Michelson, F. G. Pease, ASTROPHYS. J., No 53, 1921, p 249.

9. N. A. Yesepkina, D. V. Korol'kov, Yu. N. Pariyskiy, RADIOTELESKOPY I RADIOMETRY (Radiotelescopes and Radiometers), Moscow, Nauka, 1973.

10845
CSO: 1860

END